CHALMERS
UNIVERSITY OF TECHNOLOGY

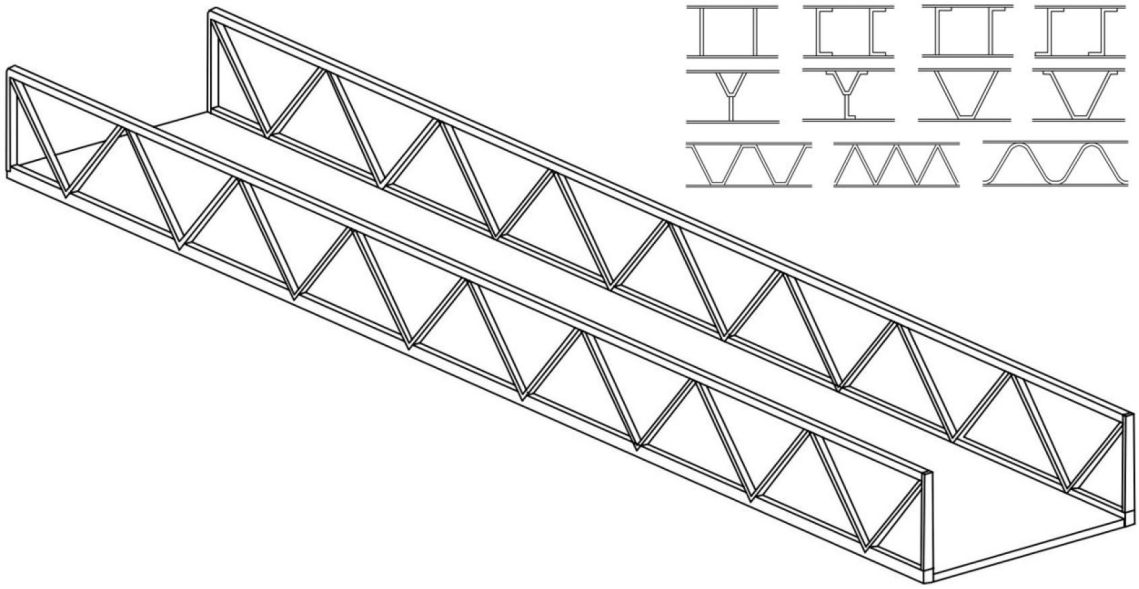

Laser Welded Steel Sandwich Panels for Pedestrian Bridge Application

A Case Study

Master's thesis in the master's program Structural Engineering and Building Technology

JOHANNA LINDQVIST
ALEXANDER SVENSSON

DEPARTMENT OF ARCHITECTURE AND CIVIL ENGINEERING

CHALMERS UNIVERSITY OF TECHNOLOGY
Gothenburg, Sweden 2022
www.chalmers.se

Master's thesis ACEX30

Laser Welded Steel Sandwich Panels for Pedestrian Bridge Application

Master's Thesis in the Master's Program Structural Engineering and Building Technology

JOHANNA LINDQVIST
ALEXANDER SVENSSON

CHALMERS
UNIVERSITY OF TECHNOLOGY

Department of Architecture and Civil Engineering
Division of Structural Engineering
Lightweight Structures
Chalmers University of Technology
Gothenburg, Sweden 2022

Laser Welded Steel Sandwich Panels for Pedestrian Bridge Application

JOHANNA LINDQVIST
ALEXANDER SVENSSON

Supervisor: Peter Nilsson Strand, WSP Sverige AB
Examiner: Professor Mohammad Al-Emrani, Department of Architecture and Civil Engineering

Department of Architecture and Civil Engineering
Division of Structural Engineering
Lightweight Structures
Chalmers University of Technology
SE-412 96 Gothenburg
Telephone +46 31 772 1000

Cover: Pedestrian bridge and core configurations for a steel sandwich panel evaluated in the thesis.

Typeset in LaTeX
Department of Architecture and Civil Engineering
Gothenburg, Sweden 2022

Laser Welded Steel Sandwich Panels for Pedestrian Bridge Applications
JOHANNA LINDQVIST
ALEXANDER SVENSSON
Department of Architecture and Civil Engineering
Chalmers University of Technology

Abstract

Evolving technologies in the field of welding enable the use of Steel Sandwich Panels (SSP) for bridge deck applications. These panels consist of two steel plates, separated by a lightweight core, acquiring a high stiffness-to-weight ratio and increased bending stiffness compared to a conventional Orthotropic Steel Deck (OSD). Laser welding enables one-sided welding and high precision, which is vital for the manufacturing of SSPs. Previous studies have mainly focused on the applicability of steel sandwich panels for road bridges, which has shown great potential to become the next generation of steel bridge decks. Increased steel prices and environmental demands are a driving force for the development and optimization of these panels.

To find an optimal deck design for a pedestrian bridge, this thesis aims to evaluate the structural response of a bridge deck exposed to the loads prevailing in a design situation. The effects of changing the bridge deck's stiffness parameters, the composite action between the deck and the surrounding structure, and the impact of locally applied wheel pressure are all being investigated. An OSD and a SSP are compared, with the production feasibility, material consumption, and cost being the main areas of comparison. Additionally, a study on pedestrian bridges in Sweden is being carried out to serve as a benchmark for this and future studies in the field.

The structural analyses' findings led to the conclusion that changing the axial, bending, and shear stiffness of the bridge deck had a negligible impact on the forces acting on the structure. Forces in the lower chord were significantly affected by the composite action between the bridge deck and truss girders. Additionally, it was demonstrated that the design of the bridge deck was determined by the wheel pressures from the service vehicle. In terms of production, it was determined that for the studied case, the SSP's welding time was 70 to 80 percent faster than an OSD's.

Keywords: Bridge decks, pedestrian bridge, steel sandwich panel, truss girders, laser welding, finite element analysis.

Lasersvetsade sandwichelement i stål för gång-och cykelbroar
JOHANNA LINDQVIST
ALEXANDER SVENSSON
Department of Architecture and Civil Engineering
Chalmers University of Technology

Sammanfattning

Ständig teknikutveckling inom svetsning möjliggör användningen av sandwichelement i stål för brodäcksapplikationer. Dessa brodäck består av två stålplåtar, åtskilda av en lätt kärna, som får en hög styvhet i relation till dess vikt och en ökad böjstyvhet jämfört med en konventionell ortotrop brobaneplatta. Lasersvetsning möjliggör ensidig svetsning och hög precision, vilket är avgörande för tillverkningen av dessa sandwichelement. Tidigare studier har främst fokuserat på användbarheten av sandwichpaneler av stål för vägbroar, vilket har visat stor potential att bli nästa generations brodäck. Ökade stålpriser och högre miljökrav är en drivkraft för utveckling och optimering av brodäck av denna typ.

För att hitta en optimal design på brodäcket för gång-och cykelbro syftar detta arbete till att utvärdera den strukturella responsen av ett brodäck som utsätts för de laster som råder vid dimensionering. Effekterna av att ändra brodäckets styvhetsparametrar, interaktionen mellan däcket och den omgivande strukturen och påverkan av lokalt applicerat hjultryck undersöks. En ortotrop brobaneplatta och en brobaneplatta av sandwichpaneler i stål jämförs, med produktionsgenomförbarhet, materialförbrukning och kostnad som de huvudsakliga jämförelseområdena. Dessutom genomförs en studie av existerande gång-och cykelbroar i Sverige för att fungera som riktmärke för detta och framtida arbeten inom området.

Resultatet av de strukturella analysernas ledde till slutsatsen att förändring av brodäckets axielstyvhet, böjstyvhet och skjuvstyvhet hade en försumbar inverkan på de krafter som verkar på strukturen. Krafterna i den nedre underramstången påverkades signifikant av interaktionen mellan brodäcket och fackverksbalkarna. Dessutom kunde det påvisas att brodäckets utformning styrs av hjultrycken från servicefordonet. När det gäller produktionen fastställdes det att för det studerade fallet var sandwichelementets svetstid 70 till 80 procent snabbare än svetstiden för en ortotrop platta.

Nyckelord: Brodäck, gång-och cykelbroar, sandwichelement, fackverksbalkar, lasersvetsning, finit element analys.

Table of Contents

Preface

This master's thesis was carried out between January and June 2022 at the master's program Structural Engineering and Building Technology at the Department of Architecture and Civil Engineering, Chalmers University of Technology. The thesis investigates the applicability of laser welded steel sandwich panels for pedestrian bridge applications.

First and foremost, we would like to thank our supervisor, Dr. Peter Nilsson Strand, who, through his commitment and expertise in the subject, has given us invaluable advice and help throughout the project. We would also like to thank Professor Mohammad al-Emrani, who through his long experience has given us valuable feedback and encouragement, and Jostein Myklebust, who has guided us through the latest in steel sandwich panel production. This work would not have been possible without the irreplaceable assistance we received from our supervisors and examinator.

Lastly, we would like to thank everyone at the WSP bridge department in Gothenburg who gave us the opportunity to carry out our project at your department.

Johanna Lindqvist and Alexander Svensson, Gothenburg, June 2022

List of Figures

List of Tables

List of Acronyms

CCSSP	Corrugated Core Steel Sandwich Panels
DAL	Directly applied load
ESL	Equivalent single layer
FEA	Finite element analysis
FSDT	First-order shear deformation theory
GMAW	Gas metal-arc welding
HLAW	Hybrid laser-arc welding
OSD	Orthtropic steel deck
RHS	Rectangular hollow section
SSP	Steel sandwich panel
2D	Two dimensional
3D	Three dimensional

Nomenclature

γ_{xx}	Shear angle
γ_{yy}	Shear angle
κ_{xx}	Twisting curvature
κ_{yy}	Twisting curvature
ν	Poisson's ratio
ρ_{xy}	Twisting deformation
χ	Reduction factor
D_{av}	Torsional stiffness
D_{sx}	Shear stiffness
D_{sy}	Shear stiffness
D_{v}	Off-diagonal term
D_{xx}	Bending stiffness
D_{yy}	Bending stiffness
$d_{d.c}$	Spacing between the stiffeners of L-core
$d_{d.f}$	Width of the flange of L-core
$d_{d.wd}$	Distance between the welds of L-core
$d_{d.wc}$	Distance between the web and first weld of L-core
d_{xx}	Axial stiffness
d_{xy}	In plane Shear stiffness
d_{yy}	Axial stiffness
E	Young's modulus of elasticity
G	Shear modulus
h	Height of deck

h_d	Cross-sectional height of L-core
L	Length of the bridge
m_{xx}	Bending moment
m_{xy}	Twisting moment
m_{yy}	Bending moment
n_{xx}	Membrane force
n_{xy}	Shear force
n_{yy}	Membrane force
Q_{fwk}	Concentrated load
Q_{serv}	Service vehicle load
q_{fk}	Uniformly distributed load
$t_{d.L}$	Thickness of the web plate of L-core
$t_{d.lf}$	Thickness of the bottom plate of L-core
$t_{d.tf}$	Thickness of the top plate of L-core
t_f	Plate thickness
t_w	Thickness of longitudinal stiffeners
v_x	Shear force
v_y	Shear force
W	Width of the bridge

1

Introduction

1.1 Background

According to a report by McKinsey & Company (2020), the construction industry is undergoing fundamental change. The industry is currently suffering from a low degree of digitalization, and annual growth over the last 20 years has been one-third of that of average economic growth. Because each project is unique, standardization is difficult. However, parallels can be drawn to other industries with unique and large projects, such as the shipbuilding industry, which has forgone industrialization, globalization, and digitalization in order to become more profitable.

The concrete deck is the most commonly used bridge deck, with its main advantages being the availability of materials, well-known long-time behavior, and vast work experience (Chen & Duan, 2014). The structure is, however, rather heavy. Steel bridge decking has traditionally been considered a last resort, used only when structural weight is essential. The conventional way of constructing such a deck is by connecting longitudinal or transversal stiffeners to a plate. These decks are called Orthotropic Steel Decks (OSD) and have been used since 1970s (Bright & Smith, 2007). However, OSD requires a lot of complex and time-consuming welding being labor-intensive, and are potentially exposed to extensive damage and high maintenance costs.

The development of Steel Sandwich Panels (SSPs) has mainly focused on marine and aerospace applications, but has shown great potential to become the next generation of steel bridge panels. A SSP consists of two steel plates separated by a lightweight core, resulting in an increased second moment of area and thus increased bending stiffness compared to a conventional OSD (Davies, 1993; Sandcore, n.d.). Case studies regarding Corrugated Core Steel Sandwich Panels (CCSSP) have been the subject of several theses over the years. For instance, Beneus and Koc (2014) focused on an existing orthotropic bridge deck, Dackman and Ek (2015) on medium-span road bridges, Arvanitis and Papadopoulos (2016) on long-span bridge applications, and Libell and Lassing (2020) on short-span road bridges.

The SSP can be built up by several different core configurations. The most effective

design is governed by the boundary conditions and loading (Nilsson Strand, 2020). Furthermore, Nilsson (2017) claims that SSPs are weight-efficient compared to conventional steel decks, with material savings of up to 50% possible. Laser welding is a welding technique that allows for one-sided welding and high precision, both of which are required for the manufacture of these panels. Steel sandwich panels for road bridge's have commonly been the subject of research. However, the use of laser welded SSPs for pedestrian bridge applications has been modestly investigated and are thereby the topic of this master's thesis.

1.2 Aim and Objective

The aim of this thesis is to examine the structural response of a pedestrian bridge, consisting of a steel sandwich panel connected to truss girders, and its feasibility regarding production. This will be done through a case study with the following objectives:

i. Find an appropriate core configuration regarding production and structural aspects through evaluation of a large number of core configurations.

ii. Study the impact of altering the stiffness parameters of the bridge deck and investigate the composite action between the bridge deck and the surrounding structure through a Finite Element Analysis (FEA), by modeling the bridge deck as an Equivalent Single Layer (ESL).

iii. Study the impact of locally applied load by modeling parts of the deck as a three-dimensional (3D) structure through a FEA and studying the stresses in the constituent parts of the deck.

iv. Perform a comparative study between the automized production of a SSP and the conventional production of an OSD regarding time and costs.

1.3 Methodology

The thesis is divided into five main parts, which consist of a literature review, an evaluation phase of possible laser-welded steel sandwich configurations and bridges, an analysis of the global effects, an analysis of the local effects, and a comparative study between an OSD and a SSP regarding production and costs. In the literature review, the aim was to gather knowledge and explore previous studies on the subject. It is done by covering the historical use of SSPs for other applications as well as the current practice of SSPs for bridges. Production, welding techniques, stiffness constants, and load-carrying behavior are also treated in the literature review.

Secondly, a pedestrian bridge research involving 57 Swedish pedestrian bridges was

carried out to serve as a benchmark for this and future studies. Regarding possible core configurations, a large number of geometrical concepts were generated using the acquired knowledge from the literature review. They were later evaluated in a workshop focusing on feasibility and structural capacity, yielding three core configurations that were best suited to the application at hand.

Thirdly, two models were created using the finite element software ABAQUS/CAE. The first model included truss girders as well as a deck with homogenized stiffness properties, subjected to a uniformly distributed load. The second model only had one truss girder and was subjected to a line load, representing half the load acting on the bridge deck. These models were used to evaluate the effect of the bridge's composite action in linear elastic and linear buckling analyses. The response due to varying stiffness parameters of the bridge deck was also studied in the analyses.

Fourthly, the bridge model's middle section was remodelled from a homogenized layer to a section with 3D shell elements. This was done to investigate the effects of locally applied load on the stress distribution in the deck and its constituent members as well as the degree of constraint of the connection between the panel and the lower chord.

Finally, the cost and production time of an OSD and a SSP were compared.

1.4 Limitations

The following limitations and simplifications have been applied on the project:

- The core configurations were only examined through a qualitative assessment.
- Only linear static and linear buckling analyses have been performed.
- Only two load types have been examined.
- The welds are modeled with kinematic couplings and no contact condition is applied between the core and face plates.
- The cost of the SSP has been limited to material costs and the time has been limited to the welding procedure only.
- The deck's orientation is perpendicular to the bridge's longitudinal direction.

1.5 Outline

The report is divided into the following chapters:

Chapter 1 introduces the topic, provides background on the problem to be studied,

and describes how the project is carried out.

Chapter 2 contains the literature review where the relevant theory for the project is presented.

Chapter 3 includes the pedestrian bridge study, and the evaluation of geometrical concepts.

Chapter 4 presents the model used in the global analysis as well as the results obtained.

Chapter 5 presents the model used in the local analysis as well as the results obtained.

Chapter 6 compares the cost and production aspects of the conventional and steel sandwich bridge deck.

Chapter 7 contains a discussion regarding the work and results presented in the thesis.

Chapter 8 provides conclusions and recommendations for further research.

2

Literature Review

2.1 Pedestrian Bridges

Bridges are important components in the transportation network and their main function is to enable transportation over or past an obstacle (Lin & Yoda, 2017). Further, it should provide structural safety and comfort for the bridge users, i.e., transfer the loads to the foundations without excessive deformations or vibrations (Chen & Duan, 2014; Lin & Yoda, 2017). Since bridges are exposed structures the need to experience safety crossing the bridge from one side to another is important. Slip resistances and guard rails are therefore necessary to ensure the experienced safety (Keil, 2013). Pedestrian bridges are advantageously manufactured in steel to reduce construction time on site. This is possible as the entire bridge or large parts of the bridge can be manufactured in a workshop and then transported and lifted on site.

2.2 Bridge Decks

Bridges are typically made up of a superstructure, bearings, a substructure, and accessories (Lin & Yoda, 2017). The bridge deck belongs to the superstructure which is the part of the bridge that is located above the bearings, which is illustrated in Figure 2.1. Except from acting as the pedestrian walkway, various structural demands are placed on the bridge deck in terms of load-bearing function (Nilsson Strand, 2020). It should be able to locally carry loads from wheel pressures, distribute the loads to the supporting structure through plate action, and, possibly, act as a flange to the main girders to increase the global stiffness.

Bridge decks can be composed of a variety of materials and geometries where concrete, steel, and timber are the most frequently used. The usage of structural steel increases the strength in both tension and compression compared to concrete and can benefit from high ductility, rapid erection time, and easy fabrication (Lin & Yoda, 2017).

The pavement is an important part of a bridge deck as it provides comfortable

walkway conditions, spreads the concentrated loads, prevents direct contact between vehicle and bridge deck, and protects the deck from meteorological conditions, minimizing corrosion and preventing mechanical damage (Keil, 2013; Lin & Yoda, 2017).

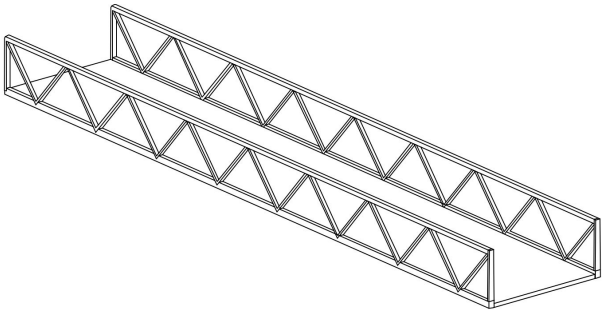

Figure 2.1: Superstructure of pedestrian bridge

2.2.1 Conventional Orthotropic Steel Decks

Conventional OSDs consist of a top steel plate and longitudinal stiffeners and have been widely used in bridge applications where the structural weight is of high importance. An important characteristic of an OSD is the high level of orthotropy due to its high longitudinal stiffness compared to its transversal stiffness. The first OSD for bridge application was introduced in 1936 and consisted of open stiffeners (Kolstein, 2007). In 1954, closed stiffeners were introduced for the first time, which resulted in improved torsional rigidity. The development has then been kept rather unchanged despite numerous problems regarding cost and durability (Bright & Smith, 2007).

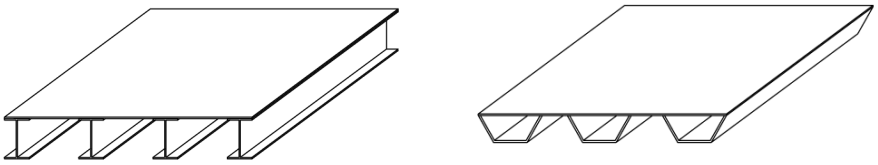

(a) Open stiffeners. **(b)** Closed stiffeners.

Figure 2.2: Orthotropic steel decks with different stiffeners.

The most significant constraints regarding the use of OSD are related to economics and fatigue-deterioration. Typically, the fabrication of OSD requires a large amount of effort associated with welding complex details, the deck-to-cross girder connection is one example, resulting in high costs (Bright & Smith, 2007).

The complexity of the welds between longitudinal stiffeners and top plate and deck-to-cross girder connections gives rise to high stress concentrations, mainly due to the effect of local loads such as wheel pressure, resulting in premature fatigue cracking (Kolstein, 2007). For that reason, conventional welding techniques are dependent on good accessibility for the welding equipment, and fillet welds or partial penetration welds have for that reason been used between the top plate and longitudinal stiffeners, resulting in reduced fatigue life (Bright & Smith, 2007).

2.2.2 Steel Sandwich panels

The development of sandwich panels was initiated in several branches as early as the 1950s and was further developed during the 1980s and 1990s, mainly for marine and aerospace purposes (Kujala & Klanac, 2005).

Sandwich panels can be made from composite or metallic components, with FRP or PU foam being common composite materials. A Steel sandwich panel is an orthotropic deck with a lightweight metal core that separates a top and bottom metal plate.

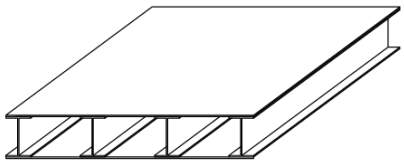

Figure 2.3: Steel sandwich panel with I-beams.

The separation of the plates and the downward shifting of the neutral layer compared to an OSD increases the second moment of area and thus the bending stiffness with only a small increase in weight (Bright & Smith, 2007; Sandcore, n.d.). Other advantages of laser-welded SSPs over conventional stiffened plates, include increased transverse bending stiffness, less distinct shear lag effect, good stiffness to weight ratio, and high manufacturing accuracy (Nilsson Strand, 2020; Kujala & Klanac, 2005). For the use of SSPs in marine applications, increased unsupported spans, reduced constructional height, and reduced assembly times were also stated (Sandcore, n.d.).

In a case study of an existing OSD and a SSP, it was shown that that the area per unit width of the cross-section, and thus the total weight, could be reduced by 23% in the SSP while maintaining its structural capacity (Beneus & Koc, 2014). If the

cross-sectional area instead was kept constant between the cases, the same study showed an stiffness increase of 82% in the direction of the corrugation.

2.3 Deck Orientation and Notations

The geometry of the SSP considered in this thesis is assumed to be rectangular with a three-dimensional coordinate system. Figure 2.4 presents the length of the panel, L, the width of the panel, W, and the height of the panel, h, with its corresponding global coordinate system. The global coordinate system is denoted with letters (x, y, z).

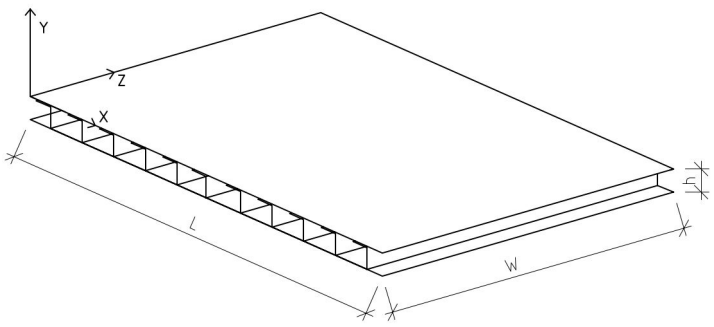

Figure 2.4: Global coordinate system.

The stiffeners can be oriented parallel or orthogonal to the length of the bridge. When the stiffeners are placed parallel to the length of the bridge (x-direction), it is called parallel deck orientation, and when the stiffeners are placed orthogonal to the length of the bridge (z-direction), it is called orthogonal deck orientation (Nilsson & Al-Emrani, 2016). The top plate is assumed to be the plate where the load is applied and has a negative sign in the downward direction (y-direction).

2.4 Welding

In the conventional way of producing a steel structure, welding plays an important part not only in its mechanical and practical properties but also in its manufacturing time. Badly welded details can result in reworks because of heat distortion or shortened lifetime (Roland, Manzon, Kujala, Brede, & Weltzenböck, 2004). To increase productivity and ensure higher quality welds, more efficient welding techniques and systems are needed. Standardized welds can be obtained by implementing an automated production method. The following sections describe techniques commonly used in laser-welded steel sandwich panels.

2.4.1 Laser Welding

The laser welding technique is what's enabling the modern SSP because it can reliably and efficiently access a joint between two steel plates from the outside. The weld is called a stake weld and is an essential component in the production of a SSP. In the bridge industry, the technique is relatively unestablished, but pilot projects have been launched in several countries and the technique is more established in industries once similar to the bridge industry with unique projects and large investments, such as the transportation industry.

Laser welding has several advantages over conventional welding, such as a reduced amount of heat distortion and residual stresses because of the low heat input, providing the section with a smaller heat affected zone (Bright & Smith, 2007). If a stake weld is used instead of a butt weld to assemble a core and a plate, filler material can be saved for the former since the laser melts the adjacent steel. Economic savings can also be obtained due to the process being up to 10 times faster compared to conventional welding methods, and the process can be automated, leading to high precision (Abbott, Caccese, Thompson, Blomquist, & Hansen, 2007). Furthermore, the technique simplifies welding and cuts preparation time on cross girders. Cut outs in the cross girders are required in conventional steel decks to allow for stiffener continuity, which is not required in a SSP (Nilsson Strand, 2020).

Even though laser welding comes with a lot of advantages it also has some drawbacks and considerations. The transition from production of conventional welding to laser welding comes with an initial cost of equipment and demands on experienced personnel (Wouters, 2005; Roland et al., 2004). Another consideration is that the laser's focus diameter is small, thus not a suitable welding technique to use when joining two parallel plates, for instance the connection between the lower chord and the bridge deck in a pedestrian bridge (Wouters, 2005).

2.4.2 Gas Metal-Arc Welding (GMAW)

The concept of Gas Metal-Arc Welding (GMAW) has been known since the 1920s (Wahab, 2014). An electrode wire is continuously fed into an electric arc by an automatic wire feeder in the GMAW process. This creates enough heat to melt metals together. This process is controlled and protected by a shielding gas.

The GMAW process provides a continuous weld with high quality at a low cost with no slag products (Dinbandhu et al., 2021). It also has a wide tolerance of the conditions on the surface, such as impurities and joint gaps. Another advantage of the GMAW is that it can be used in situations where the weld head for the hybrid laser-arc welding is too large, which can be advantageous for certain designs. However, the equipment is cumbersome, comes with a high initial cost, is quite immobile, and welding distortions are a bigger problem in comparison to the pure

laser welding and hybrid laser-arc welding processes.

2.4.3 Hybrid Laser-Arc Welding (HLAW)

Hybrid Laser Arc Welding (HLAW) is obtained by integrating gas metal-arc welding with laser welding. The technique was introduced in the late 1970s and great promise was shown with it (Steen, Eboo. M, & Clarke, 1978). However, further development was halted because of a lack of high-power lasers. The availability of high-power lasers and increased knowledge today have made the technique a viable option.

The concept of HLAW is to combine the strengths of the two welding techniques, laser welding and GMAW, to obtain a technique that has increased welding speed, penetration depth, and gap bridging ability. Because of its versatility, it can be used in many applications regarding the SSP, such as panel to panel connections and in core cycle to core cycle connections for convenience in testing (Defalco, 2007; Nilsson, Hedegård, Al-Emrani, & Atashipour, 2019).

Despite the advantages with HLAW, there are some drawbacks concerning a higher initial cost, more thorough safety measures, demands on accurate positioning and control of a large number of process parameters (Acherjee, 2018).

2.4.4 Dual Weld Lines

Nilsson, Al-Emrani, and Atashipour (2017a) investigated the effect of dual weld lines between a face plate and a core in a case study of a beam with a corrugated core. The result of the study was that dual weld lines increased the transverse shear stiffness in comparison to single weld lines. This comes as a consequence of the force couple created by the dual weld lines. The effect of the force couple was enhanced if the distance between the welds increased because of increased interaction between the adjacent plates. As a result of this increased interaction, the stresses in both the core and welds decreased while the normal stress in the top plate increased. Dual weld lines between the core and face plate are shown in Figure 2.5.

2.4.5 Contact

When welding cores with flanges to the face plates with a pure laser weld, a distance between the plates is created, denoted h_g, seen in Figure 2.5. How this distance affected the stresses for a CCSSP with dual weld lines has been studied by (Nilsson et al., 2019). In the study, it could be seen that the stresses decreased in the weld and its constituent members if contact occurred between core and face plate as it was subjected to a directly applied load (DAL). It was shown in the same report that if a distance $>50\mu$m was used, no contact was achieved between the plates during deformation and thus the stresses increased. Since the study is conducted on a CCSSP theses results cannot be directly translated to other core configuration. To

the authors' knowledge, similar studies for other core configurations do not exist. To verify contact for other core configurations, both FEAs and production experiments should be conducted on the specific core configuration.

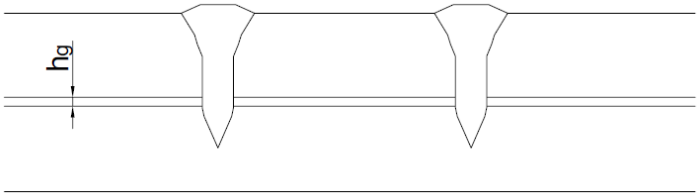

Figure 2.5: Dual weld lines between face plate and core.

2.5 Load and Actions on Pedestrian Bridges

Load models and representative values in accordance with SS-EN 1991-2 (2003) must be used when designing a pedestrian bridge in Sweden. The load models do not describe actual loads but represent the effect of traffic and should be used for serviceability and ultimate limit state calculations.

This section covers loads and actions that are used for the design and verification of pedestrian bridges. The relevant standards used within this master's thesis are presented in Table 2.1.

Table 2.1: Eurocodes used within this master's thesis.

Eurocode	**Title**	**Part**
SS-EN 1990	Eurocode:	
	Basis of structural design	
SS-EN 1991-2	Eurocode 1:	Part 2:
	Actions on structures	Traffic loads on bridges
SS-EN 1993-1-1	Eurocode 3:	Part 1-1:
	Design of steel structures	General rules and rules for buildings
SS-EN 1993-2	Eurocode 3:	Part 2:
	Design of steel structures	Steel bridges

Three static models for vertical loads due to traffic load should be taken into account; a uniformly distributed load q_{fk}, a concentrated load Q_{fwk} and loads representing a service vehicle Q_{serv} (SS-EN 1991-2, 2003).

2.5.1 Uniformly Distributed Load

The uniformly distributed load q_{fk} should only be defined and applied in the unfavorable parts of the influence surface for a specific load effect. The uniformly distributed load may be specified to cover the effect of a continuous dense crowd where such a risk exists, where the recommended value for q_{fk} is defined by Equation 2.1.

$$2.5 \leq q_{fk} = 2.0 + \frac{120}{(L + 30)} \leq 5.0 \quad [\text{kN/m}^2] \tag{2.1}$$

Where L is the loaded length in [m].

2.5.2 Concentrated Load

The concentrated load Q_{fwk} should be taken as 10 kN acting on a square surface of 0.10 x 0.10 m. If a service vehicle is allowed to drive on the pedestrian bridge, a load corresponding to a service vehicle Q_{serv} should be used instead. Thus, a service vehicle load Q_{serv} and a concentrated load Q_{fwk} should not be considered at the same time.

2.5.3 Service Vehicle

If service vehicles are allowed to be carried on a pedestrian bridge in Sweden, it will in most cases be the determining load. The service vehicle consists of a two-axle load group of 80 kN and 40 kN, as shown in Figure 2.6. The distance between the axles is 3 m, and the width of the track, wheel-centre to wheel-centre, is 1.3 m. The contact area for each wheel of such a load model is 0.20 x 0.2 m, acting at the coating level.

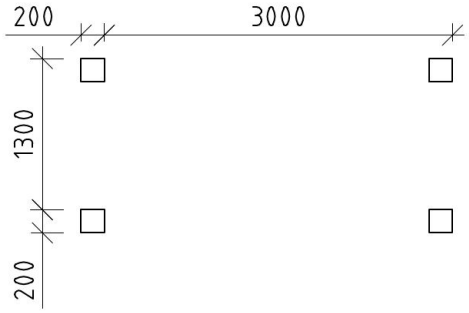

Figure 2.6: Service vehicle with a two axle load group.

2.5.4 Groups of Traffic Load

The traffic load can be divided into two groups, group 1 consisting of the uniformly distributed load q_{fk} and the braking force Q_{flk}, and group 2 consisting of the ser-

vice vehicle load Q_{serv} and Q_{flk}. The two groups are treated separately, and both combinations are presented in Table 2.2.

Table 2.2: Definition of groups.

Load type		**Vertical forces**		**Horizontal forces**
Load system		**Uniformly distributed load**	**Service vehicle**	
Groups	gr1	q_{fk}	0	Q_{flk}
of load	gr2	0	Q_{serv}	Q_{flk}

2.5.5 Load Combination

The bridge should be designed so that it fulfils the requirements of various design situations, in which the persistent design situation, the condition of normal use, is the situation considered in this thesis. Ultimate limit states is the state prior to a structural collapse, which concern the safety of people and/or the safety of the structure itself. Serviceability limit states concern the functioning of the structure under normal use and the comfort of people.

For serviceability state verification, the frequent load combinations defined in Equation 2.2 is used with the partial coefficients presented in Table 2.3 (SS-EN 1990, 2002). However, permanent loads are excluded when calculating the deflection since that is handled through an initial elevation of the structure.

$$\sum_{j\geq 1} G_{k,j} + \psi_{1,1} Q_{k,1} + \sum_{1>1} \psi_{2,i} Q_{k,i} \tag{2.2}$$

Table 2.3: Recommended values of ψ factors for footbridges (SS-EN 1990 Annex A2, 2004).

Action	**Symbol**	ψ_0	ψ_1	ψ_2
Traffic load	gr 1	0.40	0.40	0
	Q_{fwk}	0	0	0
	gr 2	0	0	0

For ultimate limit state verification, the less favorable of Equations 2.3 and 2.4 should be used to verify that internal failure or excessive deformations of the structure or structural members do not occur (SS-EN 1990, 2002). For ultimate limit states, the strength of the construction materials is governed. Partial factors according to Table 2.4 should be used.

$$\sum_{j\geq 1} \gamma_{G,j} G_{k,j} + \gamma_{Q,j} \psi_{0,1} Q_{k,1} + \gamma_{Q,i} \sum_{1>1} \psi_{0,i} Q_{k,i} \tag{2.3}$$

$$\sum_{j\geq 1} \varepsilon_j \gamma_{G,j} G_{k,j} + \gamma_{Q,j} Q_{k,1} + \gamma_{Q,i} \sum_{1>1} \psi_{0,i} Q_{k,i} \tag{2.4}$$

Table 2.4: Design values of actions (SS-EN 1990, 2002).

Design situation	**Permanent action**		**Leading variable action**	**Accompanying variable action**	
	Unfavourable	Favourable	Action	Main	Others
Equation 2.3	$1.35G_{k,j}$	$1.0G_{k,j}$		$1.5\psi_{0,1}Q_{k,1}$	$1.5\psi_{0,i}Q_{k,i}$
Equation 2.4	$1.15G_{k,j}$	$1.0G_{k,j}$	$1.5Q_{k,1}$		$1.5\psi_{0,i}Q_{k,i}$

2.6 Material Coefficients

The design values of material coefficients to be used for the calculation of structural steel components are presented in Table 2.5 (SS-EN 1993-1-1, 2005).

Table 2.5: The design values of material coefficients.

Material coefficient	**Description**	**Value**	**Unit**
E	Young's modulus of elasticity	210 000	N/mm^2
G	Shear modulus	81 000	N/mm^2
ν	Poisson's ratio	0.3	-

2.7 Structural Behavior

Fung and Tan (1998) mention three different ways to study the structural behavior of sandwich panels, namely; (1) the finite element method, (2) the grillage analogy, and (3) the thick plate analogy. The first method entails modeling the sandwich structure, consisting of face plates and core stiffeners, as an assembly of thin plates, resulting in a three-dimensional model. This is a computationally intensive method.

The grillage analogy is an approximate analysis consisting of a two-dimensional grillage of an orthogonal system of beam elements oriented along the x-and y-directions (Tan & Montague, 1991). The panel to be analyzed is first simplified from a three-dimensional structure to a two-dimensional orthotropic continuum according to the theory of Libove and Batdorf (1948). The continuum is then discretized into a grillage of beam elements, rigidly connected together, with stiffness properties given

by the continuum in terms of bending, shear, and torsion. The beam elements are subjected to out-of-plane bending and twisting about the local beam axes. In terms of reliability, the grillage analysis showed similar and converging results as the finite element analysis and is specifically suitable if a medium-sized penetration in the sandwich panel is to be modelled.

In the thick plate analogy, the plate can be analyzed by closed form solutions or finite element analysis. Tan, Fung, and Lok (1993) presented a simplified thick plate analogy for the analysis of all-steel sandwich panels, where the SSP is simplified into a two-dimensional continuum with the equivalent stiffness constants for bending and shear. The continuum is then discretized into an assembly of plate elements with the abovementioned stiffness properties. In analogy with the sandwich plate theory, the following assumptions are adapted: the deflections in z-direction are small, planes originally normal to the mid plane are assumed to remain straight but not necessarily normal to the mid plane after deformation, and in-plane deflections are negligible.

2.8 Homogenization

According to Marek and Garbowski (2015), homogenization is a technique in which a heterogeneous body is replaced by an idealized homogeneous material of equivalent stiffness. Libove and Hubka (1951) presented design formulations of elastic constants required to simplify the three dimensional structure into a two-dimensional (2D) ESL. The simplification results in a great reduction of elements and degrees of freedom, and thus less computational efforts are needed. This is specifically beneficial for design and optimization situations where a great number of iterations are needed. An illustration of a homogenization procedure can be seen in Figure 2.7.

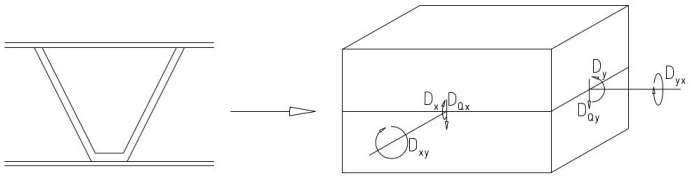

Figure 2.7: 3D V-core transformed into a 2D homogenized layer.

A disadvantage with the homogenization method occurs when it is subjected to large magnitudes of directly applied load, such as pressures from wheels (Nilsson, 2017). This is because the output from an analysis with homogenization is the average global deflection and not specific stresses and deflections in the constituent members. This means that local failures due to local loads are not considered and a separate analysis must be conducted.

2.9 Elastic Stiffness Constants

The characteristics of a steel sandwich panel, two faces separated by a lightweight core, provides high flexural rigidity in the two principal directions (Fung & Tan, 1998). Shear rigidity is high in the direction of the core stiffeners due to continuous interaction between core and face plates and low in the transverse direction due to discrete interaction between core and face plates (Nilsson, 2017). In order to simplify a 3D SSP to a 2D plate, saving computational time and effort, the stiffness properties of the panel need to be evaluated.

The elastic constants required to capture the behavior of SSPs with continuous corrugated cores were investigated and derived by Libove and Hubka (1951). These constants are required to be accurately derived for each geometry to predict accurate stresses in the constituent members, and the elastic constants used are important factors regarding the success of the transformation from a SSP to an equivalent thick plate (Nilsson, 2017; Fung & Tan, 1998).

The elastic stiffness constants derived by Libove and Hubka (1951) are valid for symmetrical sandwich panels and the stiffness properties may be considered to vary symmetrically with respect to the middle surface. In the case of non-symmetrical panel geometries, the idealized-plate material's properties must be considered to vary non-symmetrically with respect to the middle surface, and thus, additional elastic constants need to be developed.

Blaauwendraad (2010) uses the term shape-orthotropy to describe the replacement of a three-dimensional structure, a real shape, to a flat plate with orthotropic properties. The rigidities have to be determined on the basis of the geometry, cross section, and properties of the material used. This procedure is applicable if the spacing of the stiffeners is regularly arranged and there is repetition of the components.

The material used in the transformation of a 3D SSP to a ESL is assumed to be linear-elastic with Young's modulus E and Possion's ratio v.

2.9.1 Membrane Stiffness

The constitutive relationship between normal forces and normal strains for membrane plates is defined by Equation 2.5 (Blaauwendraad, 2010). The homogeneous isotropic plate is the general case of such a plate, but an orthotropic membrane plate may be the result of an isotropic top plate with added stiffeners.

$$\begin{bmatrix} n_{xx} \\ n_{yy} \\ n_{xy} \end{bmatrix} = \begin{bmatrix} d_{xx} & d_v & 0 \\ d_v & d_{yy} & 0 \\ 0 & 0 & d_{xy} \end{bmatrix} \begin{bmatrix} \varepsilon_{xx} \\ \varepsilon_{yy} \\ \gamma_{xy} \end{bmatrix} \tag{2.5}$$

The membrane forces n_{xx}, n_{yy} and n_{xy} (N/m) are related to the membrane rigidities d_{xx}, d_{yy} and d_v, and in-plane shear rigidity n_{xy}.

2.9.2 Bending Stiffness

The constitutive relationship between bending moments and curvature for the general case of an orthotropic plate are defined by Equation 2.6 (Blaauwendraad, 2010).

$$\begin{bmatrix} m_{xx} \\ m_{yy} \\ m_{xy} \end{bmatrix} = \begin{bmatrix} D_{xx} & D_v & 0 \\ D_v & D_{yy} & 0 \\ 0 & 0 & D_{av} \end{bmatrix} \begin{bmatrix} \kappa_{xx} \\ \kappa_{yy} \\ \rho_{xy} \end{bmatrix} \tag{2.6}$$

The bending moments m_{xx} and m_{yy} are defined per unit length (Nm/m) and are related to the bending rigidities D_{xx} and D_{yy} in x-and y-direction, respectively. The off-diagonal term D_v is due to Poisson's ratios v.

The twisting moments m_{xy} and m_{yx} are also defined per unit length but do not necessarily need to be equal for a structure with orthotropic properties, and the torsion rigidity D_{av} is therefore related to the average moment m_{av} of the two twisting moments.

2.9.3 Shear Stiffness

In thick plates, the transverse shear deformations are taken into account, in contrast to thin plates. The constitutive relationship between shear forces and shear angles of an orthotropic plate are defined by Equation 2.7 (Blaauwendraad, 2010).

$$\begin{bmatrix} v_x \\ v_y \end{bmatrix} = \begin{bmatrix} D_{sx} & 0 \\ 0 & D_{sy} \end{bmatrix} \begin{bmatrix} \gamma_{xx} \\ \gamma_{yy} \end{bmatrix} \tag{2.7}$$

The shear forces v_x and v_y are defined per unit length (N/m) and are related to the shear rigidities D_{sx} and D_{sy} in the x- and y-direction, respectively.

2.9.4 General Stiffness Matrix

By combining the membrane stiffness and bending stiffness in the constitutive relationships defined in Equation 2.5 and 2.6, the section stiffness matrix defined in Equation 2.8 is obtained. The stiffness matrix is used as a section property of the shell elements in the finite element model to transform the three-dimensional structure into an equivalent single layer as described in Section 2.7.

$$\begin{bmatrix} n_{xx} \\ n_{yy} \\ n_{xy} \\ m_{xx} \\ m_{yy} \\ m_{xy} \end{bmatrix} = \begin{bmatrix} d_{xx} & d_v & 0 & 0 & 0 & 0 \\ d_v & d_{yy} & 0 & 0 & 0 & 0 \\ 0 & 0 & d_{xy} & 0 & 0 & 0 \\ 0 & 0 & 0 & D_{xx} & D_v & 0 \\ 0 & 0 & 0 & D_v & D_{yy} & 0 \\ 0 & 0 & 0 & 0 & 0 & D_{av} \end{bmatrix} \begin{bmatrix} \varepsilon_{xx} \\ \varepsilon_{yy} \\ \gamma_{xy} \\ \kappa_{xx} \\ \kappa_{yy} \\ \rho_{xy} \end{bmatrix} \tag{2.8}$$

The shear stiffness in the constitutive relationship defined in Equation 2.7 is used separately as a section property of the shell element in the finite element model.

2.9.5 Weld Stiffness

To obtain a model that reflects the behavior of a real SSP, the stiffness of the welds can be a relevant parameter. Libove and Hubka (1951) assumed that a single line weld would reflect a rotationally rigid behavior. Nilsson and Al-Emrani (2016) studied the effect of rotational stiffness of the weld region and its impact on the transverse shear stiffness. They concluded that an assumption of a rigid connection resulted in an overestimation of the transverse shear stiffness and that the real behavior rather corresponds to something in-between a rigid connection and a hinge. Nilsson, Al-Emrani, and Atashipour (2017b) also concluded that the rotational stiffness of the weld region in a CCSSP has a negligible impact on the shear stiffness in the case of dual weld lines but is substantial in the case of a single weld line. However, the rotational weld stiffness is important when determining the stresses in the weld for both cases.

2.9.6 Plate Theory

Libove and Batdorf (1948) developed a small-deflection theory for flat orthotropic plates that is suitable for sandwich plates. The ordinary plate theory, based on the assumption that the plate is isotropic and the deflections due to shear may be neglected, cannot be used for the sandwich plates because of the orthotropic behavior in their flexural properties and the relatively low stiffness of the core, resulting in significant shear deformations. The first-order shear deformation theory (FSDT), which is commonly referred to as the Reissner-Mindlin theory, is the basis for the small-deflection theory by Libove and Batdorf (1948) where such effects are taken into account. The first-order shear deformation theory yields a constant shear strain through the plate thickness due to a linear distribution of in-plane deformations (Chiriac & Vrabie, 2016). Planes originally normal to the mid plane are assumed to remain straight but not necessarily normal to the mid plane after deformation (Libove & Hubka, 1951). For the analysis of an ESL, various plate theories can be used, but the first-order shear deformation theory has been shown to be sufficiently accurate considering global deformations, for example, in the design

of bridge structures (Nilsson et al., 2017b). However, local stresses in the constituent members of the bridge deck can not be treated by an ESL.

2.9.7 Shear Lag

Kollár and Tarján (2021) explains shear lag by investigating the stress distribution in a flange of an I-beam when it is subjected to a transverse load for two different cases. The first case is a beam that is based on the Euler-Bernouli theory where plane sections remain plane. The second case does not have this boundary and deformations due to shear are therefore included. Figure 2.8 illustrates the stress distribution in the two cases. In Figure 2.8(a), the stresses are evenly distributed, while in Figure 2.8(b), the stresses are non-linearly distributed with the peak stress adjacent to the web. This effect is called shear lag and can be explained by the shear strain in the flanges causing higher deformations adjacent to the web and analogously higher longitudinal stresses. This corresponds better with a real beam, and the effect of shear lag increases with increased flange width since only a part of the flange will be used.

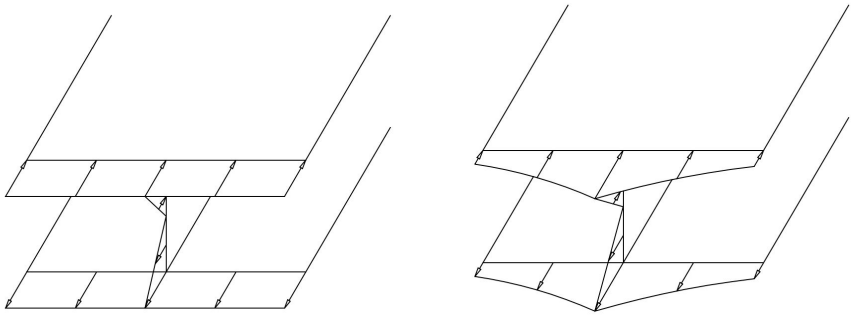

(a) Stress distribution with the Euler-Bernouli assumption.

(b) Stress distribution with shear deformations included.

Figure 2.8: Stress distribution in an I-beam subjected to transverse load.

To account for shear lag in a beam with an analytical method the effective width method can be used. In this method the maximum stress is estimated to act on a part of the flange. This method is difficult to apply since the stress distribution over the flange is required to calculate the effective width. Tenchev (1996) compared several analysis methods to establish a convenient diagram to be used in the calculation of the effective width where the ratio of width over length and shear stiffness over axial stiffness is used, as shown in Figure 2.9. Previous studies of shear lag have shown that these parameters, along with loading and support conditions, affect shear stiffness (Reissner, 1941; Moffatt & Dowling, 1975).

The relation between plate thickness t_f and the overall thickness of longitudinal stiffeners t_w was also investigated in (Tenchev, 1996) . It could be seen that small differences in this ratio did not affect the shear lag, but with a difference of 0.05 $\geq t_f/t_w \leq 5$, a variation of 30% was obtained.

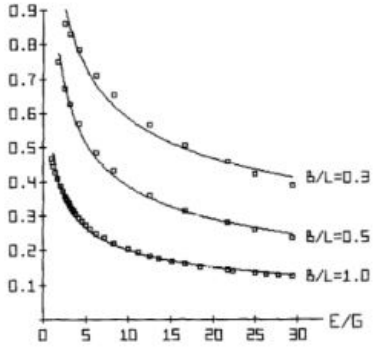

Figure 2.9: Shear lag coefficient (Tenchev, 1996).

2.10 Failure Modes

A structure's ultimate strength is determined by its failure modes. For a SSP, the failures can be divided into two categories: global collapse of the panel and local collapse of the steel face plate or core (Romanoff & Kujala, 2002). The geometry of the SSP and the load conditions determine which failure modes the structure is sensitive to. Zenkert (1997) summarizes different failure modes for a corrugated core, and these are reproduced in Figure 2.10.

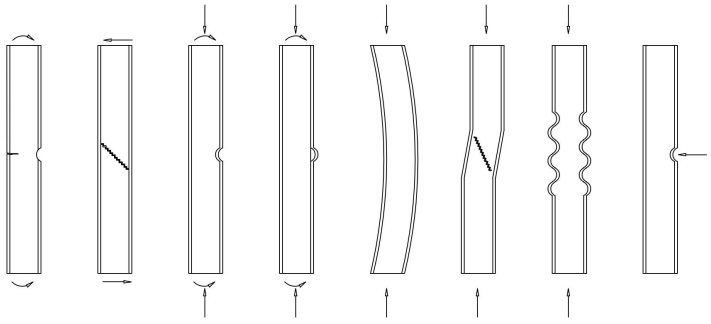

Figure 2.10: Failure modes: plate yielding and/or plate fracture, core shear failure, 2x face wrinkling, general buckling, shear crimping, face dimpling and local indentation. Created by authors, inspired by Zenkert (1997).

2.10.1 Global Collapse

According to Sandcore (n.d.), the most common reason for global collapse in a panel is a result of a local collapse in the plate and/or in the core. If this is not what initiates the collapse, the second most common cause is plastic buckling, which in turn can lead to plastic hinges in sensitive areas, around welds or in the span's middle.

2.10.1.1 Buckling of the Panel

A panel can buckle as a column if either the boundary and load conditions are fulfilled or if the plate has a high slenderness ratio, meaning that the plate has a high thickness-to-length ratio. For the former to be true, the panel must be supported on two edges and subjected to a load acting on its entire width (Romanoff & Kujala, 2002). The critical buckling stress is based on the Euler theory with a modification to account for a wider width in comparison to "real" columns. If the critical buckling stress is reached, the panel will collapse because there is no post-critical strength in a column (Al-Emrani & Åkesson, 2020).

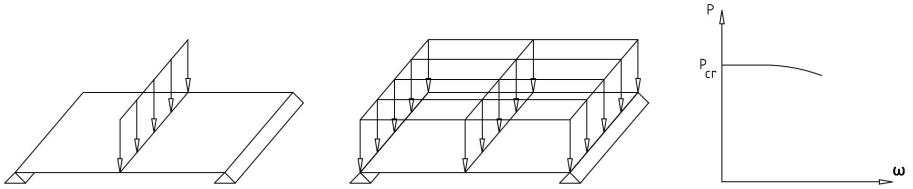

Figure 2.11: Column buckling behavior.

For every other case that is not described in the previous section, the panel will buckle as a plate (Romanoff & Kujala, 2002). If characterized by its slenderness ratio, it has a low value, and the difference for the panel to behave as a plate is that the slenderness ratio is compared to its width instead of length (Al-Emrani & Åkesson, 2020). Also, in contrast to the column behavior, the plate behavior is characterized by its post-critical reserve strength.

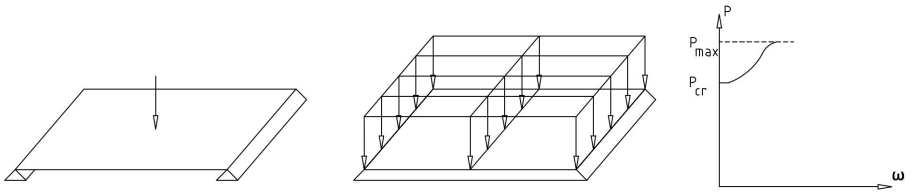

Figure 2.12: Plate buckling behavior.

This reserve strength comes from a redistribution of stresses that occur following buckling. The stiffer parts of the panel that have not buckled attract the compression

load while a transverse membrane in tension is formed in the buckled area, providing the plate with additional strength. The last difference between the two can be seen in the expression for the critical strength of plate buckling, and that is the buckling factor k that describes the loading conditions.

2.10.1.2 Plastic Hinges

Studies to calculate the plastic hinge mechanism in SSP were conducted in (Chen & Han, 1987). In the report, an upper and lower bound solution were presented. The applicability of the methods is, however, limited due to the complex input parameters. To use the methods, the plastic moment is needed as well as the deciding failure mode.

2.10.2 Local Collapse Face Plate

Failure of the face plate can be divided into three failure mechanisms: buckling, denting, or yielding (Romanoff & Kujala, 2002). However, for the specific case only buckling and yielding are relevant.

2.10.2.1 Buckling

Local buckling failure in the face plate is assumed to occur due to shear stresses and/or axial compressive stresses acting parallel or perpendicular to the stiffeners. If a combination of the above stresses occurs, it is called a biaxial stress. The occurrence of these stresses is common, and interaction formulas are applied to obtain accurate answers (Romanoff & Kujala, 2002).

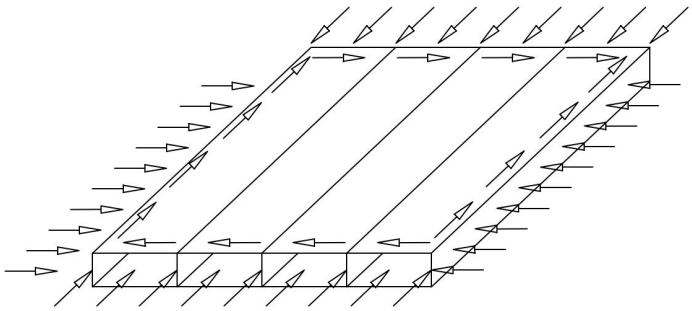

Figure 2.13: Loads in top plate.

2.10.2.2 Yielding

If the maximum allowed stress exceeds the maximum principal stress in the plate, yielding or fracturing of the steel component will occur (Zenkert, 1997). To calculate the maximum stress in a SSP, the von Mises yield criterion is used. For SSPs with

thick plates yielding will be the determining failure mode (Romanoff & Kujala, 2002).

2.10.3 Local Collapse Core

The core is subjected to loads parallel to the stiffener in the form of bending and compression as well as in-plane shear load. These loads can be, as in the face plate, treated separately or combined. The loading situation makes the core prone to buckling and yielding. Plastic collapse can also occur due to high local loads from wheels.

2.10.4 Failure Modes in a Steel Sandwich Panel

A summary of the failure modes in a SSP are as follows:

- Yielding most likely caused by local loads, but can theoretically occur from global loads.
- Buckling of the face plate in the weak direction.
- Buckling of the core due to locally applied wheel pressure.
- Buckling of the entire panel.
- Failure of the welds.
- Fatigue failure in the weld region.

3

Current Practice of Pedestrian Bridge decks and Core Configurations

3.1 Current Practice of Pedestrian Bridge Decks in Sweden

To understand the state of pedestrian bridges in Sweden, a review of 57 pedestrian bridges with conventional orthotropic steel decks is conducted on bridges built between 1970 and 2015. From the review, four different bridge decks can be distinguished. The first, second, and third deck types consist of a top steel plate with transversal stiffeners welded to it. The load is transferred directly to the main girders. The fourth deck type has transversal stiffeners, similar to the first deck type, but with the addition of longitudinal stiffeners between the plate and the transversal ones. In the majority of cases, the main girders of the bridges are made as trusses. The different deck types are presented in Table 3.1 and illustrations can be seen in Figure 3.1. The deck types are presented in plan, elevation and sectional view, showing the various cross-section of the orthotropic steel decks in front of the lower chord.

Table 3.1: Deck type information and mean weight per unit area.

Deck type	Type of stiffeners	Number of bridges	Mean weight per unit area [kg/m^2]
1	Transversal I-beam stiffeners	17	114.8
2	Transversal rectangular stiffeners	21	100.4
3	Transversal trapezoidal stiffeners	6	108.0
4	Longitudinal stiffeners	13	123.3

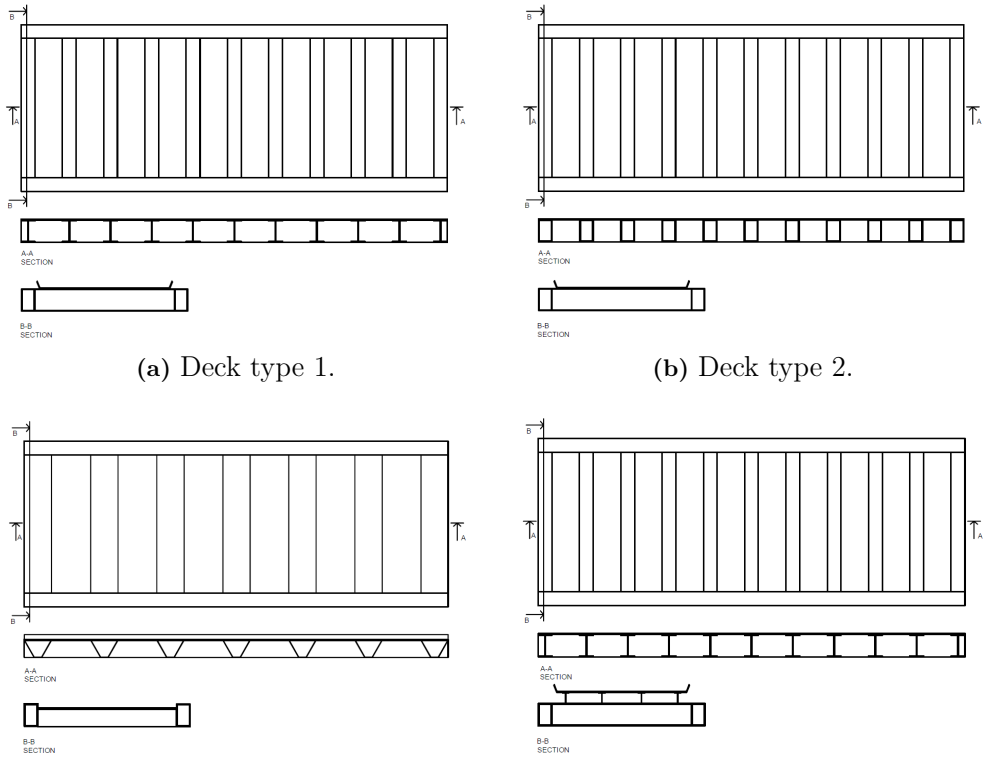

(a) Deck type 1.

(b) Deck type 2.

(c) Deck type 3.

(d) Deck type 4.

Figure 3.1: Plan, elevation and sectional view for the different deck types.

The review of existing pedestrian bridges and the material consumption of their orthotropic steel bridge decks will serve as a benchmark for studies with more economical and sustainable bridges with lower material consumption. The amount of material in the bridge decks is presented as weight per unit area of the deck. From Table 3.1, it can be noted that the deck with transversal rectangular stiffeners has the lowest mean weight per unit area. This deck type has been used throughout the years but was most frequently used from the 1970s until the 1990s. The crossbeams have historically been mechanically fastened to the face plate, yielding a sensitive and corrosion-exposed connection. The bridge deck with both transversal and longitudinal stiffeners has the highest weight per unit area.

Figure 3.2 shows the material usage in weight per unit area over time for each deck type. The dashed line indicates the trend line for each deck type. In general, most of the bridge decks with a high weight per unit area have a thicker steel plate, often 10–12 mm, and most of the bridges that have a low weight per unit area have a thinner top plate, often 6–8 mm. However, the distribution of weight between the top plate and core is not significantly changed but follows the distribution in Table 3.4. It can, however, be noted that between 1970 and 1980, the top plate had

commonly a thickness of 8 mm, and after 1980, it was increased to a thickness of 10 or 12 mm. Annex C of SS-EN 1993-2 (2006) states that the deck plate thickness, t, should be greater than or equal to 10 mm ($t \geq 10$ mm) and the free distance between the stiffeners, e, should be equal to or less than 40 times the plate thickness ($e \leq 40t$).

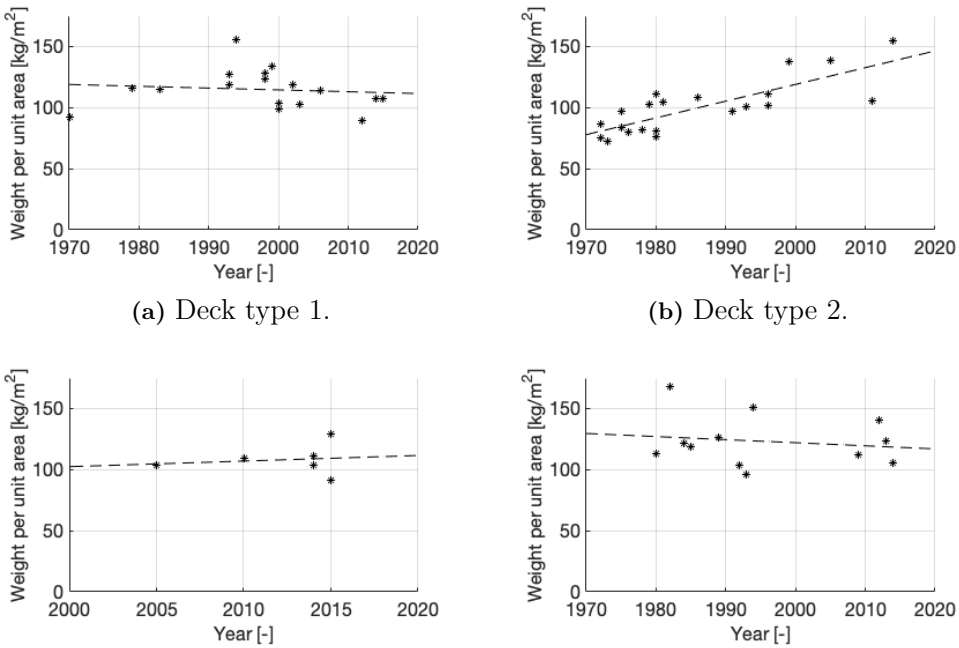

(a) Deck type 1.

(b) Deck type 2.

(c) Deck type 3.

(d) Deck type 4.

Figure 3.2: Material usage, weight per unit area over time.

The weight presented in Table 3.1 and Figure 3.2 shows the weight per unit area of each deck type. Instead, Table 3.2 displays the weight per unit area divided into decades. It can be noted that the weight was relatively low between 1970 and 1979, which can be explained by previous reasoning of plate thickness. After 1980, the mean weight per unit area has been rather unchanged, however, with large variations between the maximum and minimum weights of each decade.

Table 3.2: Weight per unit area divided on decades.

	1970 - 1979 [kg/m^2]	1980 - 1989 [kg/m^2]	1990 - 1999 [kg/m^2]	2000 - 2009 [kg/m^2]	2010 - [kg/m^2]
Max	116.1	168.2	155.4	137.5	155.1
Min	72.5	76.5	96.1	98.8	89.2
Mean	88.8	114.5	119.1	111.4	113.7

Table 3.3 shows the plate thicknesses, center-to-center distances, widths, and lengths for the bridge decks studied. The median thickness for all bridge decks is 10 mm, and the largest thickness for all deck types is 12 mm. The thicknesses have no clear correlation to the widths and lengths of the bridges. The commonly used width for a pedestrian bridge is distinguished as being around 3 m, which applies to all bridge types. Maximum and minimum values can be noted to be around 2 m and 4 m. The mean center-to-center distance between the stiffeners is almost the same for all deck types. However, the maximum and minimum values slightly differ, where deck type 1 has the maximum value and deck type 2 has the minimum value.

Table 3.3: Plate thickness, distance between stiffeners, width and length of each deck type.

Deck type		Plate thickness [mm]	Distance between stiffeners [m]	Width [m]	Length [m]
1	Max	12	1.03	4.2	31.9
	Min	8	0.49	2.5	6.0
	Mean	10.4	0.72	3.3	18.5
	Median	10	0.73	3.2	17.4
2	Max	12	0.90	4.0	45.1
	Min	8	0.30	1.8	6.0
	Mean	9.3	0.70	2.7	18.7
	Median	10	0.73	3.0	16.0
3	Max	12	0.78	3.6	41.0
	Min	8	0.60	3.0	17.0
	Mean	9.7	0.71	3.3	26.4
	Median	10	0.72	3.3	27.0
4	Max	12	0.82	4.1	39.4
	Min	6	0.62	2.2	9.9
	Mean	9.5	0.72	2.9	24.6
	Median	10	0.71	3.0	26.6

In Table 3.4 it can be seen how much the plate and the core make up of the total amount of steel in the bridge deck. In three out of four deck types, the face plates make up for approximately 70% of the steel usage. For deck type 4, it can be noted that the percentage of the core has increased since stiffeners in both transversal and longitudinal directions are used, thus increasing the weight.

Table 3.4: Proportion of plate and stiffener material.

Deck type	Plate weight per unit area [kg/m^2]	[%]	Stiffeners weight per unit area [kg/m^2]	[%]
1	79.6	71	33.2	29
2	73.3	71	29.6	29
3	76.1	71	31.8	29
4	75.5	59	51.5	41

The conventional way of connecting the crossbeams to the steel plate for bridge type one can be seen in Figure 3.3. In the rectangular cross-section, the connection is welded to the core and to the face plate, while for the I-beam it is bolted. Connections conducted in this way exposes the structure to deterioration.

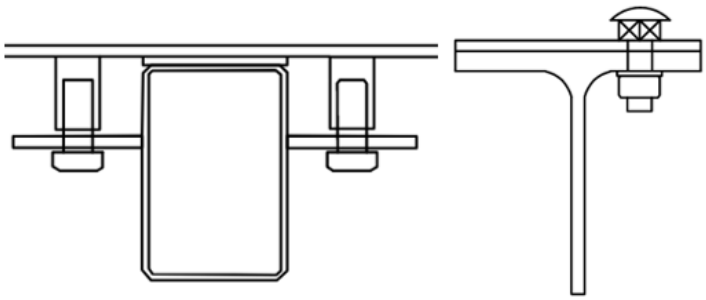

Figure 3.3: Plate connections for different for deck type 1 and 2.

A detailed summary of the collected data for each bridge is presented in Appendix A.

3.2 Core Configurations

Different core configurations are possible for a SSP, in which the most significant difference between them is the material consumption, production aspects, and the shear stiffness in the direction orthogonal to the core (Nilsson Strand, 2020). The following sections will describe the main characteristics of the most common core configurations that can be used in SSPs.

3.2.1 Straight Webs

The elastic stiffness constants of a SSP with straight webs were first derived by Holmberg (1950). The web-core sandwich panel is the most plain layout and is symmetrical over two axes. Following that, elastic stiffness constants for various

layouts of straight webs were derived, covering unsymmetrical sections over one axis with a C-core (Fung, Tan, & Lok, 1993, 1996) and over two axes with a Z-core (Fung, Tan, & Lok, 1994; Fung & Tan, 1998). The influence of patch load has been studied by Naar (1997) and secondary bending stresses by Romanoff (2007). An illustration of different core configurations for straight webs is shown in Figure 3.4. Straight webs are a suitable option if an orthotropic behavior is desired.

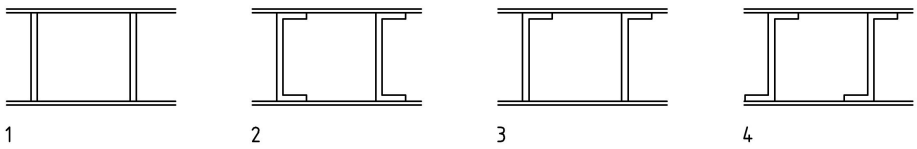

Figure 3.4: Core configurations with straight webs; (1) Web-core, (2) C-core, (3) L-Core, and (4) Z-core.

3.2.1.1 Web-core and L-core

The web-core and L-core have similar layouts and can be material-efficient from a theoretical point of view because of their plain layout. The possibility of optimizing the cross-section have no restrictions regarding cutting and bending of the core profiles, but may be restricted by welding difficulties and limitations regarding the minimum distances between the stiffeners.

The web-core configuration are made with a full penetration weld between the core and top face plate, and one stake weld between the core and bottom face plate. However, difficulties regarding the accuracy of the stake weld with respect to the web often makes it necessary to increase the web thickness, yielding an inefficient design with regard to material consumption.

The addition of flanges in the L-core configuration enables the laser-welding technique to be used and allows for dual weld lines between the core and top face plate. Thus, two stake welds between the core and top face plate, and one stake weld between the core and bottom face plate, per core profile, are required. The stake weld between the core and bottom face plate thus faces the same problem as the web-core.

Depending on the desired distance between the stiffeners, the production can be done in two ways. Either by placing all the core profiles in the right positions and using spot welding and a jigg to keep them in place, or by placing and connecting the core profiles one by one.

The layouts have a low transverse shear stiffness. If there are large distances between the stiffeners, it may be vulnerable to local deformations caused by wheel pressures.

3.2.1.2 C-core and Z-core

The C-and Z-core configuration have similar properties as the web-core and L-core, with the addition of flanges in the bottom part of the core profile. Thus, laser-welding and dual weld lines between the core and top face plate, and between the core and bottom face plate are possible. What distinguishes the Z-core from the C-core is the accessibility of the welding equipment, which yields a straightforward welding procedure from directly above. The space required to fit the weld head used for laser-welding of the C-core needs a certain height and distance between the stiffeners.

3.2.2 Corrugated Core

The elastic stiffness constants of SSP with a corrugated webs with a trapezoidal shape, namely a CCSSP, were first derived by Libove and Hubka (1951). Since then, Nordstrand, Carlsson, and Allen (1994) and Nilsson et al. (2017a) have studied the transverse shear stiffness of such a panel, and Nilsson et al. (2019) have studied the influence of production parameters in a CCSSP. Design formulations for the truss-core have been developed by Lok and Cheng (2000) and material formulations for sinusoidal corrugated cores by Bartolozzi, Pierini, Orrenius, and Baldanzini (2013). An illustration of different core configurations for corrugated webs is shown in Figure 3.5.

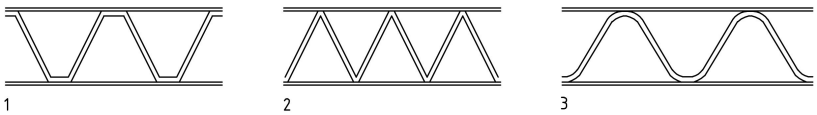

Figure 3.5: Core configurations with corrugated cores; (1) Trapezoidal-core, (2) Truss-core, and (3) Sinusoidal-Core.

3.2.2.1 Truss, Trapezoidal and Sinusoidal Core

The increased shear stiffness seen in all three cross-sections is beneficial if less orthotropic behavior is desired. Both the truss-core and sinusoidal core have a small contact point with the facing plates, which is favorable with respect to local moments and shear forces in the connection compared to the trapezoidal shaped core (Alwan & Järve, 2012). However, the small contact area restricts the truss-and sinusoidal core to having dual weld lines and is generally more difficult to produce. The disadvantages of corrugated cores are that they are material-intensive and constitute a large portion of the cross-sectional area of the panel.

In terms of manufacturing, all three cores can be created by folding a plain plate. The critical part of the truss core and sinusoidal core is the process of welding the core to the facing plates. Because of the small contact area, the accuracy of the stake

welds are important, meaning that the welds needs to be applied in the exact right spot from a perspective that hides the connection.

3.2.3 Hot-Rolled Cores

The elastic stiffness constants of a SSP with rectangular hollow sections (RHS) were first derived by Romanoff and Kujala (2002). Further on, Bright and Smith (2007) conducted fatigue tests on cores with two and four stake welds in each connection. Hot-rolled sections have been proposed as a cost-effective solution because the core is complete and requires no further preparation and is considered stable during construction. An illustration of the different core configurations with hot-rolled cores is shown in Figure 3.6.

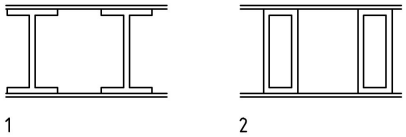

Figure 3.6: Core configurations with hot rolled cores; (1) I-core/IPE, and (2) O-core/RHS.

3.2.3.1 Rectangular Hollow Section core and I-core

Hot rolled sections are available in a limited number of layouts and geometric profiles. Because the process of folding and cutting sheets is eliminated, this is advantageous for the production of a SSP. I-sections and rectangular hollow sections are examples of geometric profiles that is suitable for this application and dual weld lines are possible to obtain.

The limitation of the supply of hot rolled sections reduces the optimization from continuous to discrete variables in terms of height and width. Rectangular hollow sections are material-intensive and constitutes a large proportion of the cross-sectional area, making it inefficient in terms of material usage. Additionally, hot-rolled sections have larger initial imperfections than folded profiles made by modern folding techniques, which results in challenges in automized production.

The process of making a SSP out of I-beams is straight forward. However, due to accessibility for the weld head to fit between, the height and the distance between the I-beams can be a limiting factor. A SSP with a RHS-core can be manufactured in one of two ways: first, by using stake welds from the outside to connect the core and face plates. In order to complete both sides, the SSP must be rotated. Second, in the corners of the O-core, the core can be welded to the face plate. The section can then be enclosed with a second face plate, and stake welds can be done from the outside.

3.2.4 Multi-Supporting Cores

Romanoff and Kujala (2002) derived elastic stiffness constants for V-core. St-Pierre, Deshpande, and Fleck (2015) studied the low velocity impact response and the dynamic indentation response of a SSP consisting of Y-core. An illustration of the different core configurations for multi-supporting cores is shown in Figure 3.7.

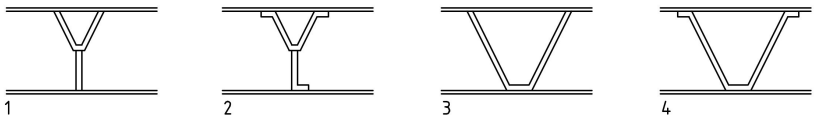

Figure 3.7: Core configurations with multiple supports to the top plate; (1) Y-core, (2) Y-core with flanges, (3) V-Core, and (4) V-core with flanges.

3.2.4.1 V-core and Y-core

The top plate is supported in two positions by both cores, and the loads are transferred to the bottom plate at a single point. This is advantageous in terms of local loads caused by wheel pressure. Flanges can be used to enable dual weld lines in all positions. Additional benefits include the ability to optimize geometric properties due to the ease of producing cores and the accessibility of the welds. The Y-core has the disadvantage of requiring two cold-formed profiles to be welded together to complete the cross-section, causing distortions in the element prior to attachment to the face plate. The V-core has the disadvantage of consuming a significant amount of space.

Depending on the layout of the cross section, there are two ways of producing a V-core. Six stake welds are required in each horizontal part if flanges are used. If flanges are not used, full penetration welds between the top face plate and the core can be used instead, with stake welds connecting the bottom face plate to the core. It is possible to produce a Y-core, but is inefficient due to the previous stated reasons.

3.2.5 Multilayerd Cores

Studies covering multilayered trapezoidal shaped corrugated cores have been conducted by Hou et al. (2015). The study focuses on both numerical and analytical methods for stacked cores.

Multilayered core enables the creation of layers with different properties, such as a first layer with closely spaced stiffeners to withstand local loads and a second layer that is less dense because the load is spread over a larger area, thus reducing the effect of local loads. Having layers in different directions improves the two-way bending behavior. The disadvantages of the profiles include the need for more material since a third horizontal plate is required, the fact that more material in the neutral axis does

not always imply improved structural properties, and the fact that a multilayered core requires greater height. The production of the various layers and the assembly of the final panel both necessitate additional steps. Figure 3.8 illustrates different ways of stacking corrugated cores.

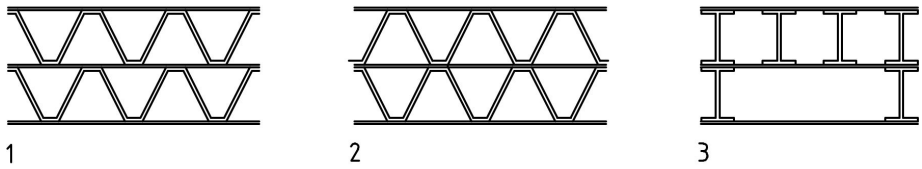

Figure 3.8: Core configurations with multilayered cores; (1) Regularly arranged, (2) Stagger arranged, and (3) First layer with closely spaced stiffeners and second layer with sparsely spaced stiffeners.

3.3 Discussion

Conventional orthotropic steel decks have large weight variations but a relatively high weight per unit area, implying that using SSPs could save weight. As a first assumption, limiting the weight to approximately 100 kg/m^2 would make the SSP competitive with the majority of OSDs.

Plate thickness must be at least 10 mm according to orthotropic steel deck requirements, which means that the steel sandwich panel's two plates must not exceed 10 mm in total in order to save weight. The core stiffeners must also be arranged more densely to resist the locally applied wheel load because the top plate thickness is reduced. The height of the orthotropic plate stiffeners is important for the deck's bending stiffness in the strong direction, but it is not as important in the SSP design because the addition of a bottom plate will contribute. In addition, the thickness of the core stiffeners for a SSP may be reduced when compared to an OSD.

Several of the cross-sections presented have advantages such as increased stiffness and good load-spreading properties, but have been deemed inapplicable due to production constraints and weight consumption without further evaluation.

3.4 Conclusion

The aim of this study was to evaluate a set of existing bridges in terms of weight and geometrical properties so that they could be used as a benchmark for further analysis of a pedestrian bridge with a steel sandwich bridge deck. Furthermore, the aim was to examine possible core configurations. The study has provided mean weight per unit area values by year or bridge type, and the examination of core configurations yielded three configurations that were suitable for the application at

hand. The following conclusions can be drawn from the findings presented in this section:

- If a SSP for pedestrian bridge application should be competitive against a OSD, the weight per unit area should be limited to approximately 100 kg/m^2, with a certain variation due to the width of the bridge.
- The L-core, V-core and Z-core have the greatest potential in an optimized SSP regarding production and weight consumption.
- The V-core and Z-core, both with flanges at the top, are beneficial in terms of production aspects, as there are practically no restrictions on how tightly the stiffeners can be placed.
- The L-core and Z-core are expected to have a similar structural behavior. However, the Z-core will have a contribution from the additional flange, which increases the weight but is advantageous from a production point of view.

4

Global Analysis

4.1 Introduction

The aim of the global analysis is to study how the deck stiffness affects the bridge response and to study the composite action between the deck and truss girders. In the global analysis, the 3D structure of the bridge deck will be transformed into an ESL by homogenization, which allows for multiple analyses in a short period of time.

The modeled bridge is an existing bridge, originally with a conventional orthotropic bridge deck. The software that have been used for the analyses is ABAQUS/CAE.

4.2 Geometry

The bridge to be studied is a pedestrian bridge consisting of a steel sandwich panel connected to two longitudinal truss girders. An illustration of the bridge is shown in Figure 4.1 with dimensions according to Figure 4.2.

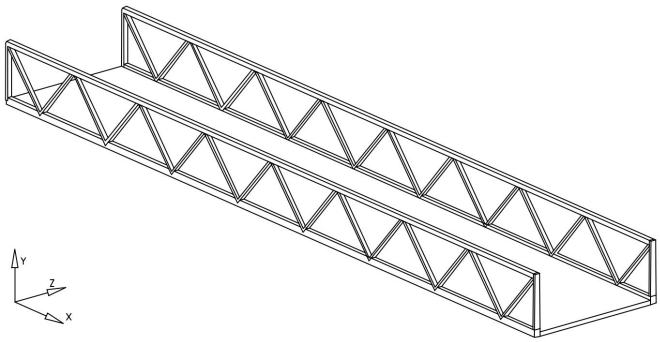

Figure 4.1: Pedestrian bridge used in the case study.

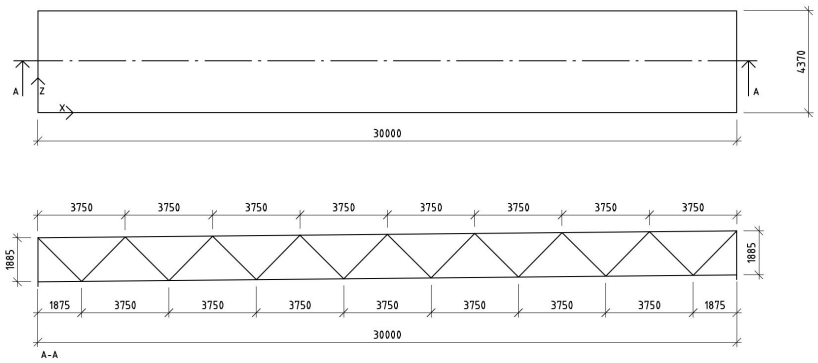

Figure 4.2: Geometry of the bridge panel and truss system.

The truss system illustrated in Figure 4.2 consists of hot-formed rectangular structural hollow sections with cross-sectional dimensions according to Table 4.1 and with steel quality S355.

Table 4.1: Cross-sectional profiles used in the model.

Type	Profiles	Description
1	VKR 150x100x6.3	Diagonal chord
2	VKR 150x100x8	Horizontal end chord
3	VKR 150x100x10	Vertical end chord
4	VKR 180x180x10	Upper chord
5	VKR 250x150x6.3	Lower chord

The bridge deck used for this case study is made out of a steel sandwich panel with a L-core configuration. An illustration of the panel can be seen in Figure 4.3 where all the necessary notations are shown. The dimensions used in this study are presented in Table 4.2.

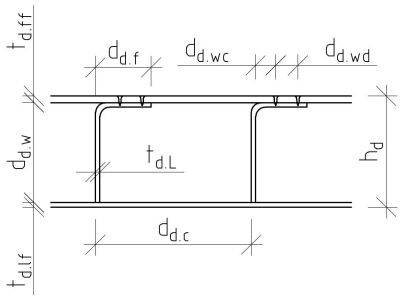

Figure 4.3: Cross-section of the steel sandwich panel used in the study.

Table 4.2: Cross-sectional dimensions for the steel sandwich panel used in the study.

Notation	Description	Value
h_d	Cross-sectional height	100 mm
$d_{d.c}$	Spacing between the stiffeners	140 mm
$d_{d.f}$	Width of the flange	50 mm
$t_{d.tf}$	Thickness of the top plate	6 mm
$t_{d.L}$	Thickness of the web plate	4 mm
$t_{d.lf}$	Thickness of the bottom plate	4 mm
$d_{d.wd}$	Distance between the welds	20 mm
$d_{d.wc}$	Distance between the web and first weld	18 mm

4.3 Stiffness and Material Properties

The truss girders are modeled with beam elements. The elastic material model is used in the truss system with Young's modulus of elasticity set to 210 GPa and Poisson's ratio set to 0.3.

Because the SSP is modeled as an ESL, the material parameters used to calculate the stiffness parameters are inserted into the analysis using the general shell stiffness model, as described in Section 2.9 where the full stiffness matrix is defined. The calculation of the elastic stiffness constants can be seen in Appendix B.

4.4 Boundary Conditions and Constraints

The boundary conditions applied in the FE analysis are made to reflect a simply supported behavior where the translation in y-direction is prevented in all four positions, the translation in x-direction is prevented on one side, and the translation in z-direction is restricted in two positions to prevent rigid body motion. The boundary conditions are set at the bottom of the vertical end beams.

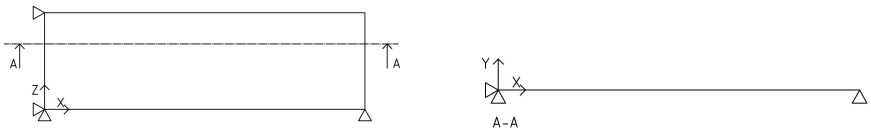

(a) Boundary conditions in the xz-plane.

(b) Boundary conditions in the xy-plane.

Figure 4.4: Boundary conditions used in the model with ABAQUS notations.

To model the composite action between the bridge deck and the truss system, kinematic couplings have been used. That means that the elements of the bottom chord and the deck edges shear degrees of freedom are fused together with no relative motion between them. This is used to mimic the real behavior of a welded connection.

4.5 Mesh

The mesh used in the analysis consists of 3-node shear deformable beam elements with second-order shape functions and 8-node shear-deformable shell elements with second order shape functions.

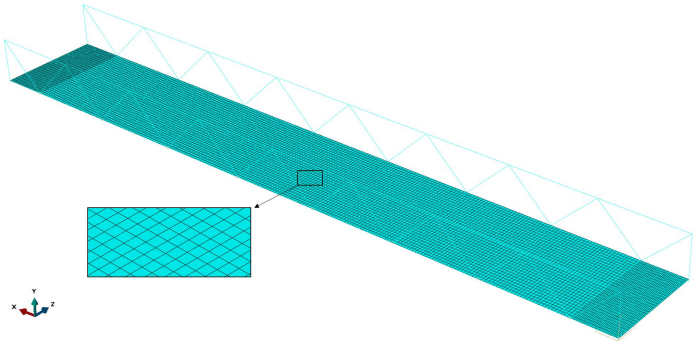

Figure 4.5: Mesh distribution in bridge deck.

To know if the mesh size selected in the model had any effect on the results, a convergence study was conducted. Where the results of the deflection and membrane forces in the deck have been compared for different mesh sizes. The result of the study can be seen in Table 4.3. The size of the mesh had no significant effect on the result, as can be seen in the table. Each edge was divided into 30 elements, which was found to be sufficient for a computationally efficient analysis with accurate results.

Table 4.3: Convergence study.

Edge division	Max displacement [m]	%	Max membrane force [N]	%
300	0.06505	0	342142	0
30	0.06505	0	342134	0

4.6 Locations of Interest

In order to study the behavior of the bridge deck and the influence of the stiffness parameters, several locations of interest have been determined. These locations are

illustrated in Figure 4.6 and created as paths in the FE-program in which load effects can be extracted.

The locations of interest are divided into four sections in the transversal direction of the bridge, where each section consists of four paths. These locations are specifically selected to investigate the distribution of forces near the connection between the diagonals in the truss system and the bridge deck.

Since the bridge is symmetric, only one side of the bridge deck is investigated. Section 1, consisting of paths 1-1, 1-2, 1-3, and 1-4, is located at the outmost part of the bridge, followed by Section 2, Section 3, and Section 4, each section labeled with the same systematics.

In the truss system, however, paths have been created in the longitudinal direction of the bridge in the upper chord and the lower chord, respectively, also illustrated in Figure 4.6.

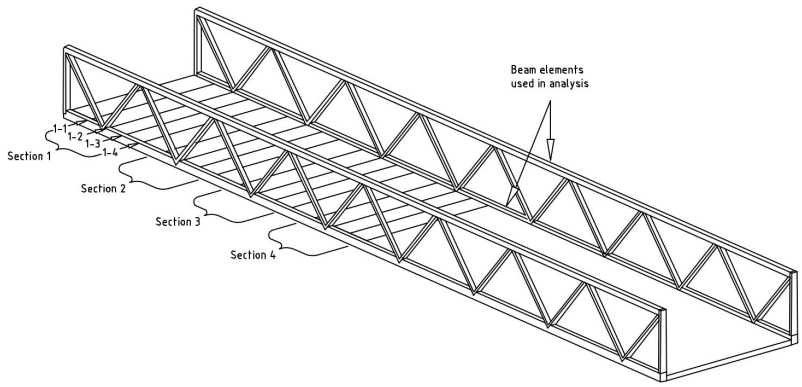

Figure 4.6: Locations of interest.

4.7 Verification of the Model

To verify the model, the bridge has been subjected to a uniformly distributed load corresponding to one of the three static models for vertical load according to Section 2.5. The uniformly distributed load has a magnitude of 5 kN/m^2 and the load combination used for the verification of deflections is the frequent combination of actions. According to SS-EN 1990 Annex A2 (2004), the partial coefficient for frequent combination, ψ_1, is set to 0.4.

The biggest difference can be noticed in the longitudinal direction, where a difference of approximately 30% between them can be seen. This can be explained by the fact that the Euler-Bernoulli theory is used in the analytical calculation, as explained in section 4.8.3. In the transversal direction, a smaller difference can be noted,

approximately 6%. However, in this case, the analytical solution presents a higher value. The difference between them could be due to the boundary condition used in the analysis, preventing translation in the y-direction for the girders.

Table 4.4: Verification of the model in terms of deflection.

Model	Direction	FEA [mm]	Analytical [mm]	Difference [%]
Global	Longitudinal	14.4	11.3	27.4
	Transversal	1.7	1.8	-5.5

4.8 Results from Global Analysis

The results of the global analysis, which included a linear static and linear buckling analysis, will be presented in this section. The results are divided into four parts; the first illustrates the force distribution in the deck, the second examines the bridge's response when stiffness parameters are changed, the third examines the impact of shear lag on this bridge, and the fourth examines the composite action between the bridge deck and truss girders.

4.8.1 Membrane Force Distribution

Figure 4.7 illustrates the membrane force distribution in the longitudinal direction of the deck. Membrane forces have been studied due to the discrete nature of the truss, where local effects are expected to arise near the truss joints.

Figure 4.7: Membrane forces in the bridge deck.

Figure 4.8 shows the distribution of membrane forces in the bridge longitudinal direction across the bridge deck according to the sections of interest presented in Section 4.6. The membrane forces are largest in the mid section, furthest from the

support, and decreases for each section closer to the support. The distribution of membrane forces thus follows the global bending moment.

Compressive and tensile forces arise in the constituent parts of the truss in order to achieve equilibrium. These forces are transmitted to the bridge deck, resulting in local effects in the bridge deck's outer areas, as shown for Sections 1, 2, and 3 of Figure 4.8.

In Section 4 of Figure 4.8, however, no significant impact of the force transmittance at discrete points can be noted which is reasonable since the shear force in mid span is zero and therefore the diagonals contribution is limited. Furthermore, the effect of shear lag may be present, as indicated by the graphs, and will be further treated in Section 4.8.3.

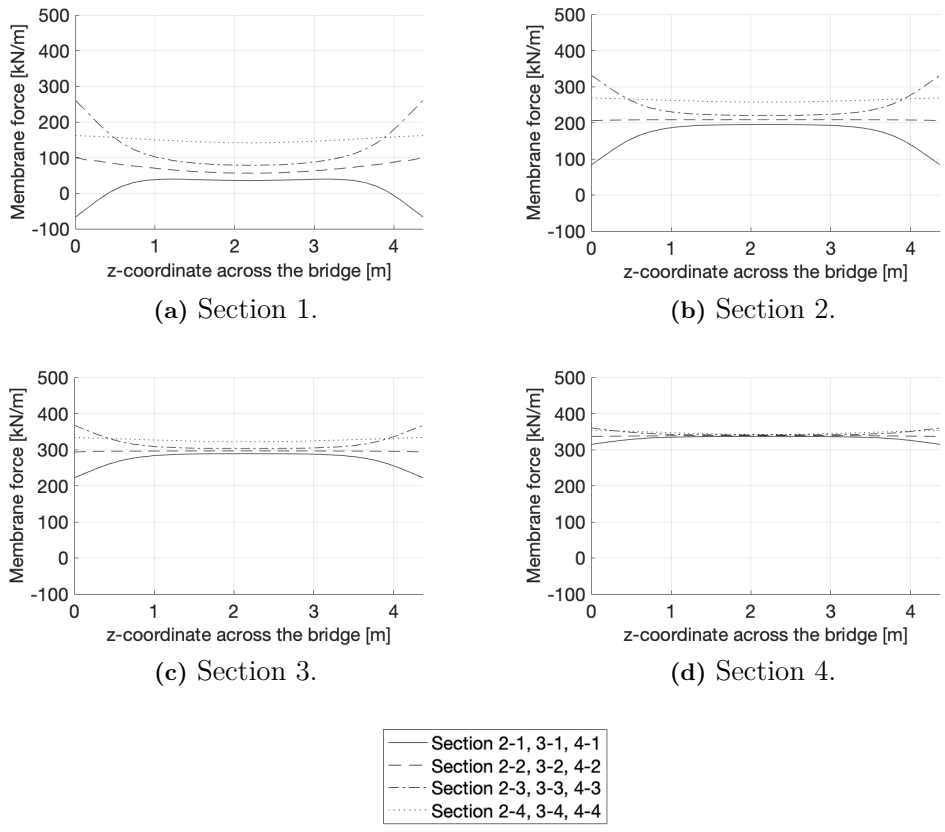

(a) Section 1. **(b)** Section 2.

(c) Section 3. **(d)** Section 4.

Figure 4.8: Membrane forces in sections across the bridge.

4.8.2 Altering Stiffness Properties

The relationship between the input and output variables of the model, i.e., the input parameters in the general stiffness matrix and the resulting normal stresses, will be

covered in this section.

Each variable will be altered from its initial value, by +20%, -20%, +40%, and -40%, respectively. The initial stiffness parameters for the deck can be seen in Appendix B and are in accordance with the layout presented in Table 4.2.

4.8.2.1 Upper Chord

Figure 4.9 and 4.10 shows the distribution of normal forces in the upper chord when the axial stiffness, in-plane shear stiffness and bending stiffness in the longitudinal direction are altered. When the parameters have been altered, no notable difference can be seen in the figures. The maximum compressive stresses obtained from the study are shown in Table 4.5, with just a slight difference between the cases.

The underlying idea of altering those parameters is for the load to transfer from the strong direction to the weak direction when the stiffness in increased and the opposite is expected when its decreased.

Table 4.5: Comparison of the normal forces in the upper chord when the axial stiffness, in-plane shear stiffness, and bending stiffness are changed.

Stiffness parameter	d_{xx}	d_{xz}	D_{xx}	Unit
Initial	-144.6	-144.6	-144.6	MPa
Increased by 20%	-144.6	-144.6	-144.6	MPa
Decreased by 20%	-144.7	-144.6	-144.8	MPa

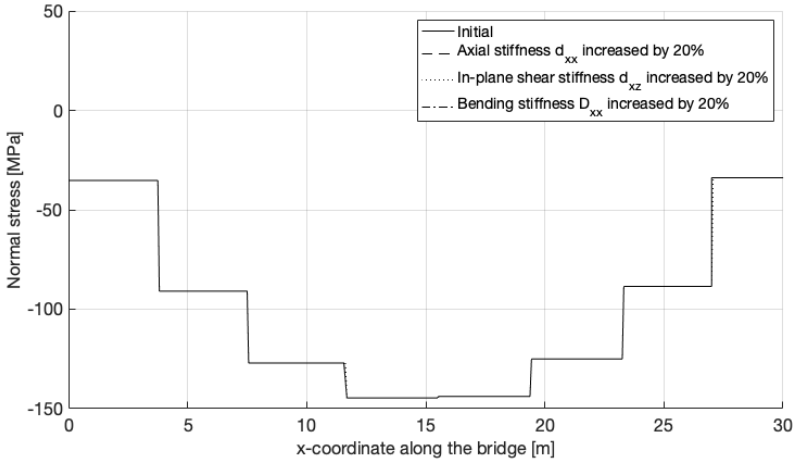

Figure 4.9: Normal stress distribution in the upper chord when the axial stiffness, in-plane shear stiffness, and bending stiffness are increased.

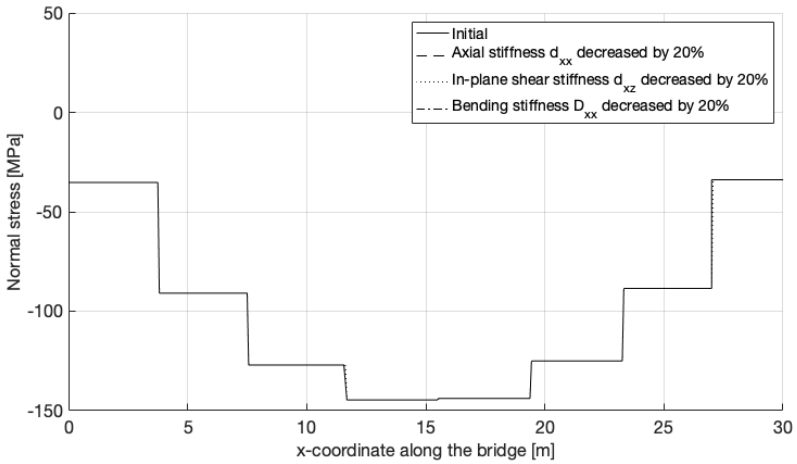

Figure 4.10: Normal stress distribution in the upper chord when the axial stiffness, in-plane shear stiffness, and bending stiffness are decreased.

4.8.2.2 Bridge Deck

Figures 4.11, 4.12, 4.13, and 4.14 show the normal stress distribution across the bridge deck, extracted from Section 4-4. The general trend for all cases is that the normal stresses decreases as the stiffness increases, and correspondingly, the normal stress increases as the stiffness decreases. The effect, however, is marginal in most of the cases. The axial stiffness of the trusses seems to have the largest impact of the normal stress distribution. The normal stress distribution when the in-plane shear stiffness is altered shows a deviant behavior in the bridge deck's middle, where the normal stresses decreases as the in-plane shear stiffness decreases.

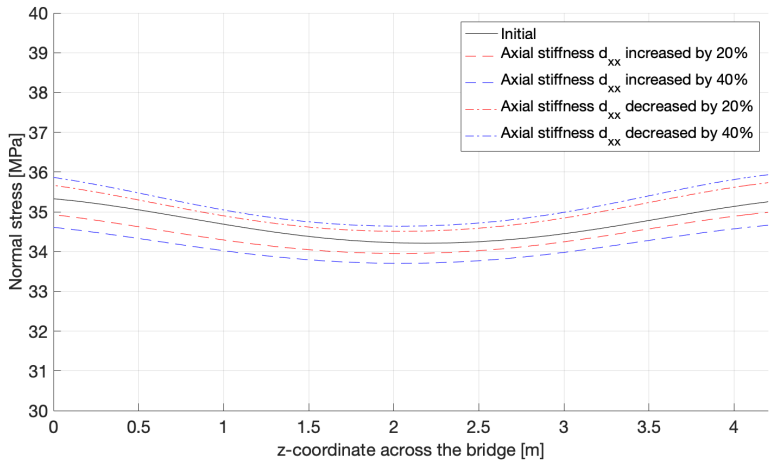

Figure 4.11: Normal stress distribution in the bridge deck when the axial stiffness is altered.

In Figure 4.12 the effect of altering the bridge decks shear stiffness is shown. It can be seen that a difference of 80% results in a modest change in normal stress and that the curve straightens when the shear stiffness is increased.

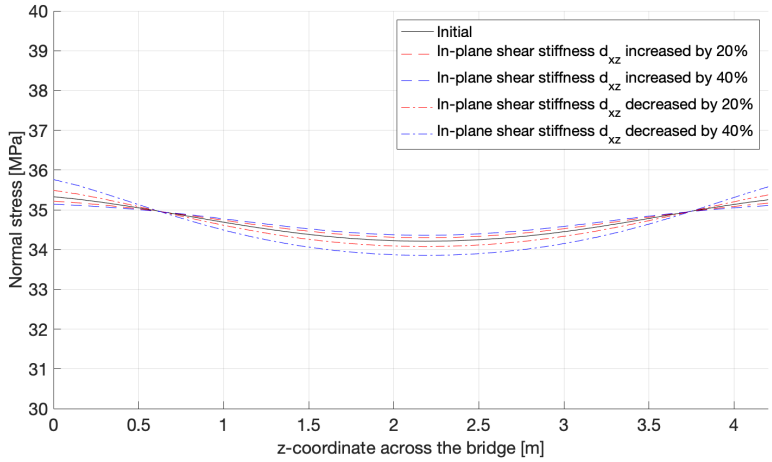

Figure 4.12: Normal stress distribution in the bridge deck when the in-plane shear stiffness is altered.

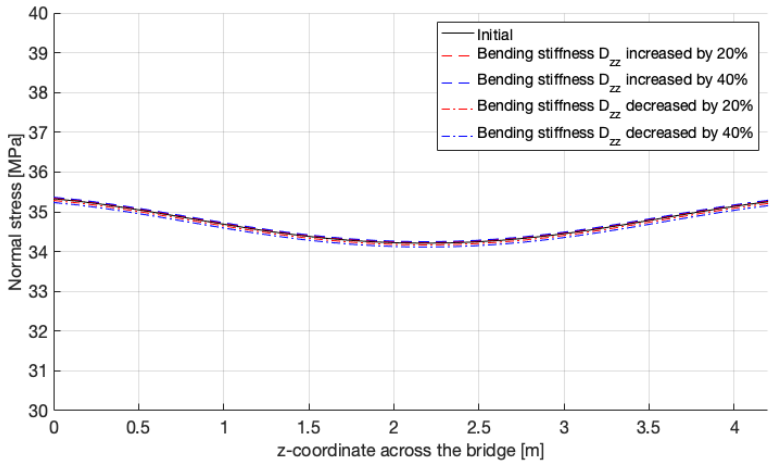

Figure 4.13: Normal stress distribution in the bridge deck when the bending stiffness is altered.

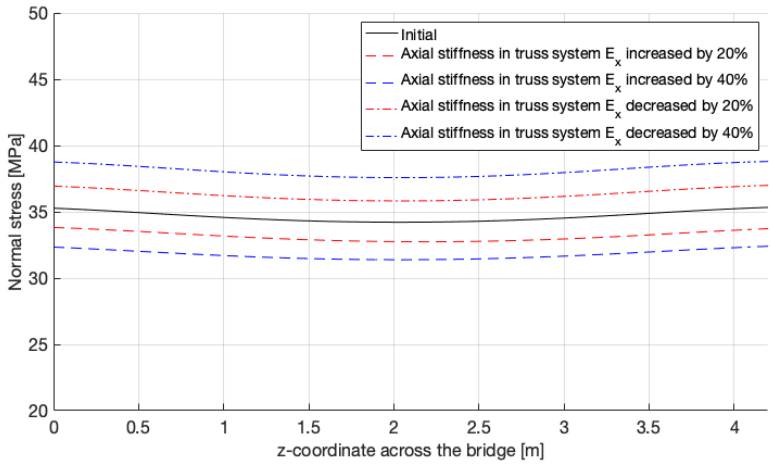

Figure 4.14: Normal stress distribution in the bridge deck when the axial stiffness in the trusses is increased.

4.8.3 Shear Lag

Shear lag causes an uneven normal stress distribution in flanges, which is generally less of a concern in bridges with a SSP because the in-plane shear stiffness is higher. An OSD with an approximate equivalent area has been modeled for comparison to see if the designed bridge deck tends to suffer from shear lag. The stiffness parameters of the OSD can be seen in Appendix C.

Figure 4.15 shows the normal stress distribution across the bridge deck, extracted

from Sections 1-2, 2-2, 3-2, and 4-2, for the sandwich deck and orthotropic deck, respectively. There is a modest difference between the normal stress distribution of each section and as expected the shear lag effect is increasing closer to the support. However, the shear-lag effects are modest and the difference between the two decks is also modest. According to Figure 2.9, a bridge with a low ratio of W/L and E/G, should have negligible shear lag effect.

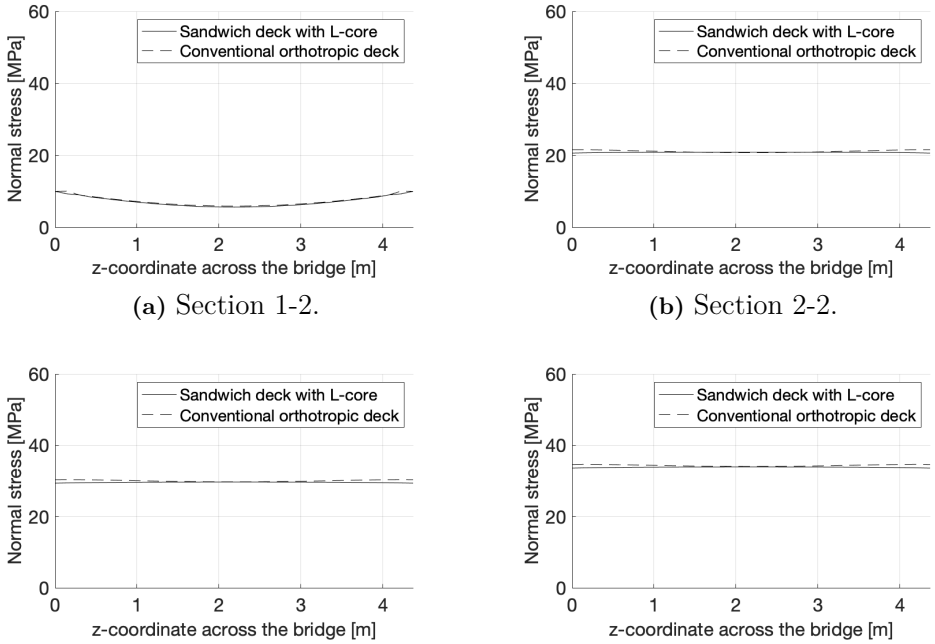

(a) Section 1-2. **(b)** Section 2-2.

(c) Section 3-2. **(d)** Section 4-2.

Figure 4.15: Shear lag effect in sections across the bridge, full bridge length.

The studied bridge is modeled with half of its length to demonstrate how length affects the shear lag effect. The sections of interest are Sections 1-2 and 2-2, which corresponds to 1/4 and 1/2 of the full length span, respectively. The results are shown in Figure 4.16, and it can be seen that a shorter span length results in a increased shear lag effect, although, the effect is modest.

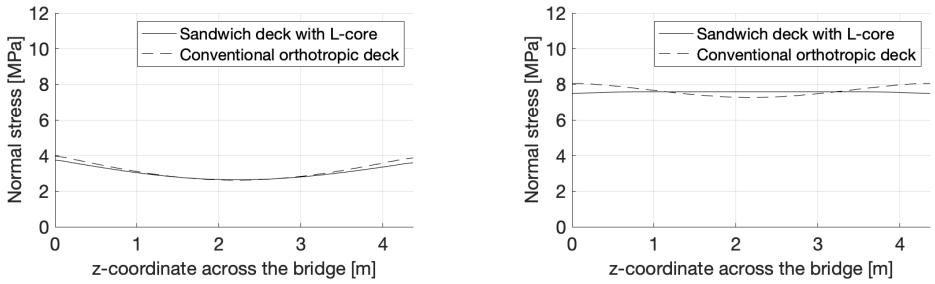

(a) Section 1-2. **(b)** Section 2-2.

Figure 4.16: Shear lag effect in sections across the bridge, half bridge length.

4.8.4 Composite Action Between the Truss System and Bridge Deck

A comparative study was carried out to examine the impact of including the composite action between the bridge deck and truss system. In the case of including composite action, kinematic couplings as described in Section 4.4 are used. In the opposite case, that means excluding the composite action between the bridge deck and truss system; only the truss system is modeled and the uniformly distributed load is transformed into a line load applied to the lower chord of each truss. Figure 4.17 shows the difference between the two models.

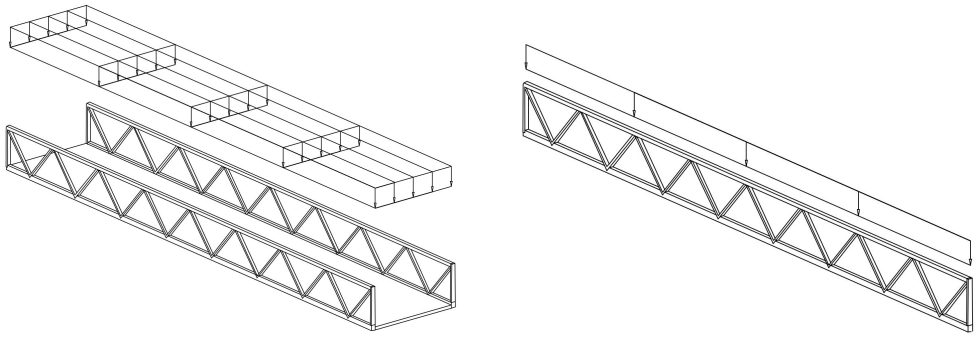

(a) Composite action included. **(b)** Composite action excluded.

Figure 4.17: Models to examine the composite action between truss system and bridge deck.

4.8.4.1 Deflection

Figure 4.18 shows the deflection when composite action is included and excluded, respectively. In both models, the deflection are obtained along the lower chord. Because the load is applied over the length of the bridge, the lines are not smooth

but vary locally along the x-axis. A significant difference can be seen between them, with the greatest difference occurring in the middle of the bridge, which is reasonable given that the deck provides additional bending stiffness to the structure.

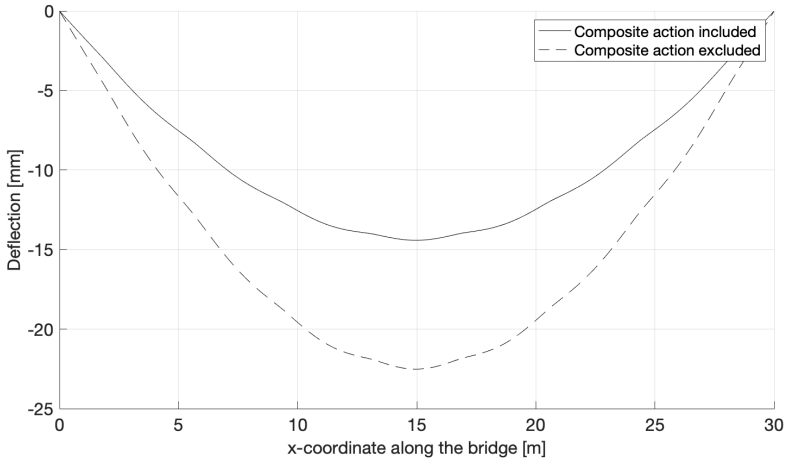

Figure 4.18: Deflection with and without composite action between the bridge deck and truss system.

4.8.4.2 Normal Stresses in Upper Chord

Figure 4.19 shows the normal stresses in the upper chord, including composite action and excluding composite action, over the beam length. In the case of composite action, there is a slight increase in normal stress which is insignificant.

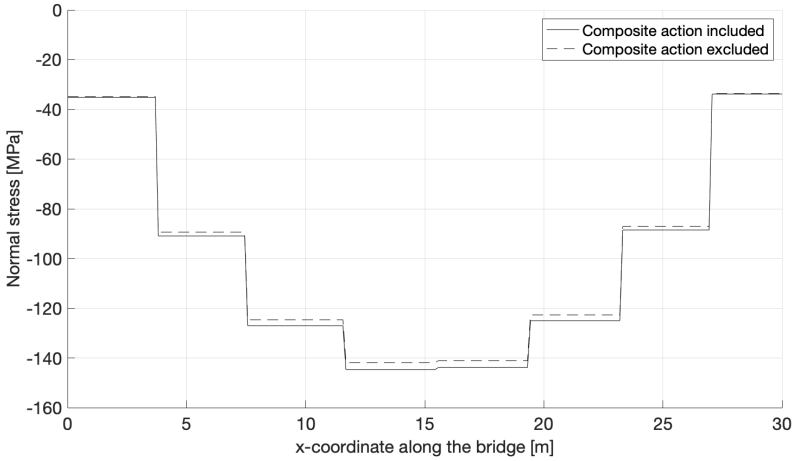

Figure 4.19: Normal stresses in upper chord with and without composite action between the bridge deck and truss system.

4.8.4.3 Normal Stresses in Lower Chord

Figure 4.20 shows the normal stresses in the lower chord, including composite action and excluding composite action, over the bridge length. The normal stress originates from the axial force in the chord. The model excluding composite action has the distribution of normal stresses as the upper chord in Figure 4.19, which is to be expected given normal force the load transfers in discrete points.

However, a different shape can be seen in the model which includes composite action. Instead, the force is distributed along the bridge deck, giving the curved distribution between the truss joints.

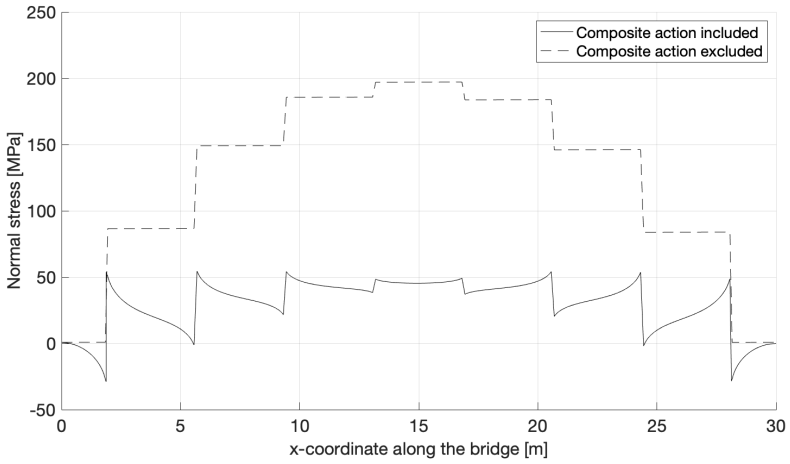

Figure 4.20: Normal stresses in lower chord with and without composite action between the bridge deck and truss system.

4.8.5 Buckling Analysis

The determining failure mode in the design of a pedestrian bridge truss girder is buckling out of the plane of the upper chord. The buckling sensitivity is dependent on the decks stiffness. Three different analyses were carried out, with the following constraints and prerequisites:

1. The lower chord is prevented to translate in the z-direction but free to rotate about the x-axis, shown in Figure 4.21. Half of the uniformly distributed load acts on the lower chord as a line load. This serve as a lower bound.

2. The deck is modeled with composite action between the bridge deck and truss system, with the transversal bending stiffness being the governing factor for how the lower chord behaves in terms of translation and rotation, shown in Figure 4.22. The load is a uniformly distributed load acting on the bridge deck,

described in section 2.5.

3. The lower chord is prevented to both translate in the z-direction and rotate about the x-axis, shown in Figure 4.23. Half of the uniformly distributed load acts on the lower chord as a line load. This serve as a upper bound.

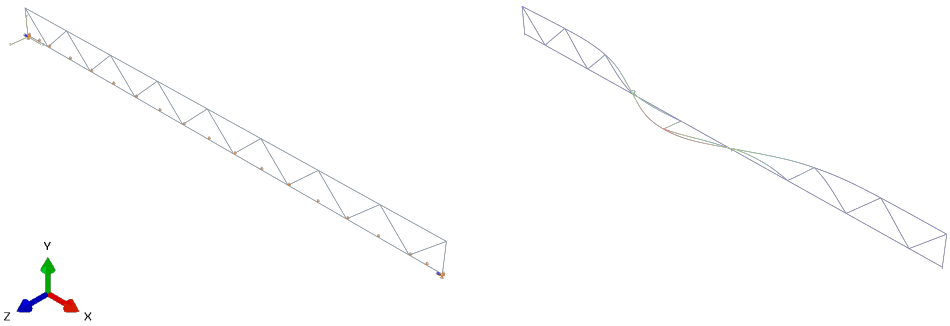

Figure 4.21: Boundary condition and buckling mode for Case 1. Eigenvalue = 3.58.

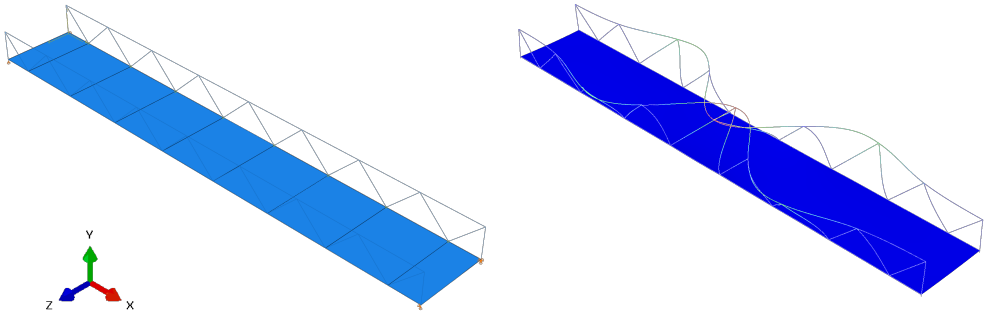

Figure 4.22: Boundary condition and buckling mode for Case 2. Eigenvalue = 4.49.

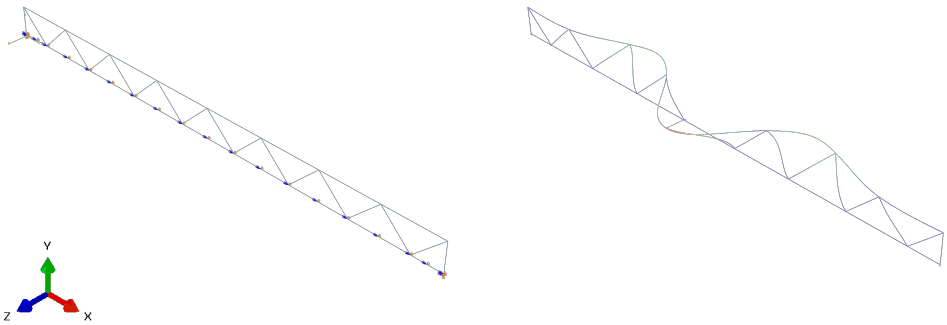

Figure 4.23: Boundary condition and buckling mode for Case 3. Eigenvalue = 4.89.

With the normal force in the upper chord given and the eigenvalues obtained from the linear static and linear buckling analyses, the reduction factors χ are obtained.

Table 4.6 summarizes the final results, where Case 2 is close to the upper bound solution.

Table 4.6: Reduction factor.

Case	Description	Eigenvalue	λ	χ
1	Composite action excluded, UR1 free	3.58	1.091	60.2%
2	Composite action included	4.49	0.966	68.9%
3	Composite action excluded, UR1 prevented	4.89	0.933	71.2%

The bending stiffness in the strong direction is the most important parameter in the deck with regard to buckling in the upper chord. For further study, a deck with approximately twice the bending stiffness of the SSP was modeled to see the effect of that parameter. The buckling mode and eigenvalue of that simulation are shown in Figure 4.24. Thus, a major increase in bending stiffness only gives a modest further increase in normal force capacity of the upper chord.

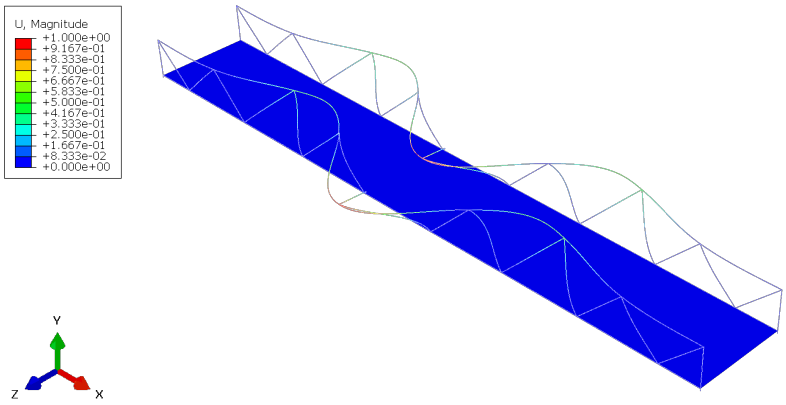

Figure 4.24: Buckling mode when the bending stiffness in transverse direction is increased. Eigenvalue = 4.66.

4.9 Discussion

The purpose of the global analysis was to investigate the structural behavior of the bridge. This was done by changing the stiffness parameters in the deck and studying normal stresses in the bridge deck and longitudinal chords of the truss, and results between a model with and without composite action was compared. Since only the global load effects was studied the bridge could be modeled as an ESL.

The results from the global analysis showed the normal stresses in the deck induced by the loading were low and that altering the bending and shear stiffness had an

insignificant effect on the normal stresses. However, an effect could be seen when the axial stiffness in the longitudinal direction was altered. The modeling of different core configurations was not done in the global analysis. This was justified because of the limited effect altering the stiffness parameters had.

The codependency of the parameters is not taken into account, which means that results that are dependent on the change of two or more parameters will be missed because one parameter is changed at a time and then reverted to the initial condition before changing the next.

Modeling the bridge deck as a two-dimensional equivalent single layer with stiffness parameters as an input to the model gives the ability to easily change the parameters given the geometry. This approach can be beneficial at an early stage and give indications for design improvements. However, the global analysis does not show the effects of locally applied load, i.e., a service vehicle, and thus a local analysis is required to further investigate that behavior.

4.10 Conclusion

To obtain the bridge's structural response subjected to a uniformly distributed load, it was modeled in the finite element program ABAQUS/CAE. To illustrate its composite action as well as showing the influence of altered stiffness parameters and shear lag, two models where established. One that includes the bridge deck and one that excludes the deck and is subjected to half the load. From the results of the studied bridge the following can be concluded:

- The global analysis indicates that altering of bending and shear stiffness in the deck did not have a significant impact on the distribution of normal stresses in the bridge deck. However, a considerable effect could be seen when the axial stiffness in the bridge deck was altered.
- The effect of shear lag was marginal for both a bridge with a SSP and an OSD.
- A study of the composite action between bridge deck and girder indicated that its important to consider composite action, it reduces the stresses and the deflection.
- Composite action gives normal stresses in the deck in the bridge's longitudinal direction, however only of a modest magnitude. Furthermore, in the deck sides, at truss joints, composite action gives rise to additional local forces in the deck that need to be considered.
- Including composite action has no effect on the normal force in the upper chord.

- In the buckling analysis, the degree of rotation of the lower chord was shown to be close to fully fixed for the analysis including interaction.

5

Local Analysis

5.1 Introduction

In the global analysis, the bridge deck was modeled as a shell with elastic stiffness constants. That is a good way to model if the load is distributed and global deformations are to be predicted, but it lacks the ability to predict the stress distribution in the constituent plates of the deck. If the load to be applied is due to local wheel pressure, the correct response is not obtained due to the discrete nature of the steel sandwich panel.

The aim of the local analysis is to examine the local effects due to wheel pressure from a service vehicle. The geometry and cross-sectional parameters are the same as in the global analysis. However, in the local analysis, a part of the bridge deck is modeled as a 3D structure while the rest of the bridge deck is maintained as in the global analysis, which can be seen in Figure 5.1. This approach makes it possible to interpret local stress distributions in the constituent plates of the deck.

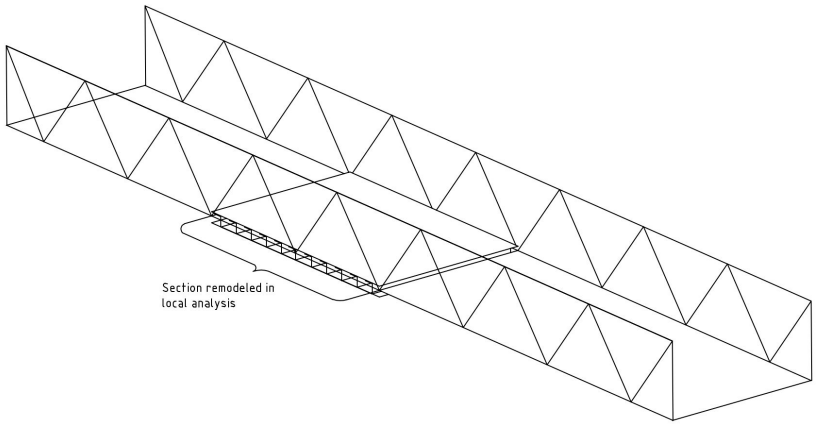

Figure 5.1: Model used in local analysis.

5.2 Load Position

In order to study the effects due to locally applied loads, one of the three static models for vertical loads due to traffic, as described in Section 2.5, is used. The load representing a service vehicle, Q_{serv}, consists of a load axle pair of 80 kN and 40 kN each with a contact area of 0.2 x 0.2 m.

Two load positions have been determined. For both placements in the transverse direction, one of the wheels in the pair is placed in the middle, that is, W/2. The longitudinal placement of the axle loads is thereby separated by the two cases:

(a) The heaviest axle load is placed at a truss joint, which is the connection between the diagonals in the truss system and the bridge deck.

(b) The heaviest axle load is placed in between two truss joints.

The two load positions are illustrated in Figure 5.2 and 5.3, respectively.

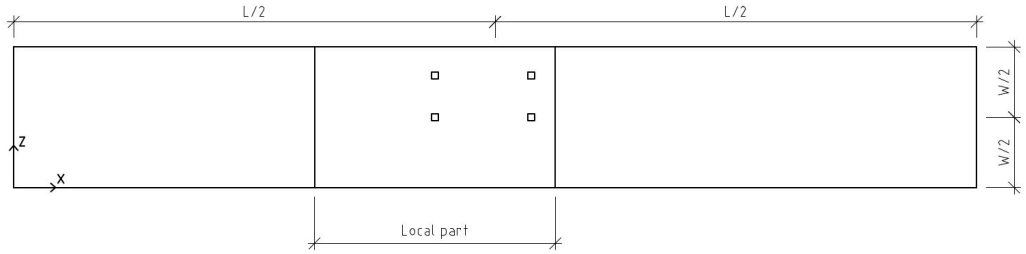

Figure 5.2: The heaviest axle load is placed at a truss joint, load position (a).

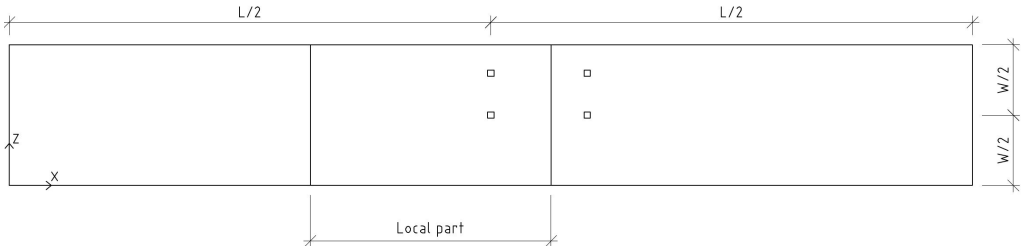

Figure 5.3: The heaviest axle load is placed between two truss joints, load position (b).

5.3 Mesh

The element type used in the local analysis is the same as in the global analysis, which is quadratic elements with quadratic shape functions. To avoid singularities, obtain accurate results, and have a computationally efficient simulation, a denser

mesh was chosen in the parts adjacent to the load, which declined towards the deck with general shell stiffness. Edge divisions on the previously mentioned partitions were made to obtain such a mesh. The chosen mesh sizes can be seen in Table 5.1.

Table 5.1: Mesh size in the constituent members of the bridge.

Element	Edge	Description	Size [mm]
Top plate	X	Mesh size between cores	10
Top plate	X	Mesh size between weld lines	5
Top plate	X	Mesh size on load application area	10
Top/bottom plate Core	Z	Mesh size in the deck	43
Top/bottom plate Core	Z	Mesh size on load application area	30
Bottom plate	X	Mesh size in bottom plate	10
Truss (ESL)	X	Mesh size in truss	50
Truss (3D)	X	Mesh size in truss	5
Bridge deck (ESL)	X	Mesh size in global bridge deck	43
Bridge deck (ESL)	Z	Mesh size in global bridge deck	50

All parts of the system are set up separately and then connected with kinematic couplings.

5.4 Verification of The Model

To verify the model, a convergence study and a comparison of the deflections are performed. The convergence study is performed with respect to the von Mises stress distribution, and the deflections are compared with the results from the global analysis and analytical calculations.

5.4.1 Convergence Study

A convergence study was carried out with regard to the von Mises stress distribution. The convergence study covers the top plate, core, and bottom plate, and the von Mises stresses are obtained from a path directly under the axle loads. The result of the convergence study can be seen in Figure 5.4 where the error from a converged solution is plotted against the total number of elements in the top plate, core, and bottom plate, respectively. The circles represent the chosen mesh size and give an error of less than 1%.

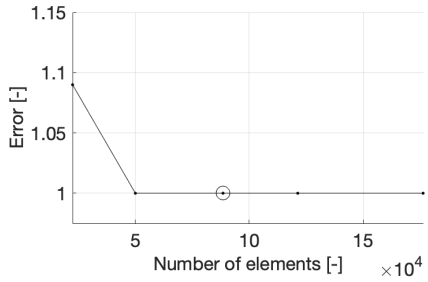

(a) Convergence study for the top plate.

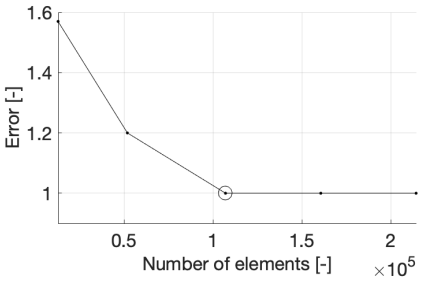

(b) Convergence study for the core.

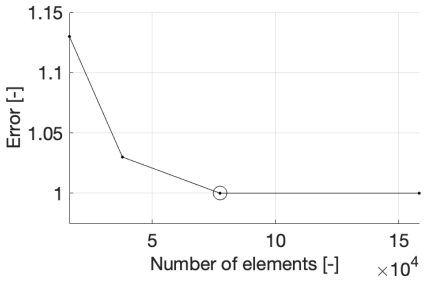

(c) Convergence study for the bottom plate.

Figure 5.4: Convergence study. The circles are representing the chosen mesh size.

5.4.2 Deflection

Figure 5.5 shows the deformed shape and deflection obtained from the finite element analysis, and Table 5.2 presents the maximum values. The biggest difference can be noticed in the longitudinal direction for both the numerical and analytical solutions. A difference between them is expected since the analytical calculation is based on the Euler-Bernoulli theory and, therefore, shear deformations in the truss are not considered.

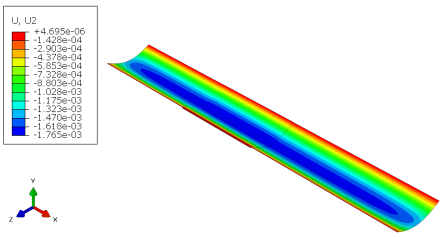

(a) Deformed shape, transversal direction.

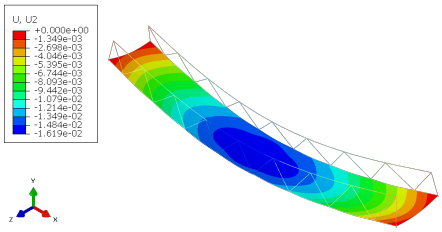

(b) Deformed shape, longitudinal direction.

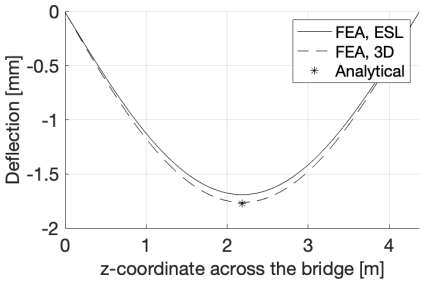

(c) Deflection, transversal direction.

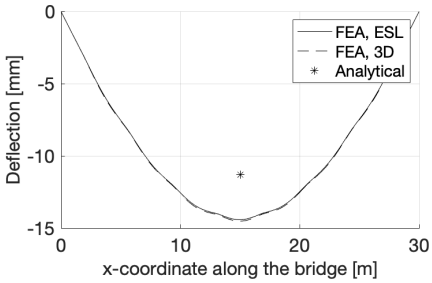

(d) Deflection, longitudinal direction.

Figure 5.5: Deformed shape and deflection in transversal and longitudinal direction of the bridge.

Table 5.2: Comparison of the analytical and numerical solution.

Model	Direction	Analytical [mm]	Numerical [mm]	L/400 [mm]	Difference [%]
Global	Longitudinal	11.3	14.4	75	27.4
	Transversal	1.8	1.7	11	-5.5
Local	Longitudinal	11.3	14.5	75	28.3
	Transversal	1.8	1.8	11	0

5.5 Result from Local Analysis

The results from a linear static analysis of the local model will be presented in this section. The results are presented for the top plate, bottom plate, and core separately. The stresses in the constituent plates of the deck, in the vicinity of the connection between the bridge deck and lower chord, are also investigated and compared to a rotationally constrained condition. Figure 5.6 shows the von Mises stress distribution on the deformed shape of the model, showing the effect of the locally applied wheel pressure.

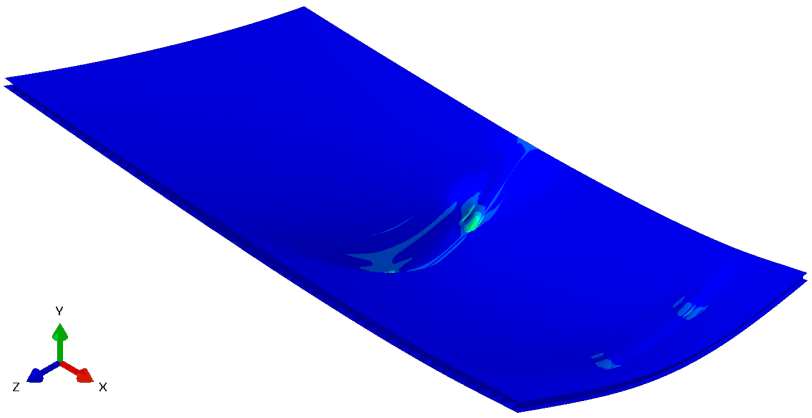

Figure 5.6: Von Mises stress distribution on deformed shape, whole bridge deck modeled in 3D. Scale factor 50.

5.5.1 Stress Distribution in the Top Plate

Figure 5.7 and 5.8 shows the von Mises stress distribution in the top plate plate for load position (a) and (b), respectively, in Pa. The stresses are obtained by extracting the stresses from the top surface of the top plate. The distribution of stresses in the top plate shows high local stress maximums directly under the heaviest axle load. The Von Mises stresses obtained for the top plate can be compared against the yield stress of the material.

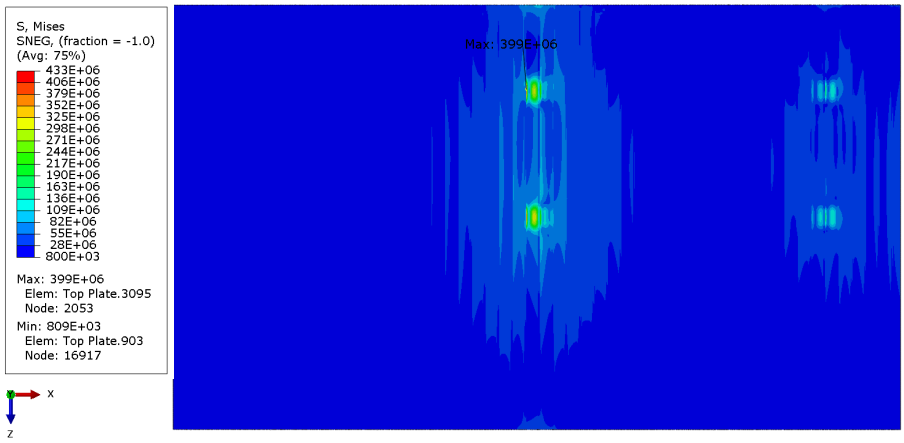

Figure 5.7: Von Mises stress distribution in the top plate for load position (a). Units in Pa.

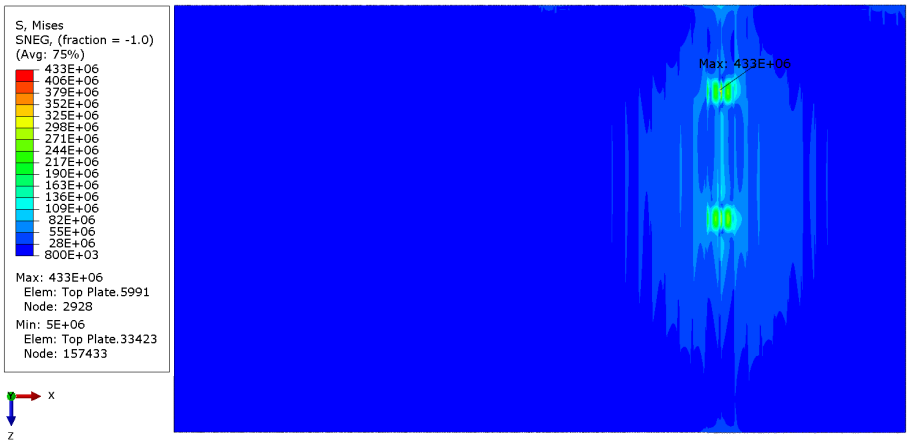

Figure 5.8: Von Mises stress distribution in the top plate for load position (b). Units in Pa.

Figure 5.9 and 5.10 show the normal stress distribution in a longitudinal and transversal direction in the top plate, respectively, caused by local bending. The stresses are extracted from the top surface of the top plate. The distribution of normal stresses in the longitudinal direction is shown in figures 5.9(a) and 5.10(a), where the maximum compressive stresses in the plate arise between the core stiffeners and the maximum tensile stresses arise in the adjacent area of the core-to-face joint. Figures 5.9(b) and 5.10(b) show the distribution of normal stresses in the transverse direction, where the maximum compressive stresses occur, but with a slightly smaller magnitude, in the above-mentioned location. The tensile stresses in the adjacent area of the core-to-face joint, however, are negligible. Instead, the maximum tensile stresses in the transverse direction arise at the edges of the bridge deck, where the deck is connected to the lower chord acting as support.

However, the distribution of normal stresses varies depending on whether the wheel is placed directly above a core stiffener or in between the core stiffeners. In the studied case, the maximum compressive stress in the longitudinal direction was found when the center line of the heaviest axle load was placed in between two core stiffeners, as seen in Figure 5.9. Similarly, the maximum tensile stress in the longitudinal direction was found when the center line of the heaviest axle load was placed directly above a core stiffener, as seen in 5.10.

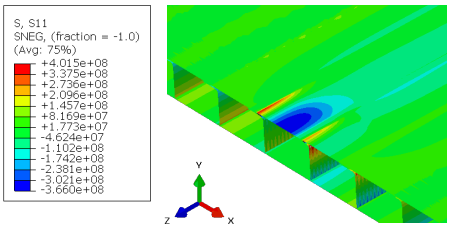

(a) Normal stresses in the longitudinal direction.

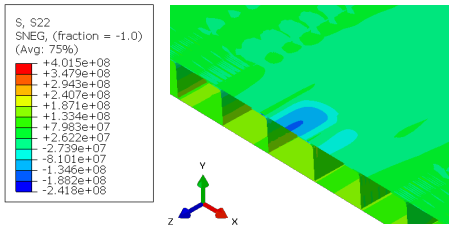

(b) Normal stresses in the transversal direction.

Figure 5.9: Normal stress distribution in the top plate, heaviest axle load placed between the core stiffeners.

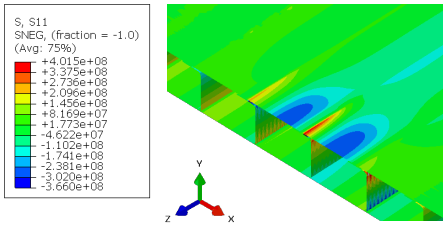

(a) Normal stresses in the longitudinal direction.

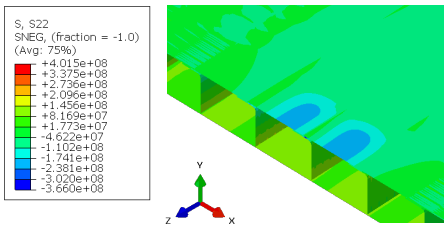

(b) Normal stresses in the transversal direction.

Figure 5.10: Normal stress distribution in the top plate, heaviest axle load placed directly above a core stiffener.

Figure 5.11 shows the distribution of normal stresses in the longitudinal direction of the top plate, directly above a core stiffener, corresponding to the two wheel placements previously described. The tensile stresses in the adjacent area of the core-to-face joint, shown as the red area in Figures 5.9 and 5.10, can be seen as the peak value in the figure. The zero point refers to the center line of the core and the core-to-face connections seen to the left refer to the two weld lines.

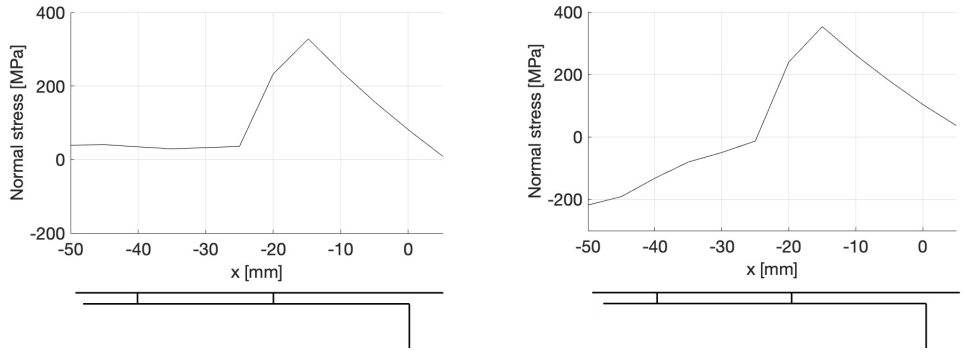

(a) The wheel is placed in between the core stiffeners.

(b) The wheel is placed directly above a core stiffener.

Figure 5.11: Normal stress distribution in the top plate, directly above the core stiffener.

Figure 5.12 shows the distribution of normal stresses in the longitudinal direction of the top plate over several core stiffeners when the wheel is placed in between the core stiffeners and when the wheel is placed directly above a core stiffener, respectively. The solid lines represent when both the displacement and rotational degrees of freedom in the kinematic coupling between the core and facing plates are constrained, corresponding to a fully rigid weld region, and the dashed lines represent when only the displacement degrees of freedom in the kinematic coupling are constrained, corresponding to a hinged connection. The actual behavior is somewhere in between a rigid and hinged connection.

As previously mentioned, the tensile stresses in the top fiber of the top plate in the adjacent area of the core-to-face joint, shown as the red area in 5.9 and 5.10, can be seen as the local maximums in Figure 5.12. The compressive stresses in the top fiber of the top plate can be seen as the local minimums, seen as the blue area in Figure 5.9 and 5.10. The compressive stresses are slightly larger when the wheel load is placed in between the core stiffeners, but the tensile stresses are almost the same regardless of how the load is related to the core stiffeners. The difference between constraining the rotational degrees of freedom or not does not have a significant impact on the normal stress distribution in the top plate. However, the weld stiffness is likely to have an impact on the stress in the weld itself, if this is to be predicted.

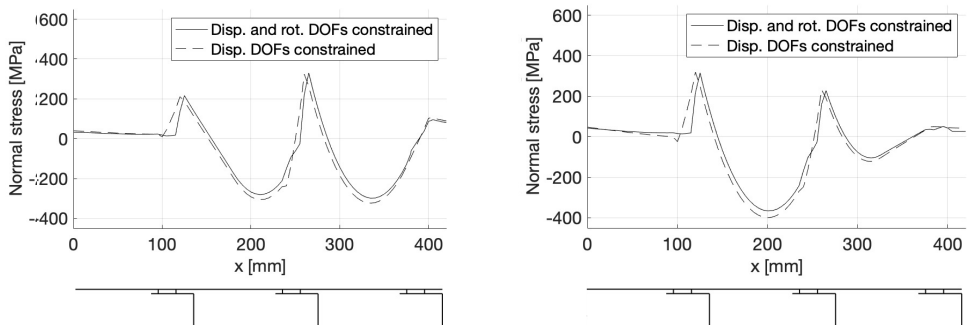

(a) The wheel is placed in between the core stiffeners.

(b) The wheel is placed directly above a core stiffener.

Figure 5.12: Normal stress distribution in the top plate, over several stiffeners.

5.5.2 Stress Distribution in the Bottom Plate

Figure 5.13 and 5.14 shows the von Mises stress distribution in the bottom plate for load position (a) and (b), respectively, in Pa. The stresses are obtained by extracting the stresses from the bottom surface of the bottom plate. The distribution of stresses in the bottom plate shows high local stress maximums directly under the heaviest axle load, but not as significant or high as the stresses obtained for the top plate as they are transferred through the core and distributed over a larger area. The maximum von Mises stresses are obtained at the edges of the bridge deck, where the deck is connected to the lower chord. The von Mises stresses obtained for the bottom plate can be compared against the yield stress of the material.

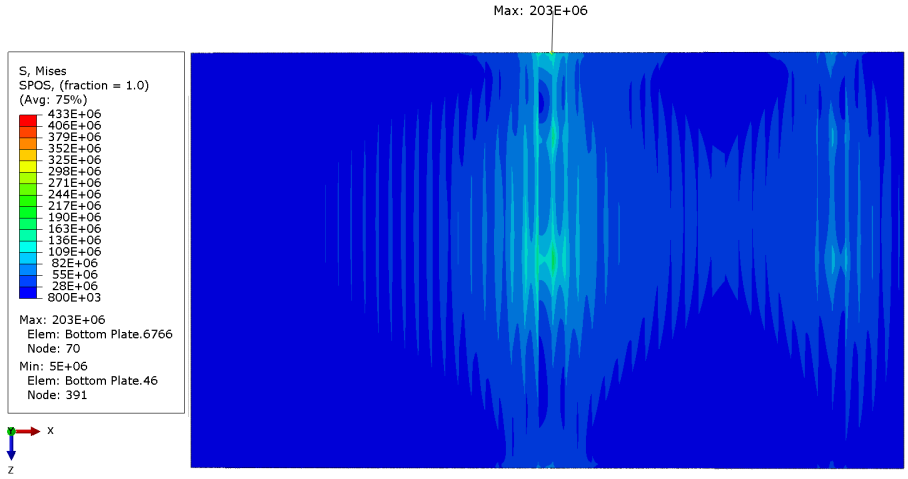

Figure 5.13: Von Mises stress distribution in the bottom plate for load position (a). Units in Pa.

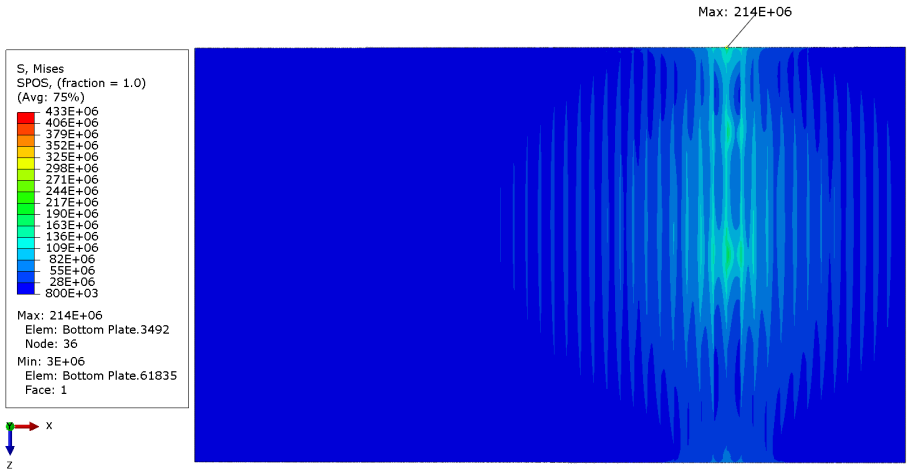

Figure 5.14: Von Mises stress distribution in the bottom plate for load position (b). Units in Pa.

5.5.3 Stress Distribution in the Core

Figure 5.15 shows the von Mises stress distribution on the deformed shape of the model. High local bending stresses caused by the wheel loads can be observed mainly in the longitudinal direction of the core. The stresses in the core are significantly higher than those in the facing plates.

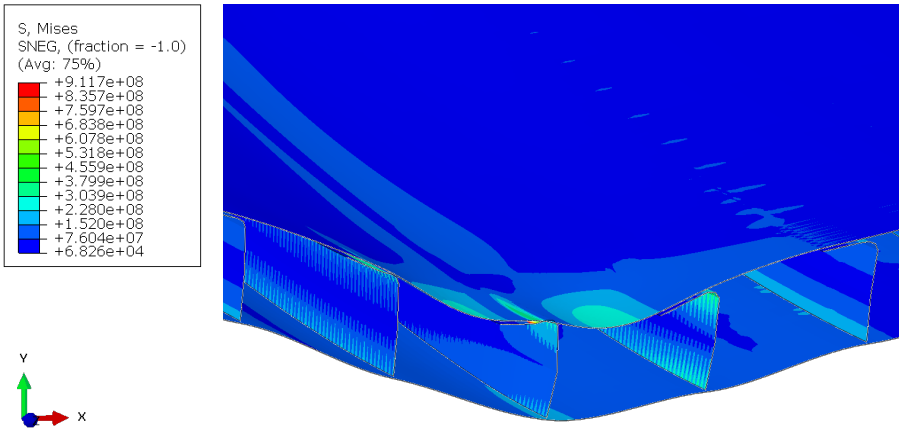

Figure 5.15: Von Mises stress distribution on deformed shape, local deformation under wheel pressure. Units in Pa.

Figures 5.16 and 5.17 show the distribution of normal stresses in longitudinal and transversal directions, respectively, where the locally applied wheel load is shown. Exceptional high compressive stresses in the longitudinal direction can be seen in the flanges of the core adjacent to the core-to-face connection, directly under the wheel load. Similarly, high tensile stresses can be seen in the same region but in the vertical part of the core. Except in the area in which the wheel loads are applied, the stresses in the core are low.

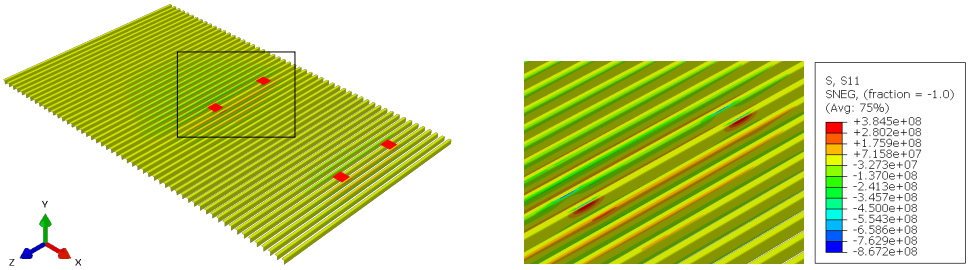

(a) Stress distribution and position of axle loads.

(b) Stress distribution in the deck at the heaviest wheel axle load.

Figure 5.16: Distribution of normal stresses in longitudinal direction.

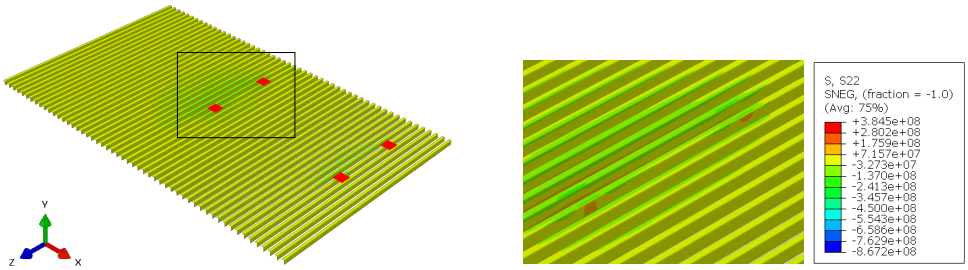

(a) Stress distribution and position of axle loads.

(b) Stress distribution in the deck at the heaviest wheel axle load.

Figure 5.17: Distribution of normal stresses in transverse direction.

The model that is used in the analysis does not consider contact between the core and facing plates, and thus, a significant positive influence of the stresses that arise from the locally applied wheel pressure and the lever arm between the vertical plates and welds is excluded. However, the analysis indicates that contact between the core and facing plates and vast modeling of the welding region is of great importance for the stress magnitudes in the constituent plates of the deck, especially in the core.

5.5.4 Degree of Constraint

In order to show the degree of constraint the bottom chord puts on the bridge deck, a section adjacent to the truss girder in the 3D part of the SSP in the model has been analyzed. Figure 5.18 shows the location of interest, a path in the longitudinal direction of the bridge adjacent to the lower chord, where membrane forces have been extracted.

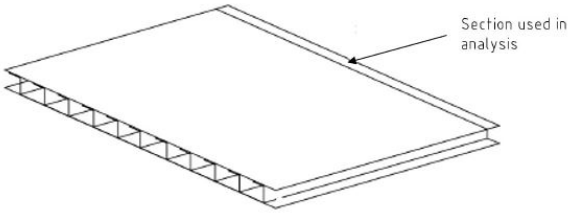

Figure 5.18: Section used to analyze the degree of constraint.

Figure 5.19 shows the stress distribution in the top and bottom plates along the previously described path. The highest magnitude is due to the heaviest axle load of 80 kN, and the lower peak is due to the lower axle load of 40 kN. The load is placed according to load position (a).

It can be noted that the compressive stresses in the transversal direction in the

bottom plate are slightly higher than the tensile stresses in the transversal direction in the top plate due to the distance from the neutral axis and the thickness of the plate. The solid lines represent the real case when the plate is attached to the lower chord. The lower chord is here free to rotate about its own axis. The dashed lines represent a case when the lower chord is prevented from rotating about its own axis and thus captures a rotational constraint behavior. The maximum compressive and tensile stresses for load position (a) are presented in Table 5.3.

Table 5.3: Stresses in top and bottom plate for load position (a).

Load position	Part	Lower chord	Stress [MPa]
(a)	Top plate	Free to rotate	62.4
		Prevented to rotate	89.4
(a)	Bottom plate	Free to rotate	-94.5
		Prevented to rotate	-140.4

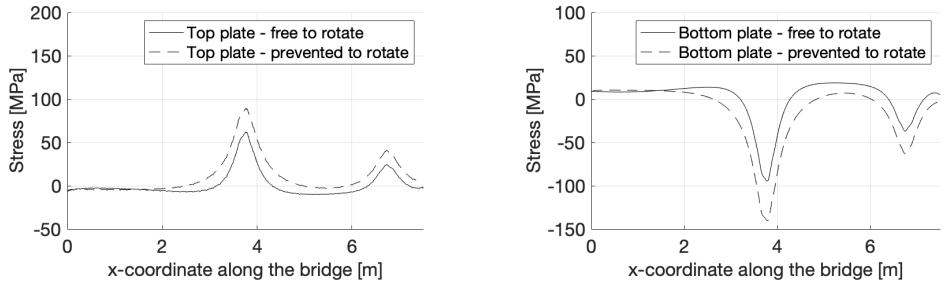

(a) Tensile stresses in top plate.

(b) Compressive stresses in bottom plate.

Figure 5.19: Stresses in top and bottom plate, load position (a).

Figure 5.20 shows the stress distribution in the top and bottom plates along the path described in Figure 5.18. The peak is due to the heaviest axle load of 80 kN and the other axle load is outside the limits of the plate modeled in 3D. The load is placed according to load position (b).

The maximum compressive and tensile stresses for load position (b) are presented in Table 5.4. The stresses obtained from placing the load according to load position (b) give slightly lower results than for load position (a). Since the axle load is placed close to a truss joint in load position (a), this gives a higher degree of constraint.

Table 5.4: Stresses in top and bottom plate for load position (b).

Load position	Part	Lower chord	Stress [MPa]
(b)	Top plate	Free to rotate	53.2
		Prevented to rotate	85.5
(b)	Bottom plate	Free to rotate	-83.8
		Prevented to rotate	-135.6

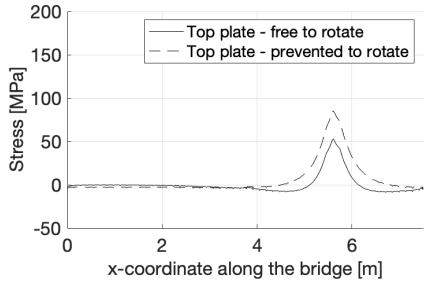

(a) Tensile stresses in top plate.

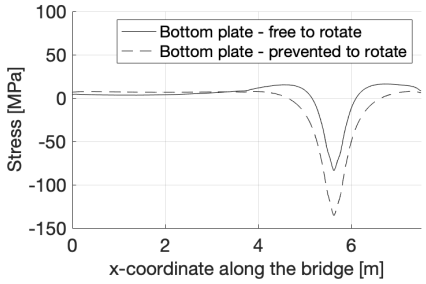

(b) Compressive stresses in bottom plate.

Figure 5.20: Stresses in top and bottom plate, load position (b).

The degree of fixation can thus be obtained by the ratio between the free and fixed conditions and is presented in Table 5.5 in terms of bending moment. The highest degree of fixation is obtained for load position (a) at 70% and the lowest is obtained for load position (b) at 62%.

Table 5.5: Bending moments and degree of contraint in the deck edge for load position (a) and (b).

Load position	Lower chord	Bending moment (in bridge deck) [kNm/m]	Degree of constraint [%]
(a)	Free to rotate	38.4	69.8
	Prevented to rotate	55.1	
(b)	Free to rotate	32.8	62.2
	Prevented to rotate	52.7	

There is a noticeable difference between the maximum stress level for load positions (a) and (b). In general, higher stresses occur when the load is placed in position (a). The truss joints are stiffening the lower chord in that region and thus attract more load, resulting in higher stresses.

5.6 Discussion

The purpose of the local analysis was to investigate the response of the bridge deck due to the effects of locally applied load. In order to keep the analysis time short, only parts of the bridge deck were modeled as a 3D shell structure, while the rest was kept as an ESL. The deflection verification and comparisons to the previously developed ESL model validated this model.

The local analysis showed local stress maximums in the core, especially in the adjacent area of the core-to-face connection. High stresses were also observed in the top plate, directly under the applied wheel load. The local bending stresses in the longitudinal direction of the core were remarkably high as a result of not including contact between the core and top plate in the analysis. The stress is thought to decrease when contact is included. In general, including contact in the analysis is considered favorable but needs to be verified to account for it.

When both the displacement and rotational degrees of freedom in the kinematic coupling are constrained, the behavior corresponds to a fully rigid weld region. In the other case, if only the displacement degrees of freedom in the kinematic coupling are constrained, the behavior corresponds to a hinged connection. When the SSP deforms due to the directly applied load, the rotational angles between the facing and core plates will diverge, which means that the weld region is not rigid. To capture the real behavior, a rotational spring that accounts for the weld region rotational stiffness should have been used instead.

The location of the wheel loads is important to consider for further analysis, and a more thorough investigation of the worst load case is necessary by taking into account the most unfavorable load case by examining the longitudinal and transverse position of the wheel loads. A study example demonstrated that wheel placement in relation to the core stiffeners is also an important factor to consider.

However, the stress magnitudes indicate that the effects due to local action are more critical than global action. Except for the locally concentrated stresses, the analysis showed that the degree of utilization in the remaining parts is relatively low.

Plate buckling in the lower plate between the stiffeners in the transversal direction can be determining in the design. However, in this specific case, part of the plate was in cross-section class three and no further studies have been conducted regarding buckling.

The results are based on the geometry of an existing bridge with one core configuration. In order to get a more comprehensive view of different core configurations and geometries and their impact on the bridge response, several configurations and different geometries could have been modeled. However, this study was a starting point,

which gives indications and a direction for further improvement and optimization.

5.7 Conclusion

To investigate the bridge's structural response subjected to locally applied wheel pressure, it was modeled in the finite element program ABAQUS/CAE. To show the stresses in the constituent plates of the bridge deck, the middle section was remodeled from an ESL to a 3D structure with shell elements. From the results of the studied bridge, the following can be concluded:

- The stress magnitudes from the locally applied wheel pressure are significantly larger than the stress magnitudes from a distributed load, especially in the core and top plate.
- The degree of rotation neither corresponded to a simply supported or fixed condition, where the first is used to calculate maximum deflections in the transversal direction and the latter is used to calculate stresses at the boundaries, respectively. The degree of constraint rather corresponded to a value between the extremes, approximately 60-70%.
- The weld rotational stiffness does not have a significant impact on the stress magnitudes in the bridge deck and its constituent plates.

6

Production and material

In the previous chapters, the structural respone of a bridge with a sandwich panel has been studied. This chapter will focus on the SSPs feasibility regarding production and investment economies. The result of this will be compared to a conventional deck.

6.1 Steel Sandwich Panel with V-Core

The V-core with flanges is determined to be the most interesting core configuration for further investigation regarding production and material due to the possibility of optimizing the design with little restriction in production.

6.1.1 Design

The design of the studied V-core is illustrated in Figure 6.1. Since the structural response of the V-core has not been investigated, emphasis has been put on obtaining a design similar to the L-core. Due to the additional contact point in each unit of the V-core, the number of stiffeners is halved in comparison to the L-core.

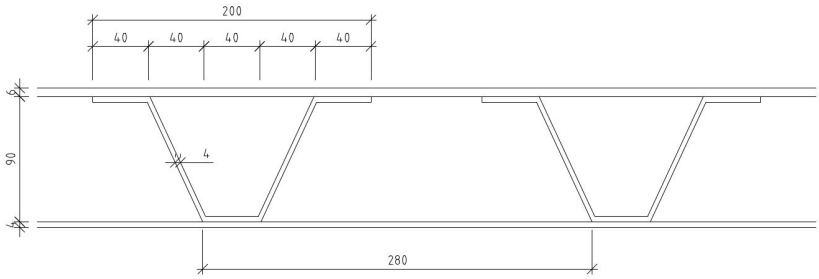

Figure 6.1: Design of the V-core used in the sandwich panel. Dimensions in mm

An illustration of the comparison between a V-and L-core can be seen in Figure 6.2 where the height and plate thickness are kept the same and thus the resulting cross-sectional areas are comparable.

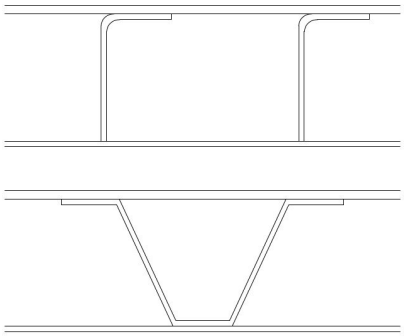

Figure 6.2: Comparison between a L-and V-core configuration.

6.1.2 Production

In the assembly of the bridge deck, the core is welded to the face plates. This is preferably done with stake welds since the accessibility is not restricted. Two weld lines are advantageous at each contact point to get a sufficiently strong connection, which results in six weld lines for each core unit. A reasonable production sequence for a SSP with a V-core can be seen in Figure 6.3 and are summarized as follows:

1. The face plates and the core profiles are purchased by an external manufacturer and delivered to the workshop in the correct lengths, widths, and profiles. Alternatively, this step can be performed directly in the workshop.

2. The top plate is placed in the manufacturing area and the core profiles are placed upside-down at the right positions using robotics, i.e., the side with the two flanges is turned downwards.

3. A proper clamping system is used to ensure contact between the core profiles and the top plate and to avoid weld distortions, and spot welding is performed to keep the components in place.

4. Laser welding with two stake welds at each contact point is performed, i.e., four weld lines per core unit. The laser welds are performed in a continuous manner from one side of the panel to another.

5. The bottom plate is placed on the assembled parts in the right position using robotics.

6. Laser welding is performed from the outer surface of the bottom plate with two stake welds per core unit.

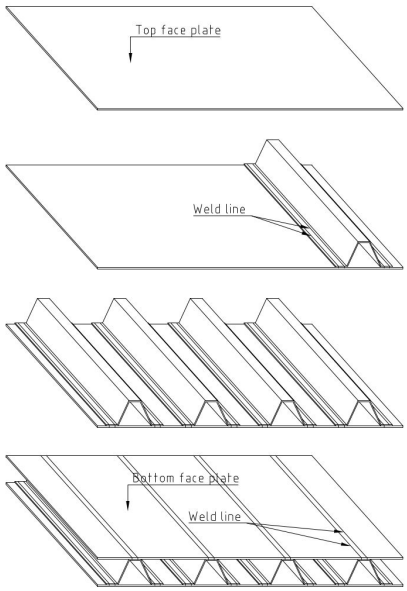

Figure 6.3: Production procedure for the sandwich panel with V-core. Spot welding and joint between core and lower chord is excluded.

The connection between the lower chord and the bridge deck is preferably performed with hybrid laser arc welding at the workshop. The connection is illustrated in Figure 6.4 and shows the weld between the core and lower chord and the longitudinal weld between the upper face plates and lower chord, respectively. The weld between the lower plate and the lower chord is not illustrated but will be the same as the weld between the upper plate and the lower chord. If accessibility is restricted, gas metal arc welding might be needed between the core and lower chord. If there are restrictions on the width of the completed bridge deck with regard to transportation, the connection between the SSP and lower chord may need to be welded on the construction site.

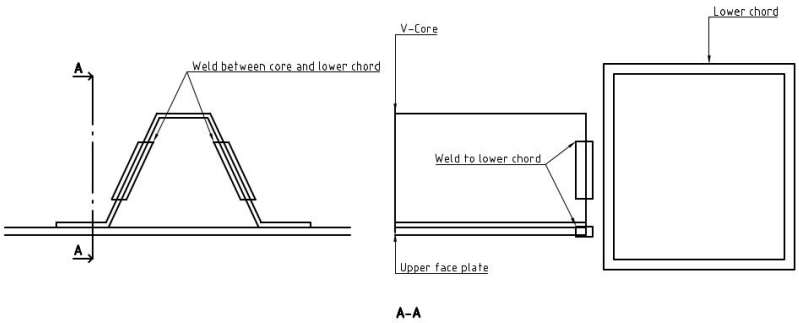

Figure 6.4: Weld required for the connection between the lower chord and bridge deck.

6.1.3 Material

In Table 6.1 the amount of material required for the bridge can be seen. The deck's dimensions are the same as those used in the structural analysis, with a length of 30 m and a width of 4.37 m. It can be noted that the weight per unit area for the V-core is approximately the same as for bridge type 3, as seen in Table 3.1.

Table 6.1: Material consumption for the V-core.

Length [m]	Width [m]	Total weight [ton]	Weight per unit area [kg/m^2]
30	4.37	14.8	108.7

6.1.4 Welding

As the bridge is 30 m long, it can be manufactured in one piece, which is advantageous as several SSPs do not have to be welded together longitudinally with connecting elements. This means that only stake welds are needed to connect the core to the face plates. The resulting time can be obtained by multiplying the total weld line length with the welding speed from the laser. In conversation with a manufacturer, a welding speed of 3.5–4 m/min can be assumed for stake welds through a 4 mm plate. According to the manufacturer, active welding accounts for 40–50% of total production time. With these parameters, the extremes of the total production time can be estimated, which is presented in Table 6.2.

Table 6.2: Production time for the V-core.

Case	Nr. weld lines	Weld line [m]	Stake weld time [h]	Assembly, spot weld and etc [h]	Total time [h]
(1) 3.5 m/min, 40% production	648	2831.8	13.48	20.23	33.7
(2) 4 m/min, 50% production	648	2831.8	11.80	11.80	23.6

6.2 Conventional Orthotropic Steel Deck

As shown in Chapter 3, an OSD with trapezoidal stiffeners in the transversal direction is common for pedestrian bridge applications and will serve as a comparison to the SSP with a V-core.

6.2.1 Production

An OSD is manufactured by welding the stiffeners to the deck plate. To obtain a sufficiently strong connection, several weld passes may be needed. Since gas metal arc welding is used to connect the stiffeners, the stiffeners must be at a certain distance to fit the welding head. Because of the length of the bridge, several OSDs must be connected to obtain the complete deck. This can be done with a v-joint between the plates. After assembling the plate, it is connected to the lower chord by welding around the stiffeners and between the plate and the lower chord.

6.2.2 Design

The design of the studied bridge deck is illustrated in Figure 6.5 and has been used for the evaluation in this section. In comparison to the SSP, the stiffeners of the OSD are placed at a larger center-to-center distance, and in order to manage the locally applied load from a service vehicle, a significantly thicker face plate is required. The cross-sectional height is also greater in order to get a sufficiently high bending stiffness in the transverse direction.

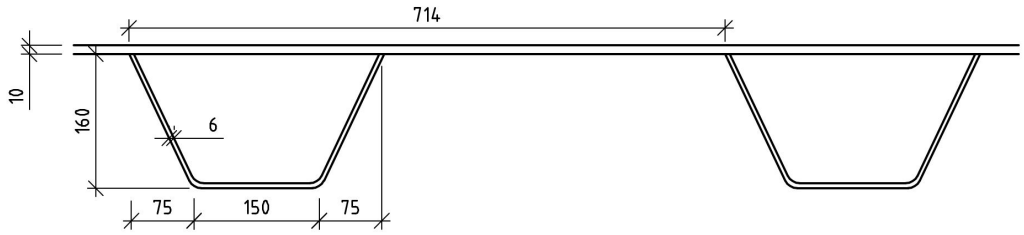

Figure 6.5: Design of the orthotropic steel deck. Dimensions in mm.

6.2.3 Material

In Table 6.3 the amount of material required for the bridge deck can be seen. It can be noted that the weight per unit area for the OSD is significantly larger than the mean value for the deck type 3, Table 3.1.

Table 6.3: Material consumption for the orthotropic steel deck.

Length [m]	Width [m]	Total weight [ton]	Weight per unit area [kg/m^2]
30	4.37	16.9	127.1

6.2.4 Welding

The welding required for the previously described deck can be seen in Table 6.4. Both welding between the core and face plate as well as longitudinally between the

panels is accounted for.

Table 6.4: Time for the welding procedure in the orthotropic steel deck.

	Nr. joints	Weld length [m]	Single weld line [m]	Weld time [h]	Assembly [h]	Total time [h]
Butt weld	10	44	352	6	20	26
Edge Preparation	10	44		22		22
Weld stiffeners	86	378	1514	25	43	68
						116

6.3 Prerequisites

Since the production of a SSP is relatively new, production lines as in conventional production do not exist. Prototypes have been built, but the cost of production exceeds that of conventional decks because production equipment, such as clamping systems, must be purchased. This complicates a cost comparison between the decks since the initial cost of equipment is not distributed over many sandwich panels. To allow for a comparison of the decks, the following prerequisites are assumed:

1. Welds to the lower chord are neglected.
2. A steel price of 20 kr/kg and a coating cost of 900 kr/m^2 is assumed.
3. The rest scrap from deck production is set at 10% for both designs.

6.4 Comparison

The aim of this comparison is to compare material cost, coating cost, and time during welding to highlight the potential of the SSP. In Table 6.5 the time needed to manufacture a conventional deck is shown. It can be seen that it takes 200 hours to complete and that production, edge preparation, and welding make up for approximately 40–60% of the time, respectively.

Table 6.5: Cost and time calculation for the orthotropic steel deck.

	Time [h]	Time [%]
Production		
Cutting	57.3	28.3
Folding	28.8	14.2
Edge preparation and welding		
Butt weld face plate (V-joint)	25.9	12.8
Edge preparation	22	10.9
Weld trapezoidal stiffener	68.2	33.7
Total	202.2	

In Table 6.6 the total time required to weld and assemble the designed SSP and OSD is summarized. It can be seen that the difference between the weld speeds for the SSP is significant, with approximately 10 hours between the optimum and conservative situation. The largest difference is, however, seen between the OSD and the SSP, where the time can be reduced by 70–80% if the welding procedure for the SSP is used. The cost of the welding procedure in a conventional OSD has been calculated to 64 KSEK. The hourly cost for the OSD during welding could then be approximated at 550 SEK/h. If the time of welding in the OSD were replaced with the SSPs time, the hourly cost would be 1892 SEK/hour for case (1) and 2703 SEK/hour for case (2).

Table 6.6: Comparison of time for the welding procedure.

Deck	Sandwich deck (1)	Sandwich deck (2)	Orthotropic steel deck
Time [h]	33.7	23.6	116.1

The material required for the SSP and OSD can be seen in Tables 6.7 and 6.8, respectively. It can be seen in the OSD that both the material used in the face plate as well as in the core is larger than in the SSP. It can also be noted that a smaller portion of the steel is in the core for the OSD, which is reasonable due to the thick face plate. Because of the design of the V-core, it can be seen that material savings of approximately 56 KSEK can be made.

Table 6.7: Cost calculation for the material in the sandwich panel.

Construction element	Nominal amount [ton]	Factor rest products	Rest products [ton]	Mass [ton]	[%]
Upper face plate	6.2	1.1	0.6	6.8	41.6
Lower face plate	4.1	1.1	0.4	4.5	27.8
Core	4.5	1.1	0.5	5.0	30.6
Total			1.5	16.3	
Cost				326.4	KSEK

Table 6.8: Cost calculation for the material in the orthotropic steel deck.

Construction element	Nominal amount [ton]	Factor rest products	Rest products [ton]	Mass [ton]	[%]
Face plate	12.4	1.1	1.2	13.7	71.7
Core	4.5	1.1	0.9	5.4	28.3
Total			2.1	19.1	
Cost				382.0	KSEK

The parts exposed to air in a bridge must have a treated surface. For a steel bridge deck, this only involves the underside surface as the top face plate is covered by pavement and the sides are covered by the lower chord. Table 6.9 shows the area needed for each case as well as the resulting cost. It can be seen that the cost will be higher for the OSD than for the SSP. This is reasonable since the underside of the SSP is a flat surface in comparison to the uneven surface of the OSD due to the stiffeners, resulting in a larger area.

Table 6.9: Coating area and cost for the sandwich panel with V-core and the orthotropic steel deck.

Deck	Orthotropic	Steel sandwich with V-core
Area [m^2]	166	131
Cost [KSEK]	150	118

6.5 Discussion

The results from the comparison showed that significant material savings could be made. However, only one deck design was investigated for each case, and the weight

per unit area of the OSD was high in comparison to other bridges in the study. Also, the structural response of the SSP with a V-core was not investigated.

In Table 6.5, it can be seen that the time spent on manufacturing an OSD is divided into the manufacture of the parts (43%) and assembly (57%). In the comparison, it was shown that time could be saved in the welding procedure if it was fully automated as for SSPs. The reduction in time due to automation was 71–80% and probably a similar comparison could have been made for the manufacturing of parts in the production if it was also automated. But this was not addressed in this comparison.

6.6 Conclusion

The aim regarding production was to conduct a comparative study between an SSP and an OSD in terms of cost and time. This has been done by establishing a realistic design on both decks and comparing their material consumption, production time during welding, and coating cost. From the results, the following can be concluded:

- Large time savings in production can be made due to automated processes in the welding and assembly procedures of a bridge deck in steel.

7

Discussion

The investigations in this thesis show the structural response of a pedestrian bridge with truss girders and a SSP subjected to a uniformly distributed load and wheel pressure from a service vehicle. The results have been compared against a conventional OSD to illustrate the difference between the two cases. Furthermore, upper and lower bounds have been modeled to evaluate to which extent it is consistent. Additionally, the production chapter demonstrated potential, which when combined with the structural analysis demonstrates the SSP's viability as a pedestrian bridge option.

Shear lag has been examined in this thesis for the full and half length of the studied bridge and the intention of this was to examine the impact of the W/L ratio and the relationship between E/G and W/L, seen in Figure 2.9. The findings of the examined bridges could demonstrate that the aforementioned conditions had only a minor effect on the bridge with half its length and no observable effect on the bridge with its entire length.

If the correlation is correct, it is interesting to consider the small effect of shear lag for future work regarding pedestrian bridges even though the range of cases examined is too small to draw any general conclusions. If the E/G ratio is also low, as it was in the study's case and is shown in Table 7.1, where the W/L ratio is shown for the mean values of each bridge type, shear lag might not be a determining factor in the design of a pedestrian bridge.

Table 7.1: Mean widths and lengths for the different bridge types.

Bridge type	1	2	3	4
Width [m]	3.3	2.7	3.3	2.9
Length [m]	18.5	18.7	26.4	24.6
W/L [-]	0.18	0.14	0.125	0.118

It should be noted that the structural analysis and the production comparison in the report used two different cross-sections for the bridge deck. This happened be-

cause the L-core was not examined as a completed design but rather only in theory during the evaluation of core configurations. As a result, the potential for producing the desired L-core was overestimated. This was discovered following the structural analysis in a discussion with an SSP manufacturer. This was not deemed to be an appropriate design to demonstrate the potential of SSPs in the production comparison. The V-core was utilized instead, which did not have the same limitations. However, the use of two different cross-sections is not thought to be a significant issue in the overall analysis because it showed little impact on altering deck stiffness. However, additional research is required to validate the design for the local analysis.

If the weight of the V-core from Chapter 6 is compared against the mean values of the different bridge types in Table 3.1, it can be seen that the weight is less than or equal to the weight of the V-core in 3 out of 4 cases. This is intriguing because the cross section can be improved, allowing weight savings. However, it must be remembered that the results are presented as a whole and do not account for the weight's dependence on width.

This might not matter if more bridges are researched and presented with a similar width. According to Nilsson (2017), using an SSP rather than a conventional solution can result in weight savings of between 10 and 50 percent for the entire bridge. These findings are corroborated by Dackman and Ek (2015) who found that using an SSP could result in material savings in the crossbeams. Figure 4.20 shows normal stresses for the lower chord with and without the composite action. It is clear that the stresses are significantly reduced if the composite action is taken into account, which is an indication of such material savings for pedestrian bridges. Therefore, a lower chord with less material might be reasonable.

8

Conclusion

The aim of this thesis was to compare the production aspects of an OSD and a SSP, as well as to investigate the structural response of a pedestrian bridge deck with truss girders. Through an evaluation of a large number of core configurations, two were selected to proceed with the structural analysis and production comparison. A finite element model was established to examine the behavior of the bridge as a result of the selected core and how it was impacted by modified stiffness parameters in the deck. The composite action's impact on the stresses and deflection in the lower chord as well as how it affected the stresses and instability of the upper chord were then studied using a model without a deck. In order to investigate the stress distribution under directly applied wheel pressure, the previous model was additionally modified. A production comparison between an OSD and an SSP was also done. The following can be concluded from the findings in this report:

- Among the evaluated core configurations, the L-core, V-core, and Z-core displayed the greatest potential in terms of structural response and manufacturing aspects.
- Altering the bending and shear stiffness of the deck did not have a significant impact on the distribution of normal stresses in the bridge deck. However, a considerable effect is seen when the axial stiffness of the bridge deck is altered.
- Including composite action reduces stresses in the lower chord significantly. However, including composite action yields local forces in the deck at the position of diagonal-to-bottom chord joints that need to be treated.
- Including composite action has no effect on the normal force in the upper chord.
- Composite action was shown to have a considerable impact on the deflection of the lower chord, excluding it yielded an increase in deflection.
- Shear lag had a negligible impact on both a bridge with a SSP and an OSD.
- In the buckling analysis the degree of rotation of the lower chord was shown

to be close to fully fixed for the analysis including interaction.

- Local stresses arising in the deck due to locally applied wheel pressure are significantly larger than the maximum stresses arising from the global bending action.
- The degree of rotation neither corresponded to a simply supported or fixed condition, where the first is used to calculate maximum deflections in the transversal direction and the latter is used to calculate stresses at the boundaries, respectively. The degree of constraint rather corresponded to a value between the extremes, approximately 60-70%.
- The weld rotational stiffness does not have a significant impact on the stress magnitudes in the bridge deck and its constituent plates.
- Large savings in production time can be achieved if the welding process is automated and stake welds are used.

A final remark is that the results of this study are based on a structural analysis and cost comparison for a specific bridge, so no generalizations can be made.

8.1 Future Studies

A suggestion for future studies is to compare the performance of an optimized steel sandwich panel and a conventional orthotropic steel deck, both in terms of the full life cycle's economic and environmental sustainability. To further establish the SSP and demonstrate its potential, a more thorough investigation of the production would be necessary.

Furthermore, it would have been interesting to look into how the design of various truss girders influences the bridge's response and to conduct a more thorough investigation that takes the contribution of the diagonals into account.

When contact between the top face plate and core was ignored, this study brought to light significant stress concentrations in the core under directly applied wheel pressure. Future studies would also benefit from an in-depth investigation of including contact in the analysis for various core configurations.

References

Abbott, S. P., Caccese, V., Thompson, L., Blomquist, P. A., & Hansen, E. E. (2007). *Automated Laser Welded High Performance Steel Sandwich Bridge Deck Development.*

Acherjee, B. (2018, 2). Hybrid laser arc welding: State-of-art review. *Optics and Laser Technology*, *99*, 60–71.

Al-Emrani, M., & Åkesson, B. (2020). *STEEL STRUCTURES Course Literature - VSM 191.*

Alwan, U., & Järve, D. (2012). *New Concept for Industrial Bridge Construction Laser Welded Steel Sandwich Panels.* Gothenburg.

Arvanitis, E., & Papadopoulos, E. (2016). *Steel-Sandwich Elements in Long-Span Bridge Applications.* Gothenburg.

Bartolozzi, G., Pierini, M., Orrenius, U., & Baldanzini, N. (2013, 6). An equivalent material formulation for sinusoidal corrugated cores of structural sandwich panels. *Composite Structures*, *100*, 173–185.

Beneus, E., & Koc, I. (2014). *Innovative road bridges with steel sandwich decks.* Gothenburg.

Blaauwendraad, J. (2010). *Plates and FEM: Surprises and Pitfalls.* Springer.

Bright, S. R., & Smith, J. W. (2007, 11). A new design for steel bridge decks using laser fabrication. *The Structural Engineer*, 49–57.

Chen, W., & Duan, L. (2014). *Bridge Engineering Handbook: Construction and Maintenance.*

Chen, W., & Han, D. (1987). *Plasticity for structural engineers.* New York.

Chiriac, R., & Vrabie, M. (2016). The First Order Shear Deformation Theory for Sandwich Plates. *Intersections/Intersecţii*, *13*(1), 37–47.

Dackman, D., & Ek, W. (2015). *Steel sandwich decks in medium span bridges.* Gothenburg.

Davies, J. M. (1993). Sandwich Panels. *Thin-Walled Structures*, *16*, 179–198.

Defalco, J. (2007). Practical Applications for Hybrid Laser Welding. *Welding journal*, 47–50.

Dinbandhu, Vishal Prajapati, Jay, J., Vora, Kumar, S., & Abhishek. (2021). Advances in gas metal arc welding process: modifications in short-circuiting transfer mode. *Advanced Welding and Deforming.*

Fung, T., & Tan, K. (1998, 7). Shear stiffness for Z-core sandwich panels. *Journal of Structural Engineering*, *124*(7), 809–816.

Fung, T., Tan, K., & Lok, T. (1993). Analysis of C-core Sandwich Plate Decking. In *Proceedings of the third (1993) international offshore and polar engineering conference* (pp. 244–249). Singapore: International Society of Offshore and Polar Engineers (ISOPE).

Fung, T., Tan, K., & Lok, T. (1994). Elastic Constants for Z-core Sandwich Panels. *Journal of Structural Engineering*, *120*(10), 3046–3055.

Fung, T., Tan, K., & Lok, T. (1996). Shear stiffness DQy for C-core sandwich panels. *Journal of Structural Engineering*, *122*, 958–966.

Holmberg, (1950). Shear-Weak Beams on Elastic Foundations. *IABSE Publications*, *10*, 69–85.

Hou, S., Shu, C., Zhao, S., Liu, T., Han, X., & Li, Q. (2015, 8). Experimental and numerical studies on multi-layered corrugated sandwich panels under crushing loading. *Composite Structures*, *126*, 371–385.

Keil, A. (2013). *Pedestrian Bridges: Ramps, Walkways, Structures.*

Kollár, L. P., & Tarján, G. (2021). Elastic beams and columns. *Mechanics of Civil Engineering Structures.*

Kolstein, M. H. (2007). *Fatigue Classification of Welded Joints in Orthotropic Steel Bridge Decks.*

Kujala, P., & Klanac, A. (2005). Steel Sandwich Panels in Marine Applications. *BRODOGRADNJA*, *56*(4), 305–314.

Libell, A., & Lassing, H. (2020). *Laser welded Corrugated Core Steel Sandwich Panels for short-span bridge application.* Gothenburg.

Libove, C., & Batdorf, S. (1948). *A general small-deflection theory for flat sandwich panels, NACA Report No. 899.*

Libove, C., & Hubka, R. E. (1951, 2). *Elastic constants for corrugated-core sandwich plates.* Washington: National Advisory Comitee for Aeronautics, Langley Aeronautical Laboratory.

Lin, W., & Yoda, T. (2017). *Bridge Engineering.*

Lok, T.-S., & Cheng, Q.-H. (2000). Elastic stiffness properties and behavior of truss-core sandwich panel. *JOURNAL OF STRUCTURAL ENGINEERING*, *126*, 552–559.

Marek, A., & Garbowski, T. (2015). Homogenization of sandwich panels. *Computer Assisted Methods in Engineering and Science*, *22*, 39–50.

McKinsey & Company. (2020). *The next normal in construction: How disruption is reshaping the world's largest ecosystem.*

Moffatt, K. R., & Dowling, P. J. (1975). Shear lag in steel box girder bridges. *Structural Engineering*, 439–448.

Naar, H. (1997). All steel Corrugated Core Sandwich Panels under Patch Loading.

Nilsson, P. (2017). *Laser-welded corrugated core steel sandwich panels for bridge application.* Gothenburg: Chalmers University of Technology.

Nilsson, P., & Al-Emrani, M. (2016). Industrialized light-weight steel bridge concept using corrugated core steel sandwich plates..

Nilsson, P., Al-Emrani, M., & Atashipour, S. R. (2017a). A numerical approach to the rotational stiffness of stake welds..

Nilsson, P., Al-Emrani, M., & Atashipour, S. R. (2017b, 8). Transverse shear stiffness of corrugated core steel sandwich panels with dual weld lines. *Thin-Walled Structures*, *117*, 98–112.

Nilsson, P., Hedegård, J., Al-Emrani, M., & Atashipour, S. R. (2019, 11). The impact of production-dependent geometric properties on fatigue-relevant stresses in laser-welded corrugated core steel sandwich panels. *Welding in the World*, *63*(6), 1801–1818.

Nilsson Strand, P. (2020). *Laser-welded corrugated core steel sandwich bridge decks.* Gothenburg.

Nordstrand, T., Carlsson, L. A., & Allen, H. G. (1994). Transverse shear stiffness of structural core sandwich. *Composite Structures*, *27*, 317–329.

Reissner, E. (1941). Least work solutions of shear lag problems. *J. Aeronaut. Sci. 8*, 284–291.

Roland, F., Manzon, L., Kujala, P., Brede, M., & Weltzenböck, J. (2004). Advanced Joining Techniques in European Shipbuilding. *Journal of Ship Production*, *20*(3), 200–210.

Romanoff, J. (2007). *Bending response of laser-welded web-core sandwich plates.* Helsinki University of Technology, Ship Laboratory.

Romanoff, J., & Kujala, P. (2002). Formulation for the strength analysis of all steel sandwich panels.

Sandcore. (n.d.). *Best Practice Guide for Sandwich Structures in Marine Applications. Eur. Comm. Contract No. FP6-506330.*

SS-EN 1990. (2002). *Eurocode - Basis of structural design.*

SS-EN 1990 Annex A2. (2004). *Eurocode - Basis of structural design.*

SS-EN 1991-2. (2003). *Eurocode 1: Actions on structures - Part 2: Traffic loads on bridges.*

SS-EN 1993-1-1. (2005). *Eurocode 3: Design of steel structures - Part 1-1: General rules and rules for buildings.*

SS-EN 1993-2. (2006). *Eurocode 3: Design of steel structures - Part 2: Steel Bridges.*

Steen, W., Eboo. M, & Clarke, J. (1978). *Arc augmented laser welding, in:Proc. of the 4th International Conference on Advances in Welding Processes, vol. 1.*

St-Pierre, L., Deshpande, V. S., & Fleck, N. A. (2015). The low velocity impact response of sandwich beams with a corrugated core or a Y-frame core. *International Journal of Mechanical Sciences*, *91*, 71–80.

Tan, K., Fung, T., & Lok, T. (1993). A simplified thick plate analogy for the analysis of all-steel sandwich panels. *The Structural Engineer*, *71*(14), 253–258.

Tan, K., & Montague, P. (1991). A simple grillage analogy for the analysis of steel sandwich panels with penetrations. *The Structural Engineer*, *69*(15), 271–276.

Tenchev, R. T. (1996). Shear lag in orthotropic beam flanges and plates with stiffeners. *International Journal of Solids and Structures*, *33*(9), 1317–1334.

Wahab, M. (2014). Welding and Bonding Technologies. *Comprehensive Materials Processing*.

Wouters, M. (2005). *Hybrid Laser-MIG welding: An investigation of geometrical considerations.* Luleå University of Technology.

Zenkert, D. (1997). *The handbook of sandwich construction.*

A

Pedestrian Bridge Study

Table A.1: Collected bridge data for deck type 1 from BaTMan.

Year	Bridge type	Span	Span length [m]	Total length [m]	Width [m]	Thickness [m]	Steel [kg/m3]	Deck [%]	Core [%]
2015	1	1	31.50	31.5	3.00	0.010	107.0	71	29
2014	1	4	30, 30, 30, 30	120.0	3.58	0.010	107.4	70	30
2012	1	1	17.00	17.0	3.00	0.008	89.2	68	32
2006	1	1	19.50	19.5	3.00	0.010	113.5	66	34
2003	1	3	9.9, 25, 9.9	44.8	3.50	0.010	102.4	73	27
2002	1	4	11.3, 18, 18, 11.3	40.6	3.50	0.010	119.1	64	36
2000	1	2	17.40	17.4	3.00	0.010	98.8	76	24
2000	1	1	30.00	30.0	2.50	0.010	104.0	72	28
1999	1	6	16, 16, 16	48.0	3.50	0.012	133.8	70	30
1998	1	1	31.90	31.9	3.00	0.012	123.6	73	27
1998	1	8	8, 11.5, 6, 19.8, 7.5, 7, 15.5, 10	85.3	3.00	0.012	128.1	74	26
1994	1	4	15, 25, 25, 15	80.0	4.20	0.010	155.4	51	49
1993	1	3	12.7, 26, 15.7	54.4	3.50	0.012	118.5	77	23
1993	1	3	20.5, 14.5, 20.5	55.5	3.14	0.012	127.3	74	26
1983	1	3	14.8, 19.2, 11.8	45.8	3.18	0.010	114.9	70	30
1979	1	3	23, 27.2, 23	73.2	4.00	0.010	116.1	68	32
1970	1	1	18.00	18.0	4.00	0.008	92.4	68	32

Table A.2: Collected bridge data for deck type 2 from BaTMan.

Year	Bridge type	Span	Span length [m]	Total length [m]	Width [m]	Thickness [m]	Steel [kg/m3]	Deck [%]	Core [%]
2014	2	2	31.5, 31.5	63.0	3.50	0.012	155.1	58	42
2011	2	2	24.9, 25.3	50.2	2.00	0.010	105.5	69	31
2005	2	1	11.30	11.3	3.05	0.012	138.2	69	31
1999	2	1	34.00	34.0	2.05	0.010	137.5	55	45
1996	2	4	10.1, 23.5, 22, 15.2	70.8	3.00	0.010	102.0	74	26
1996	2	1	25.50	25.5	2.14	0.008	110.8	54	46
1993	2	1	45.10	45.1	2.62	0.010	101.1	78	22
1991	2	6	14.2, 15, 18, 15.7, 15.7, 9.7	88.3	2.95	0.010	97.2	78	22
1986	2	3	15, 26, 26	67.0	4.00	0.010	108.8	70	30
1981	2	3	11.6, 16, 11.1	38.7	3.00	0.010	104.7	75	25
1980	2	3	11, 20, 10	41.0	1.82	0.008	76.5	83	17
1980	2	4	14, 20, 20, 10	64.0	1.82	0.008	81.2	78	22
1980	2	1	20.80	20.8	3.20	0.010	111.5	72	28
1979	2	4	10.5, 24, 24, 10.5	69.0	2.76	0.010	102.3	75	25
1978	2	1	28.00	28.0	3.02	0.008	81.6	74	26
1976	2	1	26.50	26.5	2.50	0.008	79.8	75	25
1975	2	5	18, 25.5, 12, 30, 8	93.5	3.00	0.008	83.5	72	28
1975	2	1	28.00	28.0	2.50	0.010	97.3	76	24
1973	2	3	12, 28, 16	56.0	3.00	0.008	72.5	82	18
1972	2	8	15, 15, 6, 15, 18, 9, 15, 15	108.0	3.00	0.008	86.8	72	28
1972	2	2	17.8, 17.8	35.6	2.79	0.008	75.5	86	14

Table A.3: Collected bridge data for deck type 3 from BaTMan.

Year	Bridge type	Span	Span length [m]	Total length [m]	Width [m]	Thickness [m]	Steel [kg/m3]	Deck [%]	Core [%]
2015	3	1	27.00	27.0	3.45	0.008	91.2	69	31
2015	3	1	27.60	27.6	3.16	0.012	128.7	73	27
2014	3	1	27.50	27.5	3.16	0.010	111.6	70	30
2014	3	4	17, 25.5, 25.5, 19	87.0	3.63	0.010	103.3	76	24
2010	3	1	27.50	27.5	3.00	0.008	109.3	59	41
2005	3	1	41.00	41.0	3.36	0.010	103.8	76	24

Table A.4: Collected bridge data for deck type 4 from BaTMan.

Year	Bridge type	Span	Span length [m]	Total length [m]	Width [m]	Thickness [m]	Steel [kg/m3]	Deck [%]	Core [%]
2014	4	1	24.50	24.5	2.37	0.010	105.4	71	29
2013	4	1	20.00	20.0	2.40	0.010	123.6	66	34
2012	4	1	9.90	9.9	2.59	0.010	140.5	56	44
2009	4	1	39.40	39.4	2.54	0.008	111.8	58	42
1994	4	1	27.00	27.0	3.00	0.008	150.9	38	62
1993	4	1	28.50	28.5	2.20	0.006	96.1	51	49
1992	4	3	22.8, 17, 26.1	65.9	2.50	0.008	103.8	58	42
1989	4	1	30.00	30.0	3.09	0.012	126.3	75	25
1985	4	2	13.3, 23.3	36.6	3.15	0.010	119.1	67	33
1984	4	1	28.10	28.1	3.00	0.010	121.9	62	38
1984	4	1	27.80	27.8	3.00	0.010	121.9	62	38
1982	4	1	29.30	29.3	3.63	0.012	168.2	56	44
1980	4	1	27.00	27.0	4.10	0.010	113.1	70	30

B

L-Core

Calculate the elastic stiffness constants of the L-core

Stiffness constants in the strong direction is done for the L-core and for the weak direction its made for the I-core according to Romanoff J. & Kujala P. (2002) Formulation for the strength analysis of all steel sandwich panels. The calculations are done per meter width.

By: Alexander Svensson & Johanna Lindqvist

Geometries

$t_{d.tf} := 6\ mm$	Top face plate thickness
$t_{d.L} := 4\ mm$	Core thickness
$t_{d.lf} := 4\ mm$	Bottom face plate thickness
$h := 100\ mm$	Panel height
$d_{d.w} := h - t_{d.tf} - t_{d.lf} = 0.09\ m$	Core height
$d_{d.f} := 50\ mm$	Core flange width
$d_{d.wc} := 20\ mm$	Distance between welds
$d_{d.wd} := 18\ mm$	Distance between first weld line and web of the core
$d_{d.c} := 140\ mm$	Center to center distance between L-cores

General shell stiffness

$E := 210\ GPa$	Young's modulus
$v := 0.3$	Poissons ratio
$G := \frac{E}{2 \cdot (1 + v)} = 81\ GPa$	Shear modulus
$p := \frac{d_{d.c}}{2} = 0.07\ m$	One pitch length

$d := 0.5 \cdot (t_{d.tf} + t_{d.lf}) + d_{d.w} = 0.095\ m$

Axial stiffness

$A_f := t_{d.tf} + t_{d.tf} = 0.01\ m$ — Flange area per unit width

$A_c := d_{d.w} \cdot \frac{t_{d.L}}{d_{d.c}} = 0.003\ m$ — Core area per unit width

$E_x := E \cdot (A_f + A_c) = (2.64 \cdot 10^3)\ \frac{kN}{mm}$ — Axial stiffness in stiff direction per unit width

$E_y := \frac{E \cdot A_f}{1 - v^2 \cdot \left(1 - E \cdot \frac{A_f}{E_x}\right)} = (2.139 \cdot 10^3)\ \frac{kN}{mm}$ — Axial stiffness in weak direction per unit width

$v_x := v = 0.3$

$v_y := v_x \cdot \frac{E_y}{E_x} = 0.243$

$d_{11} := \frac{E_x}{1 - v_x \cdot v_y} = (2.848 \cdot 10^3)\ \frac{kN}{mm}$

$d_{22} := \frac{E_y}{1 - v_x \cdot v_y} = (2.308 \cdot 10^3)\ \frac{kN}{mm}$

$d_{12} := \frac{v_x \cdot E_x}{1 - v_x \cdot v_y} = 854.308\ \frac{kN}{mm}$

$G_{xy} := G \cdot \frac{t_{d.L}^{\ 2}}{A_c} + G \cdot A_f = (1.31 \cdot 10^3)\ \frac{kN}{mm}$ — Horizontal shear stiffness per unit width

$d_{33} := G_{xy}$

Bending stiffness

$I_f := \frac{t_{d.tf}^3}{12} + \frac{t_{d.lf}^3}{12} + A_f \cdot \left(\frac{d}{2}\right)^2 = (2.259 \cdot 10^{-5})\ m^3$ Moment of intertia of the face plates

$I_c := \frac{d_{d.w}^3}{12} \cdot \frac{t_{d.L}}{d_{d.c}} = (1.736 \cdot 10^{-6})\ m^3$ Moment of intertia of the core

$D_x := E \cdot (I_f + I_c) = (5.108 \cdot 10^3)\ kN \cdot m$ Bending stiffness in the stiff direction per unit width

$D_y := E \cdot \frac{I_f}{\left(1 - v^2 \cdot \left(1 - E \cdot \frac{I_f}{D_x}\right)\right)} = (4.774 \cdot 10^3)\ kN \cdot m$ Bending stiffness in the weak direction per unit width

$v_x = 0.3$

$v_y := v_x \cdot \frac{D_y}{D_x} = 0.28$

$d_{44} := \frac{D_x}{1 - v_x \cdot v_y} = (5.577 \cdot 10^3)\ kN \cdot m$

$d_{55} := \frac{D_y}{1 - v_x \cdot v_y} = (5.2121 \cdot 10^3)\ kN \cdot m$

$d_{45} := v_x \cdot \frac{D_y}{1 - v_x \cdot v_y} = (1.564 \cdot 10^3)\ kN \cdot m$

$e_{xy} := \frac{\left(\left(h - \frac{t_{d.tf}}{2}\right) \cdot G \cdot t_{d.tf} + \frac{t_{d.lf}}{2} \cdot G \cdot t_{d.lf}\right)}{(G \cdot t_{d.tf} + G \cdot t_{d.lf})} = 59\ mm$

$D_{xy} := \frac{G}{3} \cdot t_{d.tf} \cdot \left(3 \cdot h \cdot (h - 2 \cdot e_{xy} - t_{d.tf}) + t_{d.tf}^2 + 3 \cdot e_{xy}^2 + 3 \cdot e_{xy} \cdot t_{d.tf}\right) + \frac{G}{3} \cdot t_{d.lf} \cdot \left(3 \cdot e_{xy}^2 - 3 \cdot e_{xy} \cdot t_{d.lf} + t_{d.lf}^2\right)$

$D_{xy} = (1.751 \cdot 10^3)\ kN \cdot m$ Torsional stiffness per unit width

$d_{66} := 0.5 \cdot D_{xy} = 875.673\ kN \cdot m$

Transverse shear stiffness

$D_{Qx} := G \cdot t_{d.tf} + G \cdot \frac{t_{d.L}}{2 \cdot p} \cdot d_{d.w} + G \cdot t_{d.lf} = (1.015 \cdot 10^{9}) \ \frac{N}{m}$ Transverse shear stiffness parallel to the corrugation per unit width

$k_{11} := D_{Qx}$

$z_1 := \frac{\left(\left(p \cdot t_{d.L}^{3} + 3 \cdot d \cdot t_{d.tf}^{3}\right) \cdot t_{d.lf}^{3}\right)}{\left(6 \cdot d \cdot t_{d.tf}^{3} \cdot t_{d.lf}^{3} + p \cdot t_{d.L}^{3} \cdot \left(t_{d.tf}^{3} + t_{d.lf}^{3}\right)\right)} = 0.463$

$\gamma_H := \frac{p^2}{d^2} \cdot \frac{1 - \nu^2}{E} \cdot \left(\frac{1}{t_{d.tf}} + \frac{1}{t_{d.lf}}\right) = (9.803 \cdot 10^{-4}) \ \frac{mm}{kN}$

$\gamma_V := 4 \cdot \frac{1 - \nu^2}{E} \cdot \left((1 - z_1) \cdot \frac{p^2}{t_{d.tf}^{3}} + (2 - 3 \cdot z_1) \cdot d \cdot \frac{p}{t_{d.L}^{3}}\right) = 1.313 \ \frac{mm}{kN}$

$D_{Q.y} := \frac{1}{\gamma_H + \gamma_V} = (7.609 \cdot 10^{5}) \ \frac{N}{m}$ Transverse shear stiffness perpendicular to the corrugation per unit width

$k_{22} := D_{Q.y}$

$D := \begin{bmatrix} d_{22} & d_{12} & 0 & 0 & 0 & 0 \\ 0 & d_{11} & 0 & 0 & 0 & 0 \\ 0 & 0 & d_{33} & 0 & 0 & 0 \\ 0 & 0 & 0 & d_{55} & d_{45} & 0 \\ 0 & 0 & 0 & 0 & d_{44} & 0 \\ 0 & 0 & 0 & 0 & 0 & d_{66} \end{bmatrix}$ Section stiffness

C

Orthotropic

Calculate the elastic stiffness constants of the orthotropic deck

Stiffness constants calculated according to Blauuwendraad, J. (2010): Plates and FEM. Dordrecht: Springer.

By: Alexander Svensson & Johanna Lindqvist

Material

$E := 210\ GPa$	Young's modulus
$v := 0.3$	Poissons ratio
$G := \frac{E}{2 \cdot (1+v)} = 81\ GPa$	Shear modulus

Geometries

$t_{fl} := 10\ mm$	Face plate thickness
$t_{st} := 6\ mm$	Thickness of stiffener
$b_{top} := 300\ mm$	Distance between inclined legs at the top plate
$b_{bot} := 150\ mm$	Distance between inclined legs at the stiffeners bottom
$b_w := 160\ mm$	Height of stiffener
$l_w := 176.7\ mm$	Length of inclined leg
$b := 0.75\ m$	Center to center distance between stiffeners

$I_z = (3.237 \cdot 10^{-5})\ m^4$	Moment of intertia of one stiffener including top face plate
$t_{top} := t_{fl}$	Top face equals the thickness of the face plate
$t_{bot} := t_{st}$	Bot and web equals the thickness of the stiffener
$t_w := t_{st}$	
$A_a := 2 \cdot t_w \cdot b_w + t_{bot} \cdot b_{bot} = 0.003\ m^2$	One stiffeners cross-sectional area
$A := \frac{b_{top} + b_{bot}}{2} \cdot b_w = 0.036\ m^2$	One stiffeners cross-sectional area including the empty space

General shell stiffness

$$i_{xy} := \frac{t_{top}^{3}}{6} = (1.667 \cdot 10^{-7})\ m^3$$ Torsional rigidity

$$I_t := \frac{4 \cdot A^2}{\left(\frac{b_{top}}{t_{top}} + 2 \cdot \frac{b_w}{t_w} + \frac{b_{bot}}{t_{bot}}\right)} = (4.785 \cdot 10^{-5})\ m^4$$ Polar moment of inertia

$$i_{yx} := \frac{1}{b} \cdot \left(I_t + \frac{t_{top}^{3} \cdot b}{6} + \frac{t_{bot}^{3} \cdot b_{bot}}{3} + \frac{2 \cdot t_w^{3} \cdot b_w}{3}\right) = (6.401 \cdot 10^{-5})\ m^3$$ Torsional rigidity

$$i_{av} := \frac{i_{xy} + i_{yx}}{2} = (3.209 \cdot 10^{-5})\ m^3$$ Torsional moment of inertia

$$d_{11} := \frac{E \cdot t_{fl}}{1 - v^2} + E \cdot \frac{A_a}{b} = (3.097 \cdot 10^{3})\ \frac{kN}{mm}$$

$$d_{12} := \frac{E \cdot t_{fl}}{(1 - v^2)} \cdot v = 692.308\ \frac{kN}{mm}$$

$$d_{22} := \frac{E \cdot t_{fl}}{1 - v^2} = (2.308 \cdot 10^{3})\ \frac{kN}{mm}$$

$$d_{33} := \frac{E \cdot t_{fl}}{1 - v^2} \cdot \frac{1 - v}{2} = 807.692\ \frac{kN}{mm}$$

$$d_{44} := \frac{E \cdot I_z}{b} = (9.063 \cdot 10^{3})\ kN \cdot m$$

$$d_{55} := \frac{E \cdot t_{fl}^{3}}{12 \cdot (1 - v^2)} = 19.231\ kN \cdot m$$

$$d_{45} := v \cdot d_{55} = 5.769\ kN \cdot m$$

$$d_{66} := \frac{G \cdot i_{av}}{2} = (1.296 \cdot 10^{3})\ kN \cdot m$$

$$D := \begin{bmatrix} d_{22} & d_{12} & 0 & 0 & 0 & 0 \\ 0 & d_{11} & 0 & 0 & 0 & 0 \\ 0 & 0 & d_{33} & 0 & 0 & 0 \\ 0 & 0 & 0 & d_{55} & d_{45} & 0 \\ 0 & 0 & 0 & 0 & d_{44} & 0 \\ 0 & 0 & 0 & 0 & 0 & d_{66} \end{bmatrix}$$ Section stiffness

D

Global verification

Global verification of the model

Calculate the defection of the bridge with distributed load with hand calculations and compare it with the result from the FEa.

By: Alexander Svensson & Johanna Lindqvist

Material

$E := 210\ GPa$ — Young's modulus

Control of the plates deflection between girders

Geometrie Deck

$t_{d.tf} := 6\ mm$ — Thickness top face plate

$t_{d.L} := 4\ mm$ — Thickness core

$t_{d.lf} := 4\ mm$ — Thickness bottom face plate

$h := 100\ mm$ — Height of panel

$d_{df} := 50\ mm$ — Length of horizontal part of the core

$d_{dc} := 140\ mm$ — Distance between stiffeners

$d_{dw} := h - t_{d.tf} - t_{d.lf} = 0.09\ m$ — Height of core

$d_{dcc} := d_{dw} - t_{d.L} = 0.086\ m$ — Height of vertical part of the core

$d := 0.5 \cdot (t_{d.tf} + t_{d.lf}) + d_{dw} = 0.095\ m$ — Distance between center of top plate and center of bottom plate

$L := 30\ m$ — Length of deck

$W := 4.37\ m$ — Width of deck

Neutral axis and moment of inertia

$$z_{na} := \frac{t_{d.tf} \cdot d_{dc} \cdot \left(\frac{t_{d.tf}}{2}\right) + t_{d.lf} \cdot d_{dc} \cdot \left(h - \frac{t_{d.lf}}{2}\right) + d_{dw} \cdot t_{d.L} \cdot \left(t_{d.tf} + \frac{d_{dw}}{2}\right) + d_{df} \cdot t_{d.L} \cdot \left(t_{d.tf} + \frac{t_{d.L}}{2}\right)}{t_{d.tf} \cdot d_{dc} + t_{d.lf} \cdot d_{dc} + d_{dw} \cdot t_{d.L} + d_{df} \cdot t_{d.L}} = 39.469 \text{ mm}$$

$$I_f := \frac{d_{dc} \cdot t_{d.tf}^3}{12} + \frac{d_{dc} \cdot t_{d.lf}^3}{12} + t_{d.tf} \cdot d_{dc} \cdot \left(z_{na} - \frac{t_{d.tf}}{2}\right)^2 + t_{d.lf} \cdot d_{dc} \cdot \left(h - z_{na} - \frac{t_{d.lf}}{2}\right)^2 = \left(3.039 \cdot 10^{-6}\right) \text{ m}^4$$

$$I_c := \frac{t_{d.L} \cdot d_{dw}^3}{12} + \frac{d_{df} \cdot t_{d.L}^3}{12} + t_{d.L} \cdot d_{dw} \cdot \left(t_{d.tf} + t_{d.L} + \left(\frac{d_{dw}}{2} - z_{na}\right)\right)^2 + d_{df} \cdot t_{d.L} \cdot \left(z_{na} - t_{d.tf} - \frac{t_{d.L}}{2}\right)^2 = \left(5.282 \cdot 10^{-7}\right) \text{ m}^4$$

$I_l := I_f + I_c = \left(3.567 \cdot 10^{-6}\right) \text{ m}^4$ Moment of inertia for stiffener including face plates

Load

$\psi := 0.4$ Factor for variable action in the frequent load combination

$q := 5 \frac{\text{kN}}{\text{m}^2}$ Distributed load

$q_{d.l} := \psi \cdot q \cdot d_{dc} = 0.28 \frac{\text{kN}}{\text{m}}$

Deflection

$u_l := \frac{5 \cdot q_{d.l} \cdot W^4}{384 \cdot E \cdot I_l} = 1.8 \text{ mm}$ Deflection hand calculations

$u_{l.FEa} := 1.7 \text{ mm}$ Deflection FEa

Control of the girders deflection

Upper Chord

$h_{uc} := 180\ mm$ $w_{uc} := 180\ mm$ $t_{uc} := 10\ mm$ Dimensions of upper chord

$A_{uc} := h_{uc} \cdot w_{uc} - \left(\left(h_{uc} - 2\ t_{uc} \right) \left(w_{uc} - 2\ t_{uc} \right) \right) = \left(6.8 \cdot 10^{3} \right)\ mm^{2}$ Area of upper chord

$I_{uc} := \frac{w_{uc} \cdot h_{uc}^{3}}{12} - \frac{\left(w_{uc} - 2\ t_{uc} \right) \cdot \left(h_{uc} - 2\ t_{uc} \right)^{3}}{12} = \left(3.287 \cdot 10^{7} \right)\ mm^{4}$ Moment of inertia upper chord

Lower Chord

$h_{lc} := 250\ mm$ $w_{lc} := 150\ mm$ $t_{lc} := 6.3\ mm$ Dimensions of lower chord

$A_{lc} := h_{lc} \cdot w_{lc} - \left(\left(h_{lc} - 2\ t_{lc} \right) \left(w_{lc} - 2\ t_{lc} \right) \right) = \left(4.881 \cdot 10^{3} \right)\ mm^{2}$ Area of lower chord

$I_{lc} := \frac{w_{lc} \cdot h_{lc}^{3}}{12} - \frac{\left(w_{lc} - 2\ t_{lc} \right) \cdot \left(h_{lc} - 2\ t_{lc} \right)^{3}}{12} = \left(4.2116 \cdot 10^{7} \right)\ mm^{4}$ Moment of inertia lower chord

Upper face plate

$t_{uf} := 6\ mm$ $w_{uf} := 4.37\ m$ Dimensions of upper face plate

$A_{uf} := t_{uf} \cdot w_{uf} = \left(2.622 \cdot 10^{4} \right)\ mm^{2}$ Area of upper face plate

$I_{uf} := \frac{w_{uf} \cdot t_{uf}^{3}}{12} = \left(7.866 \cdot 10^{4} \right)\ mm^{4}$ Moment of inertia of upper face plate

Lower face plate

$t_{lf} := 4\ mm$ $w_{lf} := 4.37\ m$ Dimensions of lower face plate

$A_{lf} := t_{lf} \cdot w_{lf} = \left(1.748 \cdot 10^{4} \right)\ mm^{2}$ Area of lower face plate

$I_{lf} := \frac{w_{lf} \cdot t_{lf}^{3}}{12} = \left(2.331 \cdot 10^{4} \right)\ mm^{4}$ Moment of inertia of lower face plate

Neutral axis

$$Z_{na} := \frac{2 \cdot A_{uc} \cdot \frac{h_{uc}}{2} + 2 \cdot A_{lc} \cdot \left(\frac{h_{uc}}{2} + 1.885\ m\right) + A_{uf} \cdot \left(\frac{h_{uc}}{2} + 1.885\ m - z_{na} + \frac{t_{uf}}{2}\right) + A_{lf} \cdot \left(\frac{h_{uc}}{2} + 1.885\ m + 60.6\ mm - \frac{t_{lf}}{2}\right)}{2\ A_{uc} + 2\ A_{lc} + A_{uf} + A_{lf}}$$

$Z_{na} = 1.594\ m$

Moment of inertia

$$I_c := I_{uc} + I_{lc} + A_{uc} \cdot \left(Z_{na} - \frac{h_{uc}}{2}\right)^2 + A_{lc} \cdot \left(Z_{na} - \left(\frac{h_{uc}}{2} + 1.885\ m\right)\right)^2 = \left(1.616 \cdot 10^{10}\right)\ mm^4$$

$$I_f := I_{uf} + I_{lf} + A_{uf} \cdot \left(Z_{na} - \left(\frac{h_{uc}}{2} + 1.885\ m - 39.5\ mm + \frac{t_{uf}}{2}\right)\right)^2 + A_{lf} \cdot \left(Z_{na} - \left(\frac{h_{uc}}{2} + 1.885\ m + 60.6\ mm - \frac{t_{lf}}{2}\right)\right)^2$$

$I_f = \left(6.498 \cdot 10^9\right)\ mm^4$

$I_{II} := 2\ I_c + I_f = \left(3.882 \cdot 10^{10}\right)\ mm^4$

Load

$q_{d.II} := \psi \cdot q \cdot W = 8.74\ \frac{kN}{m}$

Deflection

$u_{II} := \frac{5 \cdot q_{d.II} \cdot L^4}{384 \cdot E \cdot I_{II}} = 11.3\ mm$ Deflection hand calculations

$u_{II.FEa} := 14.4\ mm$ Deflection FEa

E

Buckling

Buckling of the upper chord

Calculate the reduction factor due to buckling for the bridge model including / excluding interaction

By: Alexander Svensson & Johanna Lindqvist

Material

$E := 210\ GPa$ — Young's modulus

$f_y := 420\ MPa$ — Yield stress

Sectional constants

$A := 6690\ mm^2$ — Cross-sectional area of the upper chord

$I_z := 3.19 \cdot 10^7\ mm^4$ — Moment of inertia of the upper chord

$I_y := I_z$

Eigenvalues from the finite element analysis

$$eigen := \begin{bmatrix} 3.5808 \\ 4.4875 \\ 4.8986 \end{bmatrix}$$

0: Model excluding interaction with rotation around longitudinal axis allowed
1: Model including interaction
2:Model excluding interaction with rotation around longitudinal axis restricted

Normal force in the model including interaction

Element	N_{Ed} (N)
201	−239554
202	−618279
203	−863793
204	−983527
205	−978257
206	−849950
207	−601887
208	−230282

$N_{x.average} := -670691\ N = -6.707 \cdot 10^{5}\ N$

$N_{cry} := |N_{x.average}| \cdot eigen_{1} = (3.01 \cdot 10^{3})\ kN$ Critical normal force

Normal force in the model excluding interaction

Element	$N_{Ed.EI}$
201	−237258
202	−607928
203	−847638
204	−964651
205	−959562
206	−834273
207	−592099
208	−228433

$N_{x.average} := -658980\ N$

$N_{cry.EI.RA} := |N_{x.average}| \cdot eigen_{0} = (2.36 \cdot 10^{3})\ kN$ Critical normal force, rotation allowed

$N_{cry.EI.RR} := |N_{x.average}| \cdot eigen_{2} = (3.228 \cdot 10^{3})\ kN$ Critical normal force, rotation restricted

$$N_{cr} := \begin{bmatrix} N_{cry.EI.RA} \\ N_{cry} \\ N_{cry.EI.RR} \end{bmatrix} = \begin{bmatrix} 2.36 \cdot 10^3 \\ 3.01 \cdot 10^3 \\ 3.228 \cdot 10^3 \end{bmatrix} \text{ kN}$$

$$l_{cr} := \pi \cdot \sqrt{\frac{E \cdot I_y}{N_{cr}}} = \begin{bmatrix} 5.29 \\ 4.69 \\ 4.53 \end{bmatrix} \text{ m}$$

Critical length

$$\lambda := \sqrt{\frac{A \cdot f_y}{N_{cr}}} = \begin{bmatrix} 1.091 \\ 0.966 \\ 0.933 \end{bmatrix}$$

$$\alpha := \begin{bmatrix} 0.21 \\ 0.49 \end{bmatrix}$$

0: Buckling curve a
1: Buckling curve c

$$\Phi_1 := 0.5 \cdot \left(1 + \alpha \cdot \left(\lambda_0 - 0.2\right) + \lambda_0^{\,2}\right) = \begin{bmatrix} 1.189 \\ 1.314 \end{bmatrix}$$

$$\Phi_2 := 0.5 \cdot \left(1 + \alpha \cdot \left(\lambda_1 - 0.2\right) + \lambda_1^{\,2}\right) = \begin{bmatrix} 1.047 \\ 1.155 \end{bmatrix}$$

$$\Phi_3 := 0.5 \cdot \left(1 + \alpha \cdot \left(\lambda_2 - 0.2\right) + \lambda_2^{\,2}\right) = \begin{bmatrix} 1.012 \\ 1.115 \end{bmatrix}$$

Reduction factor

$$X_1 := \frac{1}{\Phi_1 + \sqrt{\Phi_1^{\,2} - \lambda_0^{\,2}}} = \begin{bmatrix} 60.2\% \\ 48.9\% \end{bmatrix}$$

0: Model excluding interaction with rotation around longitudinal axis allowed

$$X_2 := \frac{1}{\Phi_2 + \sqrt{\Phi_2^{\,2} - \lambda_1^{\,2}}} = \begin{bmatrix} 68.9\% \\ 56\% \end{bmatrix}$$

1: Model including interaction

$$X_3 := \frac{1}{\Phi_3 + \sqrt{\Phi_3^{\,2} - \lambda_2^{\,2}}} = \begin{bmatrix} 71.2\% \\ 58\% \end{bmatrix}$$

2:Model excluding interaction with rotation around longitudinal axis restricted

DEPARTMENT OF ARCHITECTURE AND CIVIL ENGINEERING
CHALMERS UNIVERSITY OF TECHNOLOGY
Gothenburg, Sweden 2022
www.chalmers.se

CHALMERS
UNIVERSITY OF TECHNOLOGY